Development of an Intelligent Sensing Technique for Active Control of Railway Vehicles with Independently Rotating Wheels

By

Daniel Derbyshire

A thesis submitted in partial fulfilment of the requirements of the Manchester Metropolitan University for the degree of Master of Philosophy

Science & Engineering Department

Manchester Metropolitan University

2015

Abstract

This thesis continues the development of an intelligent sensing scheme; using practical techniques for estimating the vehicle variables and economic measurements, which are mounted away from any arduous environments.

The independently rotating wheelset design (IRW) de-couples the wheels; losing the mechanical feedback inherent with the conventional solid axle. The issue with the IRW, however, is that the natural curving characteristic is lost as a result, and therefore it is necessary to provide steering to the wheelset, to avoid flange contact and guide the wheelset, which can be supplied using a yaw constraint: passively or actively. As primary feedback variables aren't readily available to measure, and are costly to provide, the Kalman filter has been used to provide full state optimal estimation of the dynamic system. Involving random perturbations to return the necessary states required, the Kalman filter allows the controller and actuator to apply active steering to the IRW. This thesis applies the Kalman-Bucy filter to a closed loop system with a mechatronic vehicle. A simple P controller is used to provide a torque to the actuators. The novelty about this work is that the sensors are mounted to the vehicle body, avoiding the extreme climactic conditions that a sensor would usually see if mounted to the axle. Re-formulating the Kalman filter to include curvature and cant within the state space and output matrices has been assessed to see if the curving performance will be maintained or improved. Altering the amount of sensors used has also been assessed, to see how the curving performance is affected. This can coincide with assessing whether the system will work, should one or more of the sensors fail.

Acknowledgements

I would like to thank my director of studies, Hong Li, for her guidance and advice on this research.

I would like to thank my Mum, Dad and my girlfriend, Lucy, for their support, help and encouragement throughout my research work.

I would also like to thank the members of staff at Manchester Metropolitan University for helping me through my research.

List of Symbols

A	Semi wheelbase spacing (m)
A	State-space model matrix (continuous system)
A_k	State-space model matrix for Kalman filter
A_{kr}	State-space model matrix for Re-formulated Kalman filter
C_t	Yaw damper (kN/m)
C_y	(Primary) lateral damper (kN/m)
C	Output matrix
C_k	Output matrix for Kalman Filter
$\omega_L \omega_R$	Left and right wheel angular velocity (rad/s)
f_{11}	Longitudinal creep coefficient (MN)
f_{22}	Lateral creep coefficient (MN)
F_L, F_R	Left and right forces generated at the wheel
F_1, F_2	Lateral force
T_{w1}, T_{w2}	Control torque
G	State-space model matrix, track input
G_{kr}	State space model matrix for Kalman filter, track input
I_b	2-axle vehicle yaw inertia (kgm^2)
I_w	Wheeset Inertia (kgm^2)
$I_\emptyset$	Wheel rotational inertia (kgm^2)
K_y	(Primary) lateral stiffness (kN/m)
l	Half gauge (m)
K, K_r	Kalman-Bucy filter gain matrix
m_w	Wheelset mass (kg)
m_b	Vehicle mass (kg)
Q	Variance of random track input
Q_1	Variance of $(1/\dot{R})$
Q_2	Variance of $(\dot{\theta})$
Q_k	Track input covariance
R_k	Covariance of Measurement noise covariance
r_0	Nominal wheel radius (m)
R	Curve radius (m)
R_1, R_2	Curve radius for the leading and trailing wheelset (m)
$1/\dot{R_1}, 1/\dot{R_2}$	Curve velocity for the leading and trailing wheelset (m/s)
$R1, R2, R3, R4, R5, R6$	measurement noise covariances
v	Forward velocity (m/s)
w	Track Input

w_r	Re-formulated Kalman filter input
X	State vector
X_k, X_{kr}	Kalman-Bucy state vector
y_t	Track input (m)
$\dot{y}_t$	Track velocity input (m/s)
y_{t1}, y_{t2}	Leading and trailing lateral input (m)
$\dot{y}_{t1}, \dot{y}_{t2}$	Leading and trailing wheelsets lateral track velocity input (m/s)
$y_{w1} y_{w2}$	Leading and trailing lateral displacement (m)
$\dot{y}_{w1} \dot{y}_{w2}$	Leading and trailing lateral velocity (m/s)
y_{b1}, y_{b2}	Vehicle lateral displacement (m)
$\dot{y}_{b1}, \dot{y}_{b2}$	Vehicle lateral velocity (m/s)
Y	Output vector
Y_m	Measured output
λ	Conicity
θ	Track cant angle (rad)
$\theta_1 \theta_2$	Track cant angle for the leading and trailing wheelset (rad)
$\dot{\theta}_1 \dot{\theta}_2$	Track cant velocity for the leading and trailing wheelset (rad/s)
Ψ	Wheelset angle of attack (rad)
Ψ_{w1}, Ψ_{w2}	Angle of attack for the leading and trailing wheelset (rad)
$\dot{\Psi}_{w1}, \dot{\Psi}_{w2}$	Yaw velocities of the leading and trailing wheelsets (rad/s)
Ψ_{b1}, Ψ_{b2}	Angle of attack for the vehicle body (rad)
$\dot{\Psi}_{b1}, \dot{\Psi}_{b2}$	Body yaw velocity (rad/s)
$\dot{\phi}_L, \dot{\phi}_R$	Left and right wheel forward angular velocity (m/s)
ω_1, ω_2	Integrator time constants

Contents

Chapter 1 Introduction

1.1. Background

The Railway vehicle has been under great consideration over the last few decades; mainly to do with improving the performance of the traditional railway suspension. The automotive and aerospace industries have pioneered in applying active control to a vehicle or an aircraft in order to help improve the performance of the commuter. (Gruszecki, 2005) tested an electro-mechanical control system on a PZL-110 “Koliber” aircraft to see whether using the fly-by-wire method of navigating the vehicle could reduce the workload of the pilot and ensure a stabilised flight. The results from the in-flight testing proved that the actuator controller was capable of positioning the control surfaces with established static precision of 0.1 degrees. The automotive sector has conducted research into active means of stabilising the vehicle via means of steer-by-wire technology. (Kleine and Niekerk, 1998) provided a control strategy for the active steer-by-wire technology which resulted in sideslip limited to zero, a reduced work load for the driver and ultimately a higher stability whilst conducting dynamic manoeuvres. The automotive sector has progressed greatly in implementation of active control and has seen the production of fully active, high bandwidth body control systems, to mention, the Active control for the Mercedes CLS. The active suspension which replaced the passive suspension saw, not only improved cornering performance, but also improved ride comfort. Improvements in the automotive and aerospace industries led railway engineers to seek the same form of improved performance in the railway sector.

1.1.1 The Conventional Railway Vehicle Configuration

The current railway vehicle is comprised of a vehicle body; this is where the passengers reside. Then there are two sets of air springs which are known as the secondary suspension. This suspension is designed with passenger comfort in mind as it isolates any lateral and vertical acceleration produced whilst the vehicle is running on the track features. Then there are bogies which are the interconnection between the vehicle body and the wheelsets. The bogies are with the air springs to separate the vehicle body from the harsh vibrations experienced from the track to maintain passenger comfort. Finally, there is the primary suspension: the main purpose of the primary suspension is to maintain stability and equal weight distribution on the track to avoid derailment. The suspension configuration varies depending on the bogie design, however, usually; there are longitudinal and lateral springs and dampers which are connected between the bogie, axleboxes and/or trailing arms.

Each body has six degrees of freedom: roll, pitch, yaw and lateral, longitudinal and vertical translations. All degrees as well as vehicle configuration can be seen from the figure 1.1 (Li, 2001).

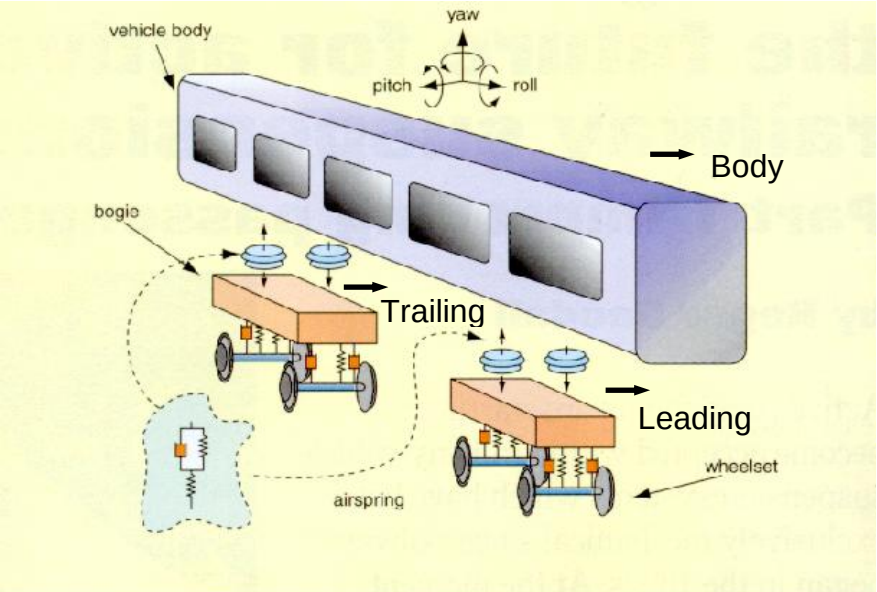

Figure 1.1 - The conventional railway vehicle configuration

1.2. Conventional Solid Axle

The conventional solid axle wheelset is comprised of two profiled wheels which are connected together with a solid axle. Each wheel has a flange, which is known as the non-linear region of the wheelset and provides a limit to the wheels lateral translation. However, with enough force, the wheel can climb its flange and de-rail.

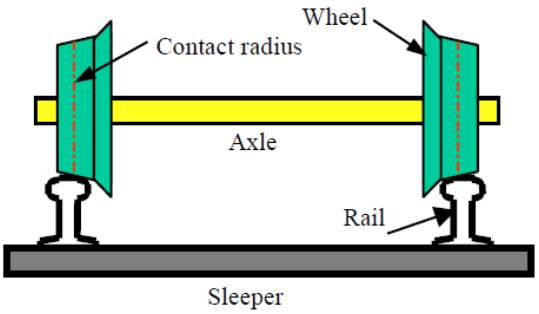

Figure 1.2 - Conventional solid axle wheelset

The shape of the wheels is the main characteristic of the wheelset; and is the main reason why the wheelset hasn't changed in design. The conical shape means that when a wheelset is running

along the track and transverses laterally, the wheels have a difference in rolling radius, which causes a difference in rotational velocities. This provides not only a self-centring characteristic, as the wheelset tends towards the centre of the track due to the difference in forward velocities, but also provides natural curving whilst mitigating a curved track feature. The solid axle has fantastic characteristics which make it perfect for mitigating the different track features.

1.2.1 The Dynamics of the Solid Axle Wheelset.

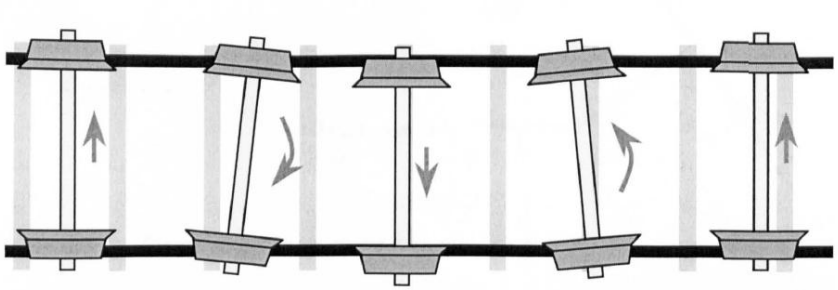

Figure 1.3 - Wheelset kinematic oscillation

Unfortunately an unconstrained (free) solid axle wheelset has some undesired characteristics: if a wheelset is rolling along the track and transverses laterally, the wheelset will produce a difference in rotational angular velocity. This difference in forward speed will create a yaw angle between the two wheels and result in the wheelset turning inward toward the centreline of the track, and overshooting, causing the wheel to transverse onto the other side of the track as shown in figure 1.3. This behaviour generates a sinusoidal motion, which is well known as the “kinematic oscillation” or hunting behaviour. As mentioned, the issue is derived from the production of differences in forward speeds or “creepages” in the lateral and longitudinal directions which create “creep forces”. It is these forces which, applied to the wheelset, provide guidance and create instability (Wickens, 1969).

1.2.2 Primary Suspension Configurations

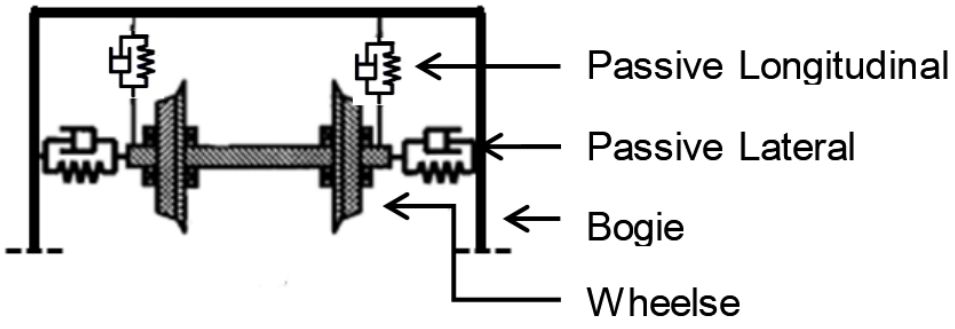

Figure 1.4 - Passive primary suspension configuration

The primary suspension has been designed to overcome the kinematic oscillatory behaviour inherent of the conventional solid-axle wheelset; to ultimately avoid any derailment risk. A typical primary suspension configuration (shown in figure 1.4) has proven to provide the stabilisation needed. However, as a result of this, the curving performance is hindered; therefore conventional vehicles have been proven to be based on a compromise between straight and curved track performance. (Goodall and Li, 2000) produced an intuitive approach to the control of the solid axle and the independently rotating wheelset. The study concluded, with the use of an open loop transfer function, that the use of a yaw torque proportional to the lateral velocity was sufficient to maintain stability and curving without interference; and that steady state conditions on the curve were achieved. It was also found that through active means, the stability margin can be increased in terms of the minimum damping ratio required for the closed loop system.

1.2.3 Independently Rotating Wheels

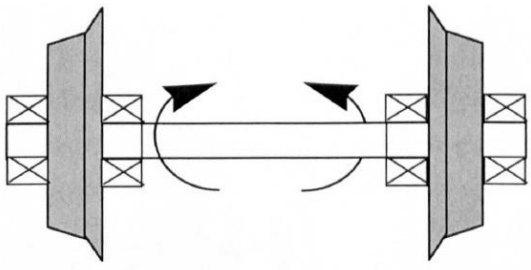

Figure 1.5 - Single independently rotating wheelset

Figure 1.5 illustrates a wheelset with independently rotating wheels, also commonly referred to as IRW. IRW is a concept which was of interest back in the 1980's, and allows the wheels to rotate freely on the axles. This, as a result, takes away any longitudinal creep forces that are usually

produced by the self-centring forces inherent of the solid axle wheelset. This extra rotational degree of freedom solves the difficult design trade-off which the conventional solid axle wheelset has between the stability on the straight track and curving performance on the curved track. The IRW significantly reduces the wear/noise at the wheel-rail interface and allows a more flexible design of railway vehicles, such as 100% low floor vehicle, which offers a larger carriage space for passengers, or the removal of the bogies altogether, which would further reduce the mass, the cost, and the design complexity of the vehicle. Furthermore, all concepts offer low floor design due to the elimination of the secondary suspension altogether and reduced wheel/rail wear, however, most require some form of actuation in order to guide the vehicle round corners.

As a result of this, IRW loses the self-guidance and track following feature that is inherent with solid-axle counterparts (R. Goodall, 1998). Work has been conducted to prevent the high lateral force exerted at the wheel and rail when the IRW manoeuvres around a curved track (Sugiyama et al., 2010), but there is still an issue with the guidance, due to the lack of longitudinal creep forces. And so providing active control has been considered as a likely solution to provide this feature.

1.3. Active Control of Wheelsets

Active control is the definition of using actuators, sensors and electronic controllers to enhance and/or replace the conventional passive suspension. It has been common for many decades for the railway industry in the power electronic control of traction systems and is now firmly established as a standard technology which has yielded substantial benefits (Iwnicki, 2006). Active suspension maintains low suspension deflections whilst maintaining ideal suspension characteristics regardless of loading and velocity. Therefore, active suspension offers a solution to provide both good stability and curving performances simultaneously. This can be provided in various methods; which will be discussed next.

1.3.1 Active Primary Suspension

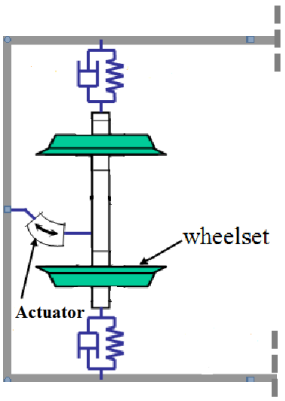

Figure 1.6 - Active primary suspension

The main objective of the active control of the primary suspension is to maintain stability whilst providing good curving. There are various configurations of the illustration in figure 1.6, which all aim to improve stability and curving, whilst maintaining good ride comfort such as Actuated Solid Wheelsets (ASW), Actuated Independently Rotating Wheelsets (AIRW), Driven Independently Rotating Wheelsets (DIRW) and Directly Steered Wheels (DSW) (Shen and Goodall, 1997; Mei and Goodall, 2000; Gretzschel and Bose, 2000). Most active control strategies proposed so far assume that some basic measurements are readily available. However, a direct measurement of those primary feedback variables, such as wheel-rail displacement, angle of attack and wheelset lateral velocity relative to the track, may prove to be difficult and expensive to achieve in practice. This is partly because of the arduous vibration and climatic environment, and also because the non-linear profiling of the wheel, and the continuously changing shape of the rail, causes difficulties for obvious measurement technologies such as optical, inductive, etc. The following literature review will underline the work in both active secondary and active primary suspension and what control laws have been established as reliable methods of providing the accurate signals to the actuators.

1.4. Aims & Objectives

The aim of this thesis is to develop a fully working active control system which may be implemented onto a mechatronic vehicle. It will provide a solution to the problem with mounting the sensors onto the axle in order to gain the full state feedback signals for optimal control of active yaw damping of the independently rotating wheels. Instead, sensors will be mounted to the vehicle body using practical and low cost sensors to overcome the arduous environment at the axle.

The objectives are as follows:

1. To develop a mathematic representation of a two axle mechatronic vehicle with IRW directly mounted to the vehicle body to use in the development of the intelligent sensing scheme.
2. To develop an intelligent sensing scheme in order to provide full state feedback for the active control of a two axle mechatronic railway vehicle with IRW.
3. To optimise the number of practical sensors used in order to provide the most cost effective option whilst providing an accurate feedback signal to the controller for active control.
4. To ensure the sensing scheme is a robust model under parameter variations.

1.5. Structure of Thesis

Chapters 2 to 5 are as follows:

Chapter 2 – This chapter will provide an insight into the work that has already been conducted on active control and its development in various methods or control to overcome certain issues which arise with each suspension design, control law and estimation technique.

Chapter 3 – This chapter will show the development of the mathematic model which will represent a single axle with IRW and a two axle mechatronic vehicle with IRW.

Chapter 4 – This chapter will be the development and optimisation of the intelligent sensing scheme as well as check for robustness.

Chapter 5 – This chapter will conclude the results from the previous chapters and will recommend further work which can be conducted.

Chapter 2 Literature Review

Through extensive literature surveys, it is clear that there are alternative methods which overcome the issue with using axle mounted sensors to provide active control to dynamic systems. The concept of body mounted sensors to return the primary feedback signals necessary for active control will be the main topic. This literature review aims to cover the development of research into active control of the railway suspension, the various concepts of active control of railway suspensions, control laws that are required for each and modern techniques that are being used to provide active control such as model-based estimation techniques.

The following literature review will convey the research that has been done using body mounted sensors and why it has been chosen as a good method of providing the controllers with the necessary feedback signals for the practical implementation of an active control scheme for a railway vehicle with independently rotating wheels. Moreover, the literature will display explain why the use of the optimal control approach with a Kalman-Bucy filter has been adopted by researchers to estimate all the states to provide accurate actuation from the actuator.

2.1. Active Control of Railway Suspensions

Active control of the suspension of a railway vehicle is well established for improving the suspension for both cornering and ride comfort (Goodall and Kortüm, 2002). Researchers have in the past questioned the need for the use of active control all together (Karnopp, 1978) and even recently, research is being investigated to try to improve the performance of the conventional solid axle with passive means of stabilisation (Jiang et al., 2013). But most have highlighted their certainty of implementation in the railway suspension design (Goodall, 1997), and how the overall progression active control of the suspension has made and how it has been introduced to operation with vehicles such as the Pendolino and TALGO trains. Most papers mentioned in (Goodall and Kortüm, 1983) discussed their future trends, as the theoretical studies suggested that active suspensions can be applied to not only the secondary suspensions, to improve ride comfort, but also to the primary suspension; whereby curving performance and stability at higher speeds can be achieved.

2.2. Active Control of Wheels or Wheelsets

Active control of the wheels or wheelsets has been studied in many variations, all of which aim to provide cost effective, robust and practically implementable methodologies. Various configurations and implementation of the active primary suspension (Shen and Goodall, 1997; Powell and

Wickens, 1996) and the control options have been proposed (Mei and Goodall, 1999; Goodall and Li, 2000; Goodall, 1998). The actuated solid wheelset has had various studies conducted all offering to provide steering without compromising the stability inherent with the solid axle. Researchers have analysed actuation being provided directly on the axle (Shen and Goodall, 1997; Pèrez et al., 2002; Pearson et al., 2004), and some have developed control strategies to provide the actuation (Mei and Goodall, 2000; Mei and Goodall, 2000; Pearson et al., 2004). Concepts have also been developed to provide actuation from the bogie to the wheelset (Pèrez et al., 2002; Tanifuji et al., 2003), again offering to provide good curving performances and stability.

Studies have shown that applying active control to the wheelset in the form of a yaw torque which is proportional to the lateral velocity of the wheelset would produce a form of damping which is stabilising and doesn't interfere with the curving performance (Goodall and Li, 2000; Li and Goodall, 1999). Active steering aims to follow the centreline of the track and keep the centreline of the wheel is radial with the curve, producing no lateral creep forces (Powell, 1998). The wheelset can however be subject to large lateral translations which would be extremely difficult to measure in order to return good controllability in practice. Therefore active guidance is key to avoiding flange contact (Powell, 1998). This will avoid any wear which could occur during the contact. This method however requires again a high bandwidth control (Goodall, 1997). The change in technological advances were surveyed (Bruni et al., 2007) to show how railway dynamics have been used in tandem with sensors, and computer processors, to create the various concepts and implementations of active control of the primary suspension of a railway vehicle.

Many active primary control strategies & controllers have been analysed (Powell, 1998; Gretzschel and Jaschinski, 2004; Michitsuji and Suda, 2006; Liang et al., 2004; Liang and Iwnicki, 2007) and have highlighted that their general performances are adequate and/or require primary feedback variables, which are impractical and costly to provide. They have also highlighted the need for track curvature and cant in order to provide active control of the vehicles, which is also difficult to provide and costly, this issue has also been concluded in many research papers such as (Mei and Goodall, 2001; Pearson et al., 2004). This is partly due to the arduous vibration and climatic environment, the profiling of the wheel and the shape of the rail which causes difficulties for obvious measurement technologies such as optical, inductive, etc. (Gretzschel and Bose, 2002).

2.3. Active control of Independently Rotating Wheels

The concept of the active control of the independently rotating wheelset was firstly studied by (Eickhoff and Harvey, 1989; Frederich, 1989; Eickhoff, 1991; Dukkipati and Narayanaswamy, 1999) and have been reviewed in a state of the art paper, which concentrates on the dynamics of the concept and highlights the key advantages of the design (Dukkipati et al., 1992). The main advantage of using the IRW with active control is the reduced control input needed by the actuator. (Goodall and Mei, 2001) introduced the actuated independently rotating wheelsets (AIRW) and compared actively controlling the conventional and the independently rotating wheelsets. They found that both offer improvements to the curving performance, however, the control torque required to actively steer the IRW was profoundly less (20Nm) than what is required to actively steer the conventional solid axle wheelset (400-500Nm). As a result, the power requirements required were low, which avoids packaging concerns. This aids the concept of creating an energy efficient, light weight and cost effective railway vehicle, which is no doubt a huge selling point to the rail industry.

Concept	Reference	Track	Torque/force Requirement	Actuator Speed	Power Requirement
Actuated Solid Wheelset	(Mei and Goodall, 2000)	Random	9.5-18 kNm (rms) 30-70 kNm (peak)	0.02 - 0.04 rad/s (rms)	-
Actuated Solid Wheelset	(Mei et al., 2002)	Curve	0.8 kNm (max)	-	-
Directly Steered Wheelset	(Mei et al., 2002)	Random	16 kNm (rms)	-	-
Directly Steered Wheelset	(Mei et al., 2002)	Curve	0.02 kN (max)	-	-
Secondary Yaw Control	(Diana et al., 2003)	Random	5 kN (max)	-	-
Secondary Yaw Control	(Diana et al., 2003)	Curve	8 kN (max)	-	-
Actuated Independently Rotating Wheelset	(Pearson, Goodall, Mei and Himmelstein, 2004)	Random	0.38 m/s (rms) 2.42 m/s (peak)	0.42 m/s (rms) 1.87 m/s (peak)	0.08kW (rms) 1.49kW (peak)
Actuated Independently Rotating Wheelset	(Mei et al., 2002)	Curve	0.04 kNm (max)	-	-
Driven Independently Rotating Wheels	(Cheli et al., 2002)	Curve	2 kN	-	-

Table 2-1 - Actuation requirements for active primary suspension configurations

Table 2.1 shows the maximum control torque, or force, required to steer, stabilise and/or guide the wheelset or vehicle. Concepts for solid axle and IRW have been chosen to compare results found from practical implementation of the control schemes. Between the various schemes, the AIRW cases had the lowest requirement on control effort. This is due to the longitudinal forces produced by the IRW are virtually zero. The loss of longitudinal creep force means that the actuated control of IRW, or AIRW was designed for guidance. (Mei et al. 2005; Mei and Goodall, 2001; Mei and Goodall 2003 and Perez et al. 2003) provided insight into the various control methods of actuating the wheelset. (Michitsuji and Suda, 2006) used a novel approach to the configuration of the IRW; using a power steered bogie design which uses gravity stiffness by non-linear tread gradient. The results showed that by the use of power steering, good curving performance was achieved. (Suda et al. 2012 and Mei et al, 2005) used a new concept of using semi-active control with the IRW, with an inverse tread to overcome the loss of steering inherent with the IRW, and provide the low floor design which is possible with the reduction in undercarriage design complexity. The article concludes that the use of an inverse tread profile will provide the resilient return to the neutral position on the track. Other concepts were developed thereafter including the driven independently rotating wheelset (DIRW) by (Gretzschel and Bose, 2000; Gretzschel and Bose, 2002; Liang and Iwnicki, 2007; Liang et al., 2004) using motors applied directly at each wheel to further improve the stability at higher speeds as well as maintain good curving performances. Directly steered wheels were also treated (Powell, 1998) whereby traction motors were coupled with a differential torque to provide individual forces at the wheels.

2.4. Control Strategies

Different control strategies have been developed to overcome individual control issues, whether it is stabilisation, steering or guidance. With the solid axle, the main issue is the inherent ‘hunting’ behaviour it exhibits when the vehicle reaches its critical speed. Therefore, the control mission is to stabilise the wheelset. Passive means of stabilising the wheelset have been shown to constrain the wheelset from a control engineer’s perspective (Goodall and Li, 2000) but they have also indicated that this will hinder the curving performance as a result. The provision of a yaw stiffness via active means has been implemented (Mei and Goodall, 2006) aiming to provide stability to the wheelset of a solid axle. Furthermore, (Mei and Goodall 2000) produced a control scheme for active stability, this time, by providing a force proportional to the wheelsets angular motion. The study was also able to provide the same kind of stability to the conventional solid axle. Other studies have attempted to not only provide stability, but also to improve the curving performance of the conventional solid axle. (Powell, 1998) compared active steering and active guidance control schemes of single axle bogies. Both active steering and active guidance controllers performed

adequately; however the latter provided a better solution as there was no flange contact which is one of the main reasons for wheel and rail wear. Active guidance has proven to be a useful control strategy for more than just the conventional solid axle. The independently rotating wheelset configuration requires some form of guidance due to the loss of the coupling between the wheels which results in poor track following performance. Therefore, active guidance is a necessity when considering the wheelset configuration. Active guidance has been applied in various methods as the wheels are now allowed to freely rotate from each other. Applying a differential torque between the wheels has been one method that has been implemented on a scaled down model of a railway vehicle (Gretzschel and Bose, 2000). Making both wheels rotate at the same speed has also proven effective. (Perez et al. 2004) proposed three strategies of providing guidance; all of which used traction motors to either equalise or maintain a differential torque at each wheel. (Gretzschel and Bose, 2002) used active guidance to keep the wheelset in tangent with the track centreline or by keeping the wheels in a radial position. This provides not only guidance, but also attempts to eliminate all unnecessary creep forces which arise when the wheelsets are negotiating a curve.

2.5. Model Based Control Strategies

(Mei and Goodall, 2000) designed a model controller for the active steering strategy applied to a solid axle. Independent controllers were designed for the yaw and lateral motions when decoupled. This aids the control of stability and curving; as they have no interconnection in the control loop. The study used genetic algorithms to fine tune the controllers in order to return maximum stability and robustness. The conclusion was that the modal controller provided a 25% better ride quality compared with the passive suspension. However, in order to control the stability, a large control torque is required, as it is trying to oppose the self-centring force generated by the coupling between the two wheels. The paper also concludes that the measurements needed to provide the control aren't possible to measure from sensors directly, but the use of practical sensors with state observers is a good method of providing a good estimate. (Mei et al. 2000) developed an optimal PI controller for the active steering of a solid-axle wheelset. The aim was to bring stabilisation and perfect curving to the solid axle wheelset which is a trade-off when passive suspension is used. With the use of the optimal control and an extended Kalman filter to estimate all of the states, active steering was achieved and lateral displacement was reduced, however, the relative yaw angle control aimed to provide the pure rolling characteristic was not achieved. Optimal control is applied to the solid axle and independently rotating wheelsets (Mei and Goodall, 1999). The study highlights the need for correct tuning of the optimal controller in order to return good performances, specific to the wheelset configuration. The study highlighted the reduced

requirement of control torque from the actuator for the IRW due to the uncoupling of the two wheels. Furthermore the use of a state estimator to return full state feedback will enable optimal control to be used. This method has been studied by (Mei and Goodall, 2000) whereby they provide a yaw torque, proportional to the lateral velocity, also known as active yaw damping, concluded by (Goodall and Li, 2000) to be a sufficient manner of stabilising the vehicle; using genetic algorithms. H-infinity controllers have also been designed by many (Zolotas et al., 2000; Akbari and Lohmann, 2010; Mei and Goodall, 2001) and offer sufficient stability margins, robust control designs and even a practical method of implementation, but can be very complex controllers which are practically difficult to implement (Goodall and Kortüm, 2002).

2.6. State Estimation Techniques

(Mei et al. 2000) developed an optimal PI controller for the active steering of a solid-axle wheelset. The aim was to bring stabilisation and perfect curving to the wheelset which is a trade-off when passive suspension is used. With the use of the optimal control and an extended Kalman filter to estimate all of the states, active steering was achieved and lateral displacement was reduced. However, the relative yaw angle control aimed to provide the pure rolling characteristic, was not achieved.

Academia and industry have looked at alternative methods of providing estimates of the signals via simple measurements such as accelerometers and gyroscopes. The H∞ control method offers a robust method of optimal control with parameter variations which are ever prevalent in dynamic systems, due to their environment (Zhou et al., 2014). The controller also provides estimation of the signals required. H∞ control has also seen its application to active control of railway and automotive vehicles (Mei and Goodall, 2001; Fallah et al., 2009). Researchers have argued that the H∞ method can become quite limited in design, however. As such, direct design and implementation of a state observer would be preferred. (Kalman, 1960) came up with a solution to the problems with prediction of random signals with random noise. Using Wiener's concept, the Wiener filter accomplishes the prediction, separation or detection of a random signal. The steady-state Kalman filter, which will return an optimal estimate of the steady state, uses a stationary gain matrix which is designed offline; this offers simplicity to an otherwise discrete and time varying filter. The Kalman filter can be extended for the state estimation of a non-linear system, which is called extended Kalman filter (EKF) (Bruni et al., 2007). (Li et al. 2002) used a recursive Kalman filter for a non-linear model. The linearized model is calculated at each iteration, based upon the current estimated state vector. This is referred to as an EKF. The results showed that the estimates of the wheel-rail lateral displacement and angle of attack are as good as the three

sensor Kalman-Bucy filter sensing scheme used in (Li and Goodall, 1999) who used it for continuous time analysis of the secondary suspension. The linear Kalman-Bucy filter has proven that it will provide good estimations of the key primary feedback variables required to actively control a wheelset (Pearson, Goodall, Mei, Shen, et al., 2004) and so too the IRW (Dukkipati and Narayanaswamy, 1999), and can perform well with estimating the low frequency deterministic track features such as curvature and cant.

Kalman filters have been subject to scrutiny due to their issues with making observers work effectively in the presence of substantial parameter changes (Mei and Goodall, 2001; Zhou et al., 2014). Moreover, there are profound non-linearities with the wheelset dynamics which has questioned the use of linear assessments to be conducted, as they do not represent the true dynamics of the system. There has, however, been studies such as (Michitsuji and Suda, 2006; Mei and Goodall, 2001) that have highlighted that, with the use of active steering or guidance, the wheels should not contact the non-linear flange region of the wheels, and therefore it can be said that the system can be assumed linear. However, these limitations are dampened by the advantages of using this type of estimator, which are that it can produce full state feedback. This can be incorporated into future applications of active control, should the designer wish to add another controller to the system, to further improve the curving performance, ride quality, or even monitor conditions such as wheel conicity, and creep coefficients. (Mei and Li, 2008a) gives a useful design approach to the active control and how taking each controller and tuning them individually will see an improved performance in damping when compared to genetic algorithms, which use a generic control structure. Furthermore, (Mei et al. 1999) demonstrates that the Kalman filter gives very good estimations of all the variables; including the track features when the filter is re-formulated.

2.7. Sensing Options for Active Primary Suspension

The sensing options have become ever more of an issue with the active control of the primary suspension. Researchers in the field have theorised and developed various methods of returning the primary feedback variables that are necessary in actuating the wheelsets and/or bogies. (Goodall and Mei, 2001) studied an intuitive method of controlling the IRW, using vehicle speed instead of wheel-rail displacement and angle of attack. Speed sensors were used to measure the relative rotational speed, in line with sensors measuring wheelset yaw velocity relative to the vehicle body. The overall result was a developed adaptive control scheme for active steering (making the wheels have zero difference in rotational speed). (Mei and Goodall, 2006) also provided an insight into the simplicity of the intuitive method of returning the absolute yaw angle of the wheelset by the use of a seismic accelerometer, which outputs the yaw acceleration of the

measured wheelset with, essentially, a second order high pass filter, as it provides a signal at frequencies below the natural frequency of the sensor. New methods of returning the absolute travelling speed have been studied by (Mei and Li, 2008; Matsumoto et al., 2012) and have found to provide useful methods in providing accurate measurements. More excitingly, image processing options have become prevalent for returning relative changes such as displacement and yaw angle. This method has been conducted by (Kim, 2011) who has found the method to be robust even with changes in climactic conditions. Most of the research that has been mentioned includes measurements being taken from the wheelset; but there are many issues with mounting the sensors to the wheelset, such as the severe climatic environment and vibrations. Therefore researchers have conducted methods of providing the feedback necessary in the control of the primary suspension, using model based sensing schemes with practical sensors mounted to the bogie and body.

2.8. Bogie and Body Mounted Sensors and Sensing Schemes

Signs of mounting practical sensors in locations, other than the axle of the railway vehicle were visible at an early stage (Zolotas and Goodall, 2000). (Diana et al. 2003) implemented active yaw damping between the car body and the bogie to stabilise the vehicle. The study demonstrated that the control strategy, which was to provide a force defined as proportional to the absolute yaw velocity of the bogie, enabled the vehicle to be stabilised above its original critical speed. (Pèrez et al. 2002) investigated the behaviour of conventional railway vehicles with bogie-based sensors providing the signals for state feedback to be used by the optimal controller to provide accurate signals for the actuator. Seven accelerometers and seven gyros were used; relative angle and displacement sensors were used in place of gyros and accelerometers which would usually be mounted to the axle, and performed well. This paper does not vary its parameters, therefore the sensing scheme will need to be checked to be considered a robust scheme. (Tanifuji et al. 2003) measured the relative yaw displacement between the bogie frame and the wheelset in the place of a yaw creep moment. This can represent as the self-steering moment which is reflected as the relative yaw displacement. The study offered good steering performance in curves of radiuses of 200m or more. (Mei and Li, 2008b) achieved effective measurements of the rail vehicle speed over a wide range of operation speeds. Importantly, they were able to provide a robust scheme against uncertainties such as parameter variations; even at low speeds where the level of vibrations at the bogie frame is minimal. (Mei and Li, 2008) presented the novel approach to use bogie mounted inertial sensors to measure the vertical excitations, pick features from the motion and measure the time delay between the two wheelsets; to ultimately provide the vehicle ground speed. The

measured signals were processed by two filters to produce estimated wheelset movements, and as there is no need for precise measurement of the track inputs. The filters used are simpler and more practically implementable when compared to a full state estimator. The approach suggests that the use of more sophisticated model-based techniques may not be necessary in the estimation of track irregularities as the filters offer an effective solution. It also shows that it is insensitive to sensor noise and is robust against uncertainties or changes in the bogie parameters. The filters were limited in terms of the signals they filtered out and so adopting a dual band filter that returns both high and low frequency signals, could further improve the performance of the system. As bogie mounted sensors had proven their accuracy, using relative sensors research was then conducted mounting practical sensors to the vehicle body. (Li et al. 2007) used body mounted sensors in line with a newly developed particle filter to estimate the parameters variations and uncertainties of the railway vehicle whilst running along the track features. Using real test data, the results consistently show that sensible estimations of the parameters were produced without the use of axle mounted sensors and, interestingly, without the need for prior knowledge on the particular initial values for the parameters to be estimated. (Zhaijun et al. 2011) used four dynamic offset sensors mounted onto the car-body; each sensor is composed of a linear Charge Couple Device, a lens and four mirrors. This method returns two images of the same track calculates formulas for the rotational and translational matrices. The offsets of the random location fixed on the car body can be obtained, but work in this area is still needed. (Ward et al. 2011) have brought together research done on vehicle-based sensor schemes to detect track defects, running gear condition monitoring and absolute train speed. The article looks at the current sensing options, which are paired with advanced processing concepts; to see whether the three main processing options are viable for practical implementation. In general, the results were positive as most bogie based sensing options in line with estimation techniques provided good estimates of the state variables. The results have also shown good comparative results when there was a parameter variation. The study does, however, highlight that, due to the provision of the sensors reducing in accuracy because of their mounting positions, high-quality accelerometers with a small operating range would be a practical solution. Furthermore, it is highlighted that mounting the sensors onto a position other than the wheelset will result in uncontrollably large errors at increasing wavelengths. It does, however, suggest that with the use of a high pass filter to accurately reconstruct the wavelengths of the input, the results will remain accurate.

2.9. Model-based Condition Monitoring and Fault Detection

Active control of the running gear of a railway vehicle is a high integrity safety critical aspect of the vehicle. Therefore, design robustness has to be prevalent for it to be considered a valid method of

controlling the vehicles dynamics. State of the art papers such as (Bruni et al., 2007) have highlighted that there are various methods of detecting faults with the strategy. Traditional fault detection is achieved through the use of hardware redundancy voting. This method, however, requires added components which come at a cost. More modern methods of fault detection include estimation and detection of the sensor faults using a Kalman filter. (Li, 2001) has used this method extensively throughout her thesis and gives good insight into how the Kalman filter can be used to estimate sensor faults to maintain sensing scheme robustness. Model-based condition monitoring uses knowledge of the system in the form of a mathematical model and vehicles measurements to perform real-time estimations of the system parameters (Charles et al., 2008). 'The best results were obtained when the Kalman filter included self-updating information about the conicity function'. (Mei and Goodall, 1999) analysed the results of a model based optimal control strategy applied to a solid axle and an IRW. Creepage coefficients and conicity were varied to represent real changes which would occur due to wear between the wheels and climactic conditions. By carefully selecting the weighting factors in the cost function, stability is found from polar extreme values. (Ward et al. 2011) uses body mounted sensors for the motorisation of the condition of the infrastructure and the rolling stock itself. The study uses high capacity communication buses and multiple sensors to collect data for such things as track defects, running gear conditions and absolute train speed. The paper highlights that the findings indicate that wheel slip/slide and absolute speed do not have to be measured with expensive equipment and can be achieved with the innovative method of using basic inertial sensors instead. This method also overcomes any issue that GPS' have when vehicles travel underground.

2.10. Summary

This literature review has brought together the work that has been done in developing the active control of railway suspensions. It has provided insight into the various wheelset and active suspension configurations. It has also provided evidence to suggest that the active control of IRW offers a more practical wheelset configuration, as it requires less control torque compared to the conventional solid axle wheelset. The review has also shown the development of various control laws to apply active control the wheelset and has given insight into the advantages and disadvantages of each. Model based state estimation techniques have been discussed, reviewing the limitations and innovations in providing the necessary feedback signals required for active control.

Chapter 3 Modelling Development

3.1. Overview

This chapter will present the development of a mathematical model of an independently rotating wheelset. It will highlight the key dynamic issues that are related with it and summarise what active control law is required in order to improve the performance. The development of the model will then be addressed to reach a final representation of the two axle mechatronic vehicle.

Firstly, it is important to understand what track inputs we are considering, prior to the development of the vehicle model, as the track input will dictate the dynamics of the equations of motion.

3.2. Track Features

The railway track is comprised of two distinct types, the straight track, and the curved track. Each track has an effect to the railway vehicle. The input forces they exhibit on the vehicle are what engineers aim to understand so that they may control the vehicle to improve the overall performance. This project is focused on applying active control to the vehicle primary suspension in order to steer the vehicle whilst maintaining suitable ride performance; and so we are to consider the lateral track inputs that are exerted when the vehicle is running on the straight track, and curves in the lateral direction.

3.2.1 Straight Track

The straight track has an input due to the inaccuracies in the laying of the track, the manufacturing of the straight steel rail and due to the fixtures themselves. Many studies (Goodall and Mei, 2001; Li, 2001) have approximated the straight track level as a random disturbance model with a power spectral density, also referred to as P.S.D. of the lateral track input y_t. The general form of spatial spectral frequency of the track alignment $y_t(x)$is given in (3.1), where $f_s[cycle/m]$ is the spatial frequency, A_r $[m^2(cycle\, m^{-1})^2]$ is the track roughness factor, which is used throughout the thesis to represent the track irregularities of a modern high-speed railway line, and x is the distance of the track.

$$S_{yt}(f_s, x) = \frac{A_r}{{f_s}^3} \qquad [m^2/cycle\ m^{-1}] \qquad (3.1)$$

A detailed explanation of the how the spatial frequency of track irregularities is converted from the frequency domain to the temporal domain is detailed in (Li, 2001). To summarise, the temporal frequency based input velocity spectrum ($s_{yt}{}'$) is:

$$s_{yt}{}'(f_t, t) = \frac{(2\pi)^2 A_r v^2}{f_t} \qquad [(m/s)^2/H_z] \qquad (3.2)$$

Where f_t is the temporal frequency, t is the time period, v is the forward velocity. The input velocity of the lateral random track input may be treated as "white noise" with a Gaussian distribution for simplicity and ease as it is difficult to obtain real track data in practice. Measured real track data is much less severe. A maximum wheel-rail deflection of less than 2mm was obtained at typical high speeds in (Mei and Goodall, 2001).

3.2.2 Curved Track

The curved track has a low-frequency, long wavelength characteristic. It is comprised of the initial straight track, then a transition from the straight track to the curve, and the curve itself. Figure 3.1 shows the track feature and highlights the main characteristics of the curved track. The civil engineer will lay the curved track in terms of what the requirements are for passenger comfort at a set speed. This is then converted into a suitable radius curvature to meet the operating requirements.

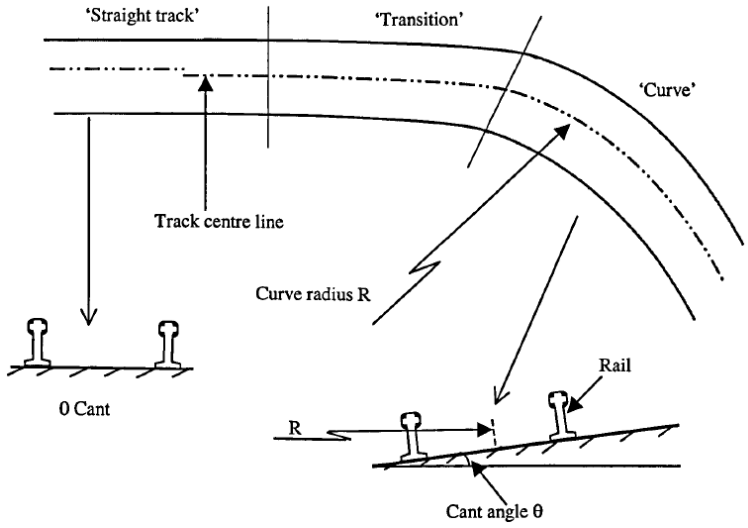

Figure 3.1 – Lateral curved track feature (Li, 2001)

The track is also canted slightly to tilt the vehicle inwards whilst it is on the curved track. This eliminates the lateral acceleration felt by the passenger and aids railway vehicles in travelling at higher speeds on curved track features; although the amount of cant is limited and so, realistically, the vehicle will have some level of cant deficiency present.

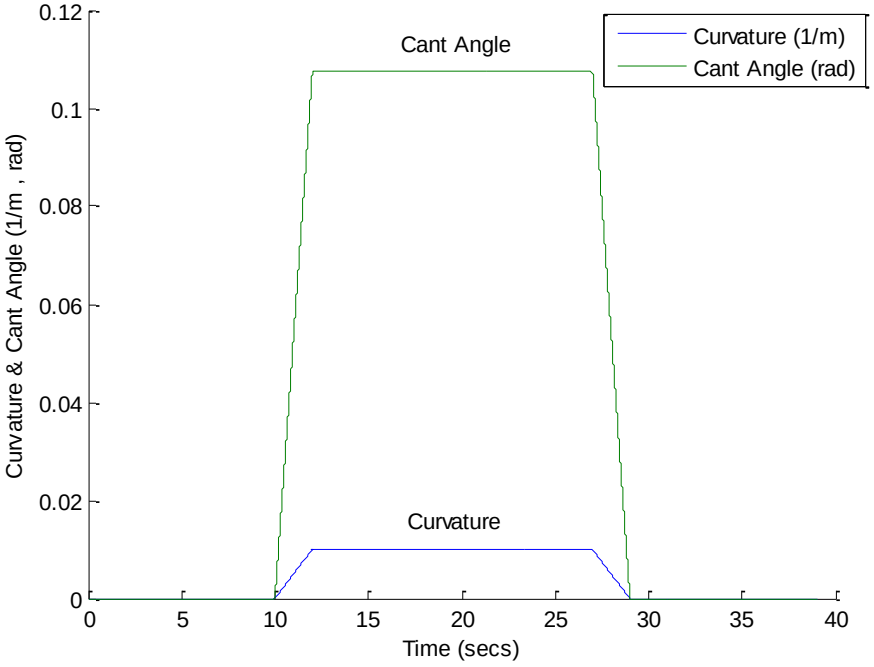

Figure 3.2 - Curved and canted track definition

Figure 3.2 plots the curvature (1/R) and cant angle (θ) in the time history. The Figure illustrates the 10 second running on the straight track, before a 2 second transient period between the straight track and the curved track, then a 15 second time period on the steady state curvature, before another transient and back onto the straight track. The same time is allocated for the cant angle as this would replicate the real track characteristic.

3.3. Independently Rotating Wheelset

The conventional solid axle has, historically, been one of the most fundamental parts of a railway vehicle and, with the use of suspension constraints, has proven to be a reliable and safe configuration. However, due to the requirements of the modern day lifestyle, we require faster, safer, more spacious and more comfortable commutes. Engineers have looked to the railway vehicle with an aim to improve its dynamics, in order to provide the demands of the modern day lifestyle. The late 20th century saw the advances in mathematical modelling and the general understanding of the dynamics of the railway vehicle, and has allowed us to understand the fundamental issues with the conventional solid axle.

The independently rotating wheelset is different from the conventional solid axle in that the wheels are allowed to rotate freely from one another. This extra degree of freedom between the wheels contributes to the longitudinal creepages; which are the main cause of the relative rotation between the wheels.

The following section is to briefly develop a mathematical model of the single independently rotating wheelset, and to highlight the kinematic oscillations present, when unconstrained. Suspension configurations will then be added to show how the issue of the loss of steering has been resolved.

The wheelset is to be modelled with three degrees of freedom: the lateral displacement y, the angle of attack Ψ and the angular rotation of the wheel's, $\emptyset$. A moving axis will be used so that the moving reference axis travels with the wheelset. Roll and spin creep motions associated with the wheelset are neglected; the reason for this is justified by (Mei et al., 1999; Mei and Goodall, 2001; Mei and Li, 2008a) as the roll and spin are all very small and due to the nature of the project. We are aiming to avoid flange contact where the non-linearities occur. Thus a linear approach to the dynamics is adopted throughout this thesis.

3.3.1 Modelling of a single axle with IRW

The following section derives the equations of motion, this has been detailed in (Li, 2001). Figure 3.3 shows how each wheel generates its angular velocity from the longitudinal forces produced at each wheel. (Andrew: repetition of 'each wheel')

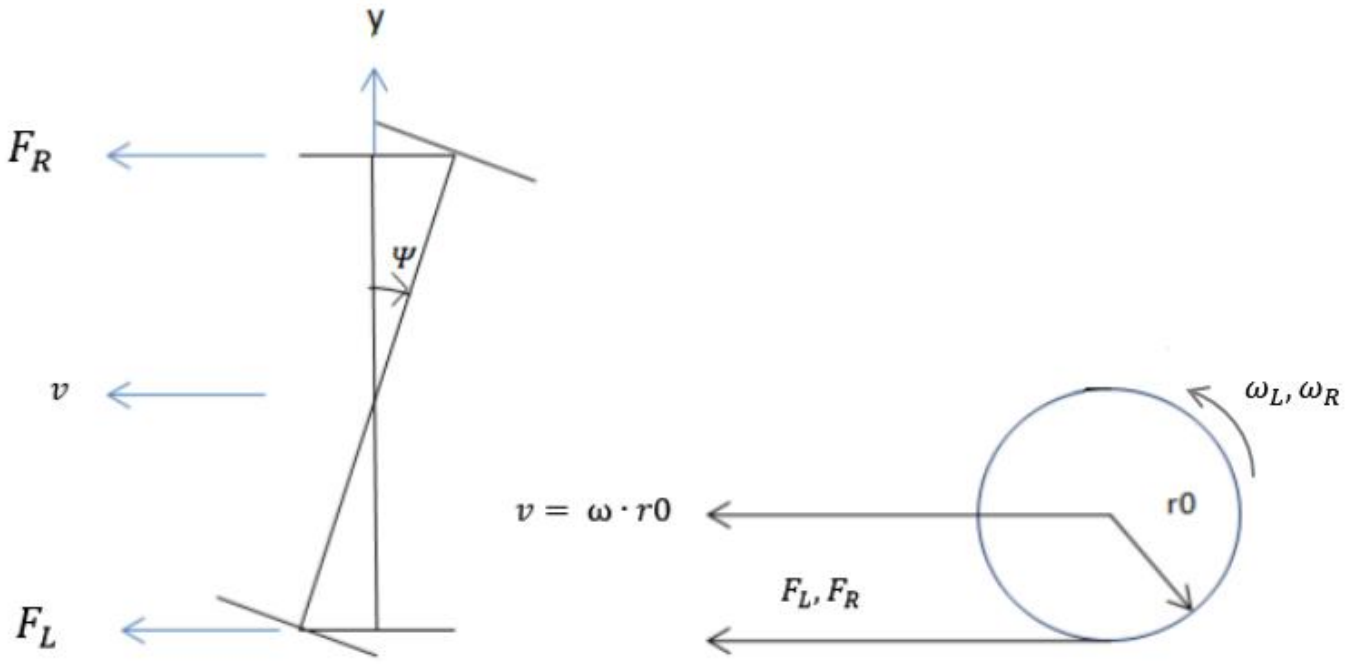

Figure 3.3 - Angular velocities of the left and right wheel

Extra states ($\dot{\emptyset_R}, \dot{\emptyset}_L$) are introduced to represent the individual rotational velocities of the left and right wheels and can be given by:

$$\omega_R = {}^{v}/_{r_0} + \dot{\emptyset}_R \qquad \omega_L = {}^{v}/_{r_0} + \dot{\emptyset}_L \tag{3.3}$$

The longitudinal creepages, γ_{1L}, γ_{1R} for the left and right wheel now incorporate the left and right angular velocities, this is detailed in (Li, 2001):

Left IRW wheel:

$$\gamma_{1L} = \frac{l}{v}\dot{\Psi} + \frac{\lambda}{r_0}y - \frac{r_0}{v}\dot{\emptyset_L} - \frac{l}{R} \tag{3.4}$$

$$\gamma_{2L} = \frac{\dot{y}}{v} - \Psi \tag{3.5}$$

Right IRW Wheel:

$$\gamma_{1R} = -\frac{l}{v}\dot{\Psi} - \frac{\lambda}{r_0}y - \frac{r_0}{v}\dot{\emptyset_R} + \frac{l}{R} \tag{3.6}$$

$$\gamma_{2R} = \frac{\dot{y}}{v} - \Psi \tag{3.7}$$

The rate of change of the rotational angular velocity between the two wheels is what creates the extra state in the yaw acceleration equation (3.15). This contributes to the longitudinal creepage and is shown in equation (3.4) and (3.6).

At small values of creepage, the relationship between force and creep can be considered linear and hence creep coefficients can be used in calculations. Therefore, the creep forces are:

$$F_{1L} = -f_{11}\gamma_{1L} \tag{3.8}$$

$$F_{1R} = f_{11}\gamma_{1R} \tag{3.9}$$

The difference of variation in rotational angular velocity, between the left and right wheel, is defined as:

$$\dot{\phi} = (\frac{\dot{\phi_R} - \dot{\phi_L}}{2}) \quad (3.10)$$

By substituting the creepage equations (3.8) and (3.9) with equation (3.10), the wheelset differential rotational angular motion is:

$$I_\phi \ddot{\phi} = \frac{r_0}{2}(F_{1L} - F_{1R}) = -\frac{f_{11} r_0}{2}(\gamma_{1L} - \gamma_{1R}) \quad (3.11)$$

The longitudinal and lateral creep forces can also be derived as follows:

$$F_x = -f_{11}\gamma_{1L} + f_{11}\gamma_{1R} \quad (3.12)$$

$$F_y = f_{22}(\gamma_{2L} + \gamma_{2R}) \quad (3.13)$$

The lateral, yaw and rotation equations of motion can then be derived from the creep forces and the centrifugal forces, and are as follows:

$$\ddot{y} = -\frac{2f_{22}}{mv}\dot{y} + \frac{2f_{22}}{m}\Psi + \frac{v^2}{R} - g\theta \quad (3.14)$$

$$\ddot{\Psi} = -\frac{2f_{11}l\lambda}{Ir_0}(y - y_t) - \frac{2f_{11}l^2}{Iv}\dot{\Psi} - \frac{2f_{11}l\dot{r_0}}{Iv}\dot{\phi} + \frac{2f_{11}l^2}{IR} \quad (3.15)$$

$$\ddot{\phi} = -\frac{f_{11}\lambda}{I_\phi}(y - y_t) - \frac{f_{11}lr_0}{I_\phi v}\dot{\Psi} - \frac{f_{11}{r_0}^2}{I_\phi v}\dot{\phi} + \frac{f_{11}lr_0}{I_\phi R} \quad (3.16)$$

When external forces and/or torques are applied to the wheelset, the equations of motion then become:

$$\ddot{y} = -\frac{2f_{22}}{mv}\dot{y} + \frac{2f_{22}}{m}\Psi + \frac{v^2}{R} - g\theta + \frac{F_y}{m} \quad (3.17)$$

$$\ddot{\Psi} = -\frac{2f_{11}l\lambda}{Ir_0}(y - y_t) - \frac{2f_{11}l^2}{Iv}\dot{\Psi} - \frac{2f_{11}lr_0}{Iv}\dot{\phi} + \frac{2f_{11}l^2}{IR} + \frac{T_\Psi}{I} \quad (3.18)$$

$$\ddot{\phi} = -\frac{f_{11}\lambda}{I_\phi}(y - y_t) - \frac{f_{11}lr_0}{I_\phi v}\dot{\Psi} - \frac{f_{11}{r_0}^2}{I_\phi v}\dot{\phi} + \frac{f_{11}lr_0}{I_\phi R} \quad (3.19)$$

The longitudinal creep induced by the wheel conicity can be written in terms of the relative lateral displacement. Analysing the relative lateral displacement between the wheel and rail will indicate how the wheelset is performing in terms of stability and curving performance.

F_y and T_Ψ are the lateral force and yaw torque that are applied to the dynamic system in order to stabilise the kinematic oscillation that arises when running along the track. (Goodall and Li, 2000) concluded that applying only a torque in the form of a yaw damper (C_t) to the wheelset will provide a control (steering) action which will not come into conflict with the provision of steady-state curving. This is not the case when the conventional solid axle is considered. Therefore the lateral force here is equal to zero.

It is clear that the variables of the wheelset model are very interactive, and produce a multi input, multi output (MIMO) system. Therefore, it is necessary to derive a state-space representation from equations 3.17 to 3.19:

$$\dot{X} = AX + Gw \tag{3.20}$$

$$Y = CX + Dw \tag{3.21}$$

Therefore the constrained wheeslet model is represented as:

$$\begin{matrix} \dot{X} & & A & & X & G & w \end{matrix}$$

$$\frac{d}{dt}\begin{bmatrix} \dot{y} \\ y - y_t \\ \dot{\Psi} \\ \Psi \\ \dot{\emptyset} \end{bmatrix} = \begin{bmatrix} -\frac{2f_{22}}{mv} & 0 & 0 & \frac{2f_{22}}{m} & 0 \\ 1 & 0 & 0 & 0 & 0 \\ 0 & -\frac{2f_{11}l\lambda}{Ir_0} & -(\frac{2f_{11}l^2}{Iv} + \frac{C_t}{I}) & 0 & -\frac{2f_{11}lr_0}{Iv} \\ 0 & 0 & 1 & 0 & 0 \\ 0 & -\frac{f_{11}\lambda}{I_\emptyset} & -\frac{f_{11}lr_0}{I_\emptyset v} & 0 & -\frac{f_{11}{r_0}^2}{I_\emptyset v} \end{bmatrix} \begin{bmatrix} \dot{y} \\ y - y_t \\ \dot{\Psi} \\ \Psi \\ \dot{\emptyset} \end{bmatrix} + \begin{bmatrix} v^2 & -g & 0 \\ 0 & 0 & -1 \\ \frac{2f_{11}l^2}{I} & 0 & 0 \\ 0 & 0 & 0 \\ \frac{f_{11}lr_0}{I_\emptyset} & 0 & 0 \end{bmatrix} \begin{bmatrix} \frac{1}{R} \\ \theta \\ \dot{y_t} \end{bmatrix}$$

3.22 - State Space Representation and Input Matrix

Where:

$$X = [\dot{y} \quad y - y_t \quad \dot{\Psi} \quad \Psi \quad \dot{\emptyset}]^T \qquad\qquad w = \left[\frac{1}{R} \quad \theta \quad \dot{y_t}\right]^T$$

The output equation given in equation 3.23 is configured to represent the measurements. In this case the outputs are the wheelset lateral acceleration, yaw velocity, and the difference in rotational velocity between the left and the right wheel; these are all chosen as they are cheap and easy to measure with accelerometers, yaw and roll gyros.

$$Y = \begin{bmatrix} \ddot{y} \\ \dot{\psi} \\ \dot{\phi} \end{bmatrix} = \underbrace{\begin{bmatrix} -\frac{2f_{22}}{mv} & 0 & 0 & \frac{2f_{22}}{m} & 0 \\ 0 & 0 & 1 & 0 & 0 \\ 0 & 0 & 0 & 0 & 1 \end{bmatrix}}_{C} \underbrace{\begin{bmatrix} \dot{y} \\ y - y_t \\ \dot{\psi} \\ \Psi \\ \dot{\phi} \end{bmatrix}}_{X} + \underbrace{\begin{bmatrix} v^2 & -g & 0 \\ 0 & 0 & 0 \\ 0 & 0 & 0 \end{bmatrix}}_{D} \underbrace{\begin{bmatrix} \frac{1}{R} \\ \theta \\ \dot{y}_t \end{bmatrix}}_{w}$$

3.23 – 3 Sensor Output Equation

Where the input signals are curvature $(1/R)$ and cant (θ) for the deterministic track and the random lateral track velocity is $(\dot{y}_t)$.

Table 3.1 provides typical values of the parameters given to the system.

Symbol	Quantity	Value
m	Wheelset mass	1250kg
θ	Track cant	6°
v	Forward velocity	13.3 m/s
λ	conicity	0.15
l	Half gauge	0.75 m
f_{11}	Longitudinal creep coefficient	10 MN
f_{22}	Lateral creep coefficient	10 MN
I	Wheelset yaw inertia	700 kgm^2
$I_\emptyset$	Wheel rotational Inertia	100 kgm^2
r_0	Nominal wheel radius	0.5 m
R	Curve radius	100 m
A_r	Track roughness factor	0.33e-8

Table 3.1 - Parameters for a single IRW

Figure 3.4 provides a graphical illustration of the unconstrained IRW (without a yaw damper present) compared to the IRW with yaw damping. MATLAB™ contains a function (lsim) which simulates the time response of a dynamic system with defined inputs. They are, in this application, the straight and curved track.

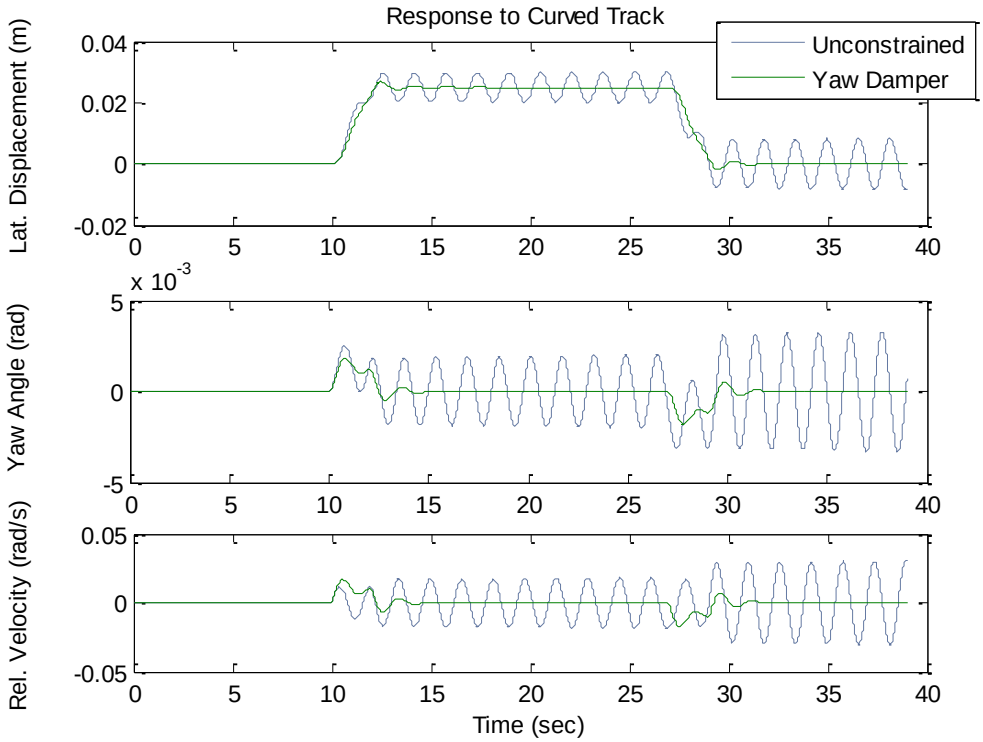

Figure 3.4 - Response to curved track input

The figures show the relative lateral displacement between the wheel and rail, angle of attack and relative speed of the wheel rotation. The response shows that with the use of a simple yaw damper ($C_t = 2.8\,\mathrm{kNms/rad}$) the steering needed to maintain a good curving performance is achieved. The yaw damping produces a zero steady state curving characteristic which is a natural curving performance. This indicates that the IRW has a self-restoring capability, which has been studied in detail by (Chi et al., 2009). It also means that the wheels will not contact the non-linear region of the wheel profile, commonly referred to as the flange, which causes a large amount of wear between the two surfaces. Reducing the amount of wear reduces the cost for re-skimming the rails and extends the lifetime of a wheelset; which ultimately makes a more cost effective design.

Figure 3.4 highlights that some form of steering control is required in order to steer each wheel in the positive direction around the curved track as the unconstrained wheelset, not only fails to follow the track, but also shows kinematic instability.

3.4. Modelling of Two Axle Mechatronic Vehicle with IRW

This section of the thesis will show the development of a two axle independently rotating wheelset model. A plan view of a two-axle mechatronic vehicle, which consists of a vehicle body and two independently rotating wheelsets, is considered; as shown in figure 3.5. Bogies are removed as they are no longer needed to isolate any unwanted vibrations which would usually be felt by the

passengers when solid axle wheelsets are fitted. They are attached to the vehicle body by lateral stiffness (K_y) and damper (C_y) in parallel; the values of which have been chosen to give a satisfactory ride quality on the vehicle body, purely through passive means. The torque input shown in the figure can be from passive components to stabilise the system or from actuators in the form of active control.

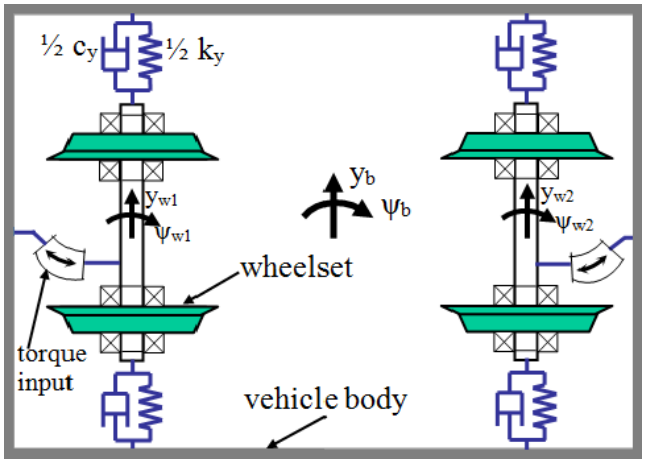

Figure 3.5 - Plan view of a two-axle IRW vehicle

3.4.1 Free Body Diagram of Two Axle Mechatronic Vehicle with IRW

Firstly, we must understand how the dynamics of the vehicle interact; and to indicate the axis system to apply positive directions in order to provide an accurate and consistent dynamic representation for the vehicle. This will then allow us to apply Newton's 2nd Law and to ultimately write the Equation of motion for each state.

Figure 3.6 shows a plan view of the two-axle IRW vehicle on the curved track. This consists of a vehicle body and two wheelsets.

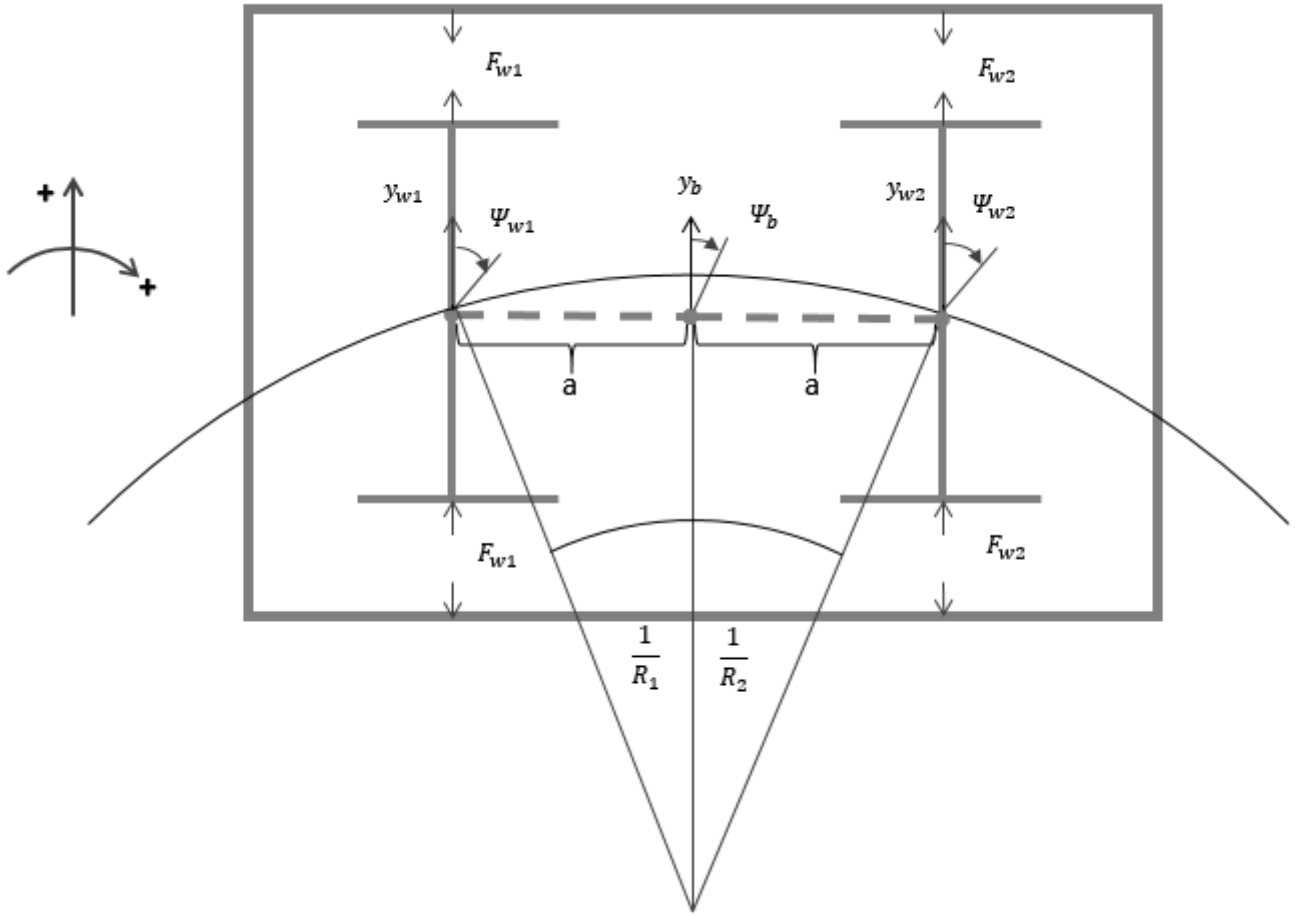

Figure 3.6 - Free body diagram of a two-axle vehicle

The vehicle doesn't have any bogies as the proposed scheme does not require a secondary mass in between the vehicle body and wheelsets in order to isolate vibrations which cause the passenger discomfort. This free body diagram will show the interaction between the wheelsets and body in order for us to produce the equations of motion we require for mathematical modelling. The passive primary suspension is designed to provide satisfactory ride comfort and to stabilise the vehicle. No longitudinal springs or dampers are shown in Figure **3**.6; although in practice, there would be some form of passive suspension present to transmit the traction and braking forces from the wheels to the vehicle body.

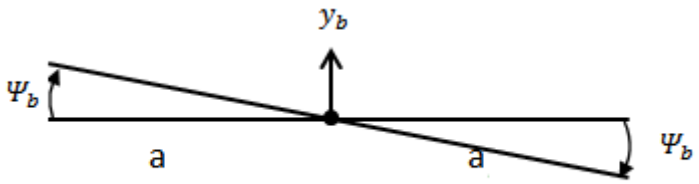

Figure 3.7 - Extra yaw angle free body diagram

Figure 3.7 details the additional lateral displacement due to the body's yaw motion. Where y_b defines the body's lateral movement, a is the distance from the centre of the body to the wheelsets axle; and Ψ_b is the body's yaw movement.

The leading and trailing wheelset forces, $F_{w1}$and F_{w2} can be equated as follows:-

Leading Wheelset:

$$F_{w1} = C_y\left(\left(\dot{y}_b + a.\dot{\Psi}_b\right) - \dot{y}_{w1}\right) + K_y\left(\left(y_b + a.\Psi_b\right) - y_{w1}\right) \quad (3.24)$$

Trailing Wheelset:

$$F_{w2} = C_y\left(\left(\dot{y}_b - a.\dot{\Psi}_b\right) - \dot{y}_{w2}\right) + K_y\left(\left(y_b - a.\Psi_b\right) - y_{w2}\right) \quad (3.25)$$

Likewise the torque that is produced due to the body's yawing can be moved to the local axis of the front and rear axles.

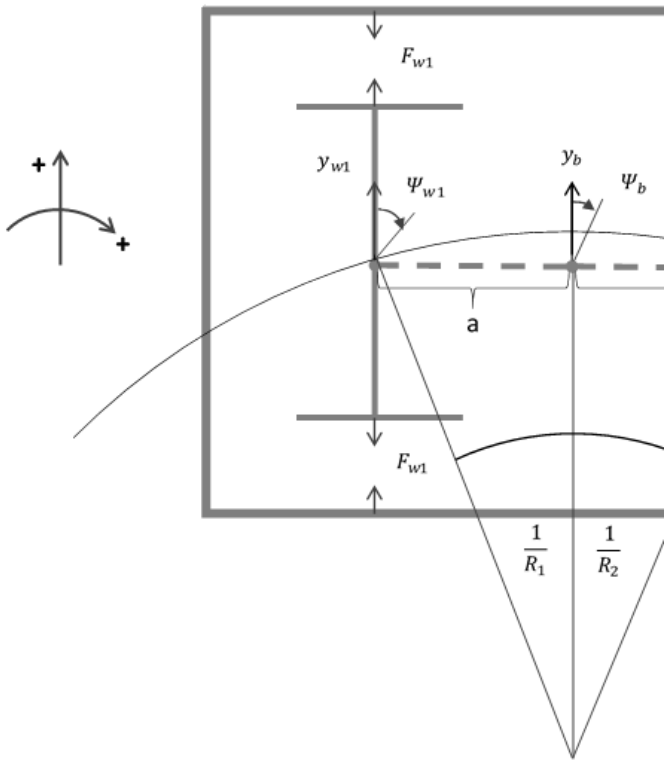

Figure 3.8 - Extra yaw angle due to interaction

Figure 3.8 shows the original free body diagram of the front axle. Localising the body's yaw to the front and rear wheelsets' local axis, the equations for the Ψ_{b1} and Ψ_{b2} are:

$$\Psi_{b1} = \Psi_b + (\frac{a}{R_1}) \tag{3.26}$$

$$\Psi_{b2} = \Psi_b - (\frac{a}{R_2}) \tag{3.27}$$

The control torque at each wheel can now be generated using a local axis system:

$$T_{w1} = C_t((\Psi_b + (\frac{\dot{a}}{R_1}) - \dot{\Psi}_{w1})) \tag{3.28}$$

$$T_{w2} = C_t((\Psi_b - (\frac{\dot{a}}{R_2}) - \dot{\Psi}_{w2})) \tag{3.29}$$

Ideally the control torque generated would be equal to the wheelsets' yaw velocity:

$$T_{w1} = -C_t(\dot{\Psi}_{w1}) \tag{3.30}$$

$$T_{w2} = -C_t(\dot{\Psi}_{w2}) \tag{3.31}$$

This has been proven to provide a direct control to positively steer the wheelsets (Goodall and Li, 2000).

3.4.2 Modelling the Body's Equations of Motion

The equations of motion for the body's lateral and yaw degrees of freedom can be written as follows:

$$m_b\ddot{y}_b = -F_{stability} - F_{centrifugal} \tag{3.32}$$

$$I_b\ddot{\Psi}_b = -a.F_{stability} - T_{stability} \tag{3.33}$$

We can now expand equations (3.32) and (3.33) to represent the forces and torques:

$$m_b\ddot{y}_b = -(F_1 + F_2) - m_b v^2(\frac{1}{2R_1} + \frac{1}{2R_2}) - m_b g(\frac{\theta_1}{2} + \frac{\theta_2}{2}) \tag{3.34}$$

$$I_b\ddot{\Psi}_b = -a.(F_1 - F_2) - T_{w1} - T_{w2} \tag{3.35}$$

3.4.3 Mathematical Modelling of a Two Axle Vehicle with IRW

The equations of motion for this plan view model of the vehicle running along both curved and random tracks are given in equations (3.36 ~ (3.43); where all variables are related to the local track reference.

$$m_w\ddot{y}_{w1} + \left(\frac{2f_{22}}{v} + c_y\right)\dot{y}_{w1} + k_y y_{w1} - 2f_{22}\Psi_{w1} - c_y\dot{y}_b - k_y y_b - c_y a\dot{\Psi}_b - k_y a\Psi_b = m_w\left(\frac{v^2}{R_1} - g\theta_1\right) \quad (3.36)$$

$$I_w\ddot{\Psi}_{w1} + \frac{2f_{11}l^2}{v}\dot{\Psi}_{w1} + \frac{2f_{11}lr_0}{v}\dot{\emptyset}_{w1} + \frac{2f_{11}l\lambda}{r_0}y_{w1} = \frac{2f_{11}l^2}{R_1} + \frac{2f_{11}l\lambda}{r_0}y_{t1} + T_{w1} \quad (3.37)$$

$$I_\emptyset\ddot{\emptyset}_{w1} + \frac{f_{11}{r_0}^2}{v}\dot{\emptyset}_{w1} + \frac{f_{11}lr_0}{v}\dot{\Psi}_{w1} + f_{11}\lambda y_{w1} = \frac{f_{11}lr_0}{R_1} + f_{11}\lambda y_{t1} \quad (3.38)$$

$$m_w\ddot{y}_{w2} + \left(\frac{2f_{22}}{v} + c_y\right)\dot{y}_{w2} + k_y y_{w2} - 2f_{22}\Psi_{w2} - c_y\dot{y}_b - k_y y_b + c_y a\dot{\Psi}_b + k_y a\Psi_b = m_w\left(\frac{v^2}{R_2} - g\theta_2\right) \quad (3.39)$$

$$I_w\ddot{\Psi}_{w2} + \frac{2f_{11}l^2}{v}\dot{\Psi}_{w2} + \frac{2f_{11}lr_0}{v}\dot{\emptyset}_{w2} + \frac{2f_{11}l\lambda}{r_0}y_{w2} = \frac{2f_{11}l^2}{R_2} + \frac{2f_{11}l\lambda}{r_0}y_{t2} + T_{w1} \quad (3.40)$$

$$I_\emptyset\ddot{\emptyset}_{w2} + \frac{f_{11}{r_0}^2}{v}\dot{\emptyset}_{w2} + \frac{f_{11}lr_0}{v}\dot{\Psi}_{w2} + f_{11}\lambda y_{w2} = \frac{f_{11}lr_0}{R_2} + f_{11}\lambda y_{t2} \quad (3.41)$$

$$m_b\ddot{y}_b + 2C_y\dot{y}_b + 2k_y y_b - C_y\dot{y}_{w1} - k_y y_{w1} - C_y\dot{y}_{w2} - k_y y_{w2} = m_b v^2\left(\frac{1}{2R_1} + \frac{1}{2R_2}\right) - m_b g\left(\frac{\theta_1}{2} + \frac{\theta_2}{2}\right) \quad (3.42)$$

$$I_b\ddot{\Psi}_b + 2a^2c_y\dot{\Psi}_b + 2a^2k_y\Psi_b - aC_y\dot{y}_{w1} - ak_y y_{w1} + aC_y\dot{y}_{w2} + ak_y y_{w2} = -T_{w1} - T_{w2} \quad (3.43)$$

It is clearly indicated that the two axle mechatronic vehicle is a highly interactive MIMO system. Therefore, for the system analysis and control design, it is desirable to derive a state-space representation from equations 3.36 to 3.43.

The state space matrix equation is written in the form:

$$\dot{X} = A \cdot X + B \cdot w \tag{3.44}$$

$$\dot{X} = \frac{d}{dt}\left[\dot{y_{w1}} \quad y_{w1} - y_{t1} \quad \dot{\Psi_{w1}} \quad \Psi_{w1} \quad \dot{\emptyset_{w1}} \quad \dot{y_{w2}} \quad y_{w2} - y_{t2} \quad \dot{\Psi_{w2}} \quad \Psi_{w2} \quad \dot{\emptyset_{w2}} \quad \dot{y_b} \quad y_b - \left(\frac{y_{t1}+y_{t2}}{2}\right) \quad \dot{\Psi_b} \quad \Psi_b \quad y_{t1} \quad y_{t2}\right]^T$$

$$A = \begin{bmatrix}
-\left(\frac{2f_{22}}{m_w v} + \frac{c}{m_w}\right) & -\frac{k}{m_w} & 0 & \frac{2f_{22}}{m_w} & 0 & 0 & 0 & 0 & 0 & 0 & \frac{c}{m_w} & \frac{k}{m_w} & \frac{ca}{m_w} & \frac{ka}{m_w} & -\frac{k}{2m_w} & \frac{k}{2m_w} \\
1 & 0 & 0 & 0 & 0 & 0 & 0 & 0 & 0 & 0 & 0 & 0 & 0 & 0 & 0 & 0 \\
0 & -\frac{2f_{11}l\lambda}{Ir_0} & -\left(\frac{2f_{11}l^2}{Iv} + \frac{c_t}{I}\right) & 0 & -\frac{2f_{11}lr_0}{Iv} & 0 & 0 & 0 & 0 & 0 & 0 & 0 & 0 & 0 & 0 & 0 \\
0 & 0 & 1 & 0 & 0 & 0 & 0 & 0 & 0 & 0 & 0 & 0 & 0 & 0 & 0 & 0 \\
0 & -\frac{f_{11}\lambda}{I_\emptyset} & -\frac{f_{11}lr_0}{I_\emptyset v} & 0 & -\left(\frac{f_{11}{r_0}^2}{I_\emptyset v} + \frac{c_r}{I_\emptyset}\right) & 0 & 0 & 0 & 0 & 0 & 0 & 0 & 0 & 0 & 0 & 0 \\
0 & 0 & 0 & 0 & 0 & -\left(\frac{2f_{22}}{m_w v} + \frac{c}{m_w}\right) & -\frac{k}{m_w} & 0 & \frac{2f_{22}}{m_w} & 0 & \frac{c}{m_w} & \frac{k}{m_w} & -\frac{ca}{m_w} & -\frac{ka}{m_w} & \frac{k}{2m_w} & -\frac{k}{2m_w} \\
0 & 0 & 0 & 0 & 0 & 1 & 0 & 0 & 0 & 0 & 0 & 0 & 0 & 0 & 0 & 0 \\
0 & 0 & 0 & 0 & 0 & 0 & -\frac{2f_{11}l\lambda}{Ir_0} & -\left(\frac{2f_{11}l^2}{Iv} + \frac{c_t}{I}\right) & 0 & -\frac{2f_{11}lr_0}{Iv} & 0 & 0 & 0 & 0 & 0 & 0 \\
0 & 0 & 0 & 0 & 0 & 0 & 0 & 1 & 0 & 0 & 0 & 0 & 0 & 0 & 0 & 0 \\
0 & 0 & 0 & 0 & 0 & 0 & -\frac{f_{11}\lambda}{I_\emptyset} & -\frac{f_{11}lr_0}{I_\emptyset v} & 0 & -\left(\frac{f_{11}{r_0}^2}{I_\emptyset v} + \frac{c_r}{I_\emptyset}\right) & 0 & 0 & 0 & 0 & 0 & 0 \\
\frac{c}{m_b} & \frac{k}{m_b} & 0 & 0 & 0 & \frac{c}{m_b} & \frac{k}{m_b} & 0 & 0 & 0 & -\frac{2c}{m_b} & -\frac{2k}{m_b} & 0 & 0 & 0 & 0 \\
0 & 0 & 0 & 0 & 0 & 0 & 0 & 0 & 0 & 0 & 1 & 0 & 0 & 0 & 0 & 0 \\
\frac{ca}{I_b} & \frac{ka}{I_b} & \frac{c_t}{I_b} & 0 & 0 & -\frac{ca}{I_b} & -\frac{ka}{I_b} & \frac{c_t}{I_b} & 0 & 0 & 0 & 0 & -\frac{2ca^2}{I_b} & -\frac{2ka^2}{I_b} & \frac{ka}{I_b} & -\frac{ka}{I_b} \\
0 & 0 & 0 & 0 & 0 & 0 & 0 & 0 & 0 & 0 & 0 & 0 & 1 & 0 & 0 & 0 \\
0 & 0 & 0 & 0 & 0 & 0 & 0 & 0 & 0 & 0 & 0 & 0 & 0 & 0 & -\omega_1 & 0 \\
0 & 0 & 0 & 0 & 0 & 0 & 0 & 0 & 0 & 0 & 0 & 0 & 0 & 0 & 0 & -\omega_1
\end{bmatrix}$$

Equation 3.45 - State space representation of two axle IRW vehicle

$$X = \left[\dot{y_{w1}} \quad y_{w1} - y_{t1} \quad \dot{\Psi_{w1}} \quad \Psi_{w1} \quad \dot{\emptyset_{w1}} \quad \dot{y_{w2}} \quad y_{w2} - y_{t2} \quad \dot{\Psi_{w2}} \quad \Psi_{w2} \quad \dot{\emptyset_{w2}} \quad \dot{y_b} \quad y_b - \left(\frac{y_{t1} + y_{t2}}{2}\right) \quad \dot{\Psi_b} \quad \Psi_b \quad y_{t1} \quad y_{t2}\right]^T$$

$$G = \begin{bmatrix}
v^2 & -g & 0 & 0 & 0 & 0 \\
0 & 0 & 0 & 0 & -1 & 0 \\
\frac{2f_{11}l^2}{I} & 0 & 0 & 0 & 0 & 0 \\
0 & 0 & 0 & 0 & 0 & 0 \\
\frac{f_{11}lr_0}{I_\emptyset} & 0 & 0 & 0 & 0 & 0 \\
0 & 0 & v^2 & -g & 0 & 0 \\
0 & 0 & 0 & 0 & 0 & -1 \\
0 & 0 & \frac{2f_{11}l^2}{I} & 0 & 0 & 0 \\
0 & 0 & 0 & 0 & 0 & 0 \\
0 & 0 & \frac{f_{11}lr_0}{I_\emptyset} & 0 & 0 & 0 \\
\frac{v^2}{2} & -\frac{g}{2} & \frac{v^2}{2} & -\frac{g}{2} & 0 & 0 \\
0 & 0 & 0 & 0 & -\frac{1}{2} & -\frac{1}{2} \\
0 & 0 & 0 & 0 & 0 & 0 \\
0 & 0 & 0 & 0 & 0 & 0 \\
0 & 0 & 0 & 0 & 1 & 0 \\
0 & 0 & 0 & 0 & 0 & 1
\end{bmatrix}$$

Equation 3.46 - Two axle IRW vehicle input matrix

$$w = \left[\frac{1}{R_1} \quad \theta_1 \quad \frac{1}{R_2} \quad \theta_2 \quad \dot{y_{t1}} \quad \dot{y_{t2}}\right]^T$$

y_{t1} and y_{t2} are represented in the state space matrix to improve the response accuracy of the high degree of freedom representation of the mechatronic vehicle. Including the track lateral, displacement in the state space matrix returns the 1st derivative (lateral track velocity) in the input matrix. This has a Gaussian white noise characteristic which can be used to generate the offline gain matrix which will be used in the intelligent sensing scheme.

Small damping (C_r) is included between the independently rotating wheels. This is done as the damping improves the stability of the dynamic system and increases the critical speed of the vehicle.

ω_1 which represents the lateral track displacements' integration time constant should ideally be set to zero for pure integrators but small time constants are used to satisfy the equation rule.

3.4.4 Simulation Results

Figure 3.9 and figure 3.10 present the wheel-rail leading and trailing relative lateral displacement and angle of attack of a vehicle with passive suspension, respectively.

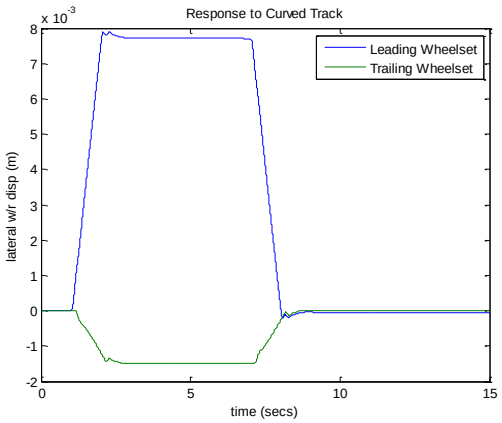

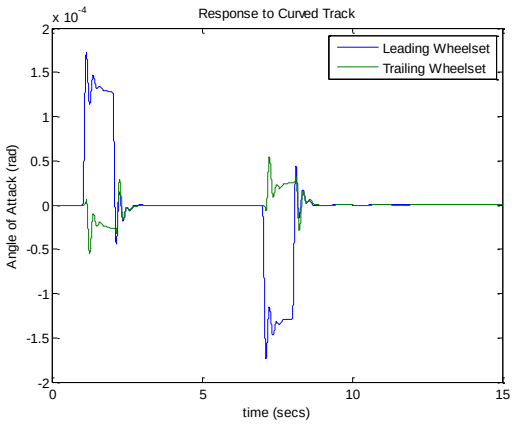

Figure 3.9 – Vehicle with passive suspension (Lateral Displacement) **Figure 3.10 - Vehicle with passive suspension (Angle of attack)**

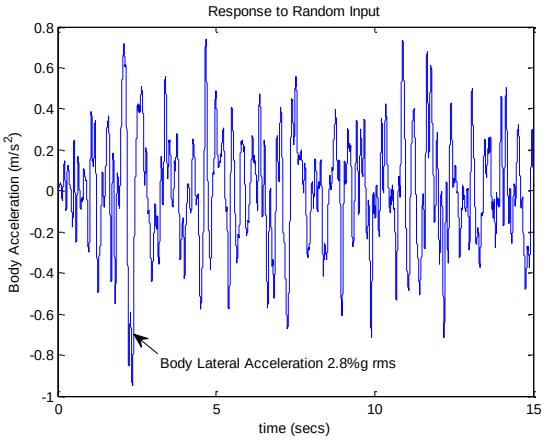

Figure 3.11 – Ride performance of paasive vehicle model

The figures show that the leading and trailing wheelsets respond differently to one another. The leading wheelset displaces laterally by 7.9mm and produces a yaw angle of 0.17mrad. The non-linear flange contact region comes into contact between 6-10mm of lateral displacement (Powell, 1998; Mei and Goodall, 2001). Therefore, the passive suspension doesn't control the vehicle to avoid the flange contact region. The results also show that both wheelsets displace laterally and yaw in opposite directions. This difference in direction of steer is caused by the interaction between the leading and trailing wheelset being connected to the body, which returns a positive and negative yaw applied to the leading and trailing wheelset. The difference in direction causes further wear to occur and ideally, both wheelsets would travel in a positive direction and produce zero yaw angles; this would imply that the wheels are curving natural, and are avoiding any wearing of the wheel and rail. Figure 3.11 presents the vehicle body lateral acceleration, using a passive suspension. The figure shows that the vehicle body exerts 2.8%g of lateral acceleration felt to the passenger of the vehicle. Any more than 4% g force exerted on the passenger will cause discomfort.

3.5. Conclusion

This chapter has shown the development of a mathematical representation of a single axle, independently rotating wheelset taking lateral, yaw and rotational degrees of freedom into account from the plan view. The track inputs have been created to represent the two inputs that the dynamic system will respond to. The simulation results have indicated that the wheelset loses its steering capability due to the decoupling of the wheels. A form of yaw torque is provided in order to steer the wheels, this can be provided by either passive or active means.

A free body diagram of a two axle mechatronic vehicle has been illustrated. The body's local reference has been adapted to each moving axis of the wheelsets so that the interaction between each wheelset connected to the vehicle body is represented accurately. An 8 degree of freedom system has then been developed as a result.

The simulation responses of the two IRW axle vehicle, with passive suspension, have been presented. The responses have highlighted the key issues with the vehicles' curving and straight track performance.

Chapter 4 Intelligent Sensing Scheme Development

4.1. Summary

This chapter will show the development of a sensing scheme and why this method of actively steering has been chosen. This chapter will give a brief overview of the Kalman filter algorithms, and will explain the design for the Kalman-Bucy filter; highlighting the drawbacks of the state estimator and how to optimise the system. The chapter will show how re-formulating the Kalman-Bucy filter returns a better curving performance; and how altering the amount of sensors used affects the accuracy of the intelligent sensing scheme. The robustness of the sensing scheme will also be analysed, to show that the scheme can maintain its performance under varying parameters. An optimisation process of the sensing scheme will be drawn and concluded; which shall be based on straight and curved track performance, and on how many sensors are used in the process.

4.2. Kalman-Bucy Filter Applied to a Single IRW Axle

4.2.1 Overview

It is understood that the IRW loses its self-steering capability due to the de-coupling of the wheels. And therefore a steering action is required to navigate the wheelset. This can be provided by the use of yaw dampers (as shown in the previous section) or, by active means. In order to actively steer the IRW, feedback signals are required to provide the controller with the correct force, or torque, which is required to steer the wheelset during curving. With the use of an estimation technique in conjunction with an optimal controller to produce a full state representation of the system using only practical sensors, active steering is possible, in theory. The following section will briefly explain the function of the Kalman filter and how it can be applied to the dynamic system to produce the full state estimation of the dynamic states in order to actively steer the wheelset.

Kalman filtering is an optimal state estimation process applied to a dynamic system that involves random perturbations. More precisely, the Kalman filter gives a linear, unbiased, and minimum error variance recursive algorithm to optimally estimate the unknown state of a dynamic system from noisy data taken at discrete real-time intervals (Chui and Chen, 2009; Grewal and Andrews, 1993).

The Kalman filter works by taking measured stochastic input data and estimating the state. This will come with an error. The states is then updated with an offline weighting system to provide a final optimal state estimation. The Kalman filter is ideally suited for real time estimating as it does not require the entire past observed data to be stored; and can use the last old estimate to update itself.

There are various types of Kalman filters, which can be applied to a dynamic system, to observe its response to a given input. The Kalman-Bucy filter is a continuous time version of the Kalman filter and is based on the state space model. Given we have represented our dynamic system as a linear time domain state space format, we will continue with the use of the Kalman-Bucy Filter, as the state estimator will be used in conjunction with an optimal control method to provide an optimal state representation of the vehicle, which we can then use to develop our practical sensing scheme to provide active steering for the mechatronic vehicle with IRW.

4.2.2 Re-formulated Kalman-Bucy filter

Research undertaken by (Li and Goodall, 1999) has shown that by re-formulating the Kalman-Bucy filter to include the curved track features (curvature and cant angle), it can provide an improved estimation of the states.

The re-formulated state-space and output equations are given in equations (4.1) and (4.2):

$$\hat{\dot{X}}_k = A_k \cdot \hat{X}_k + K_r(y_m - \hat{y}_k) \tag{4.1}$$

$$\hat{Y}_k = C_k \cdot \hat{X}_k \tag{4.2}$$

Where:

$$\hat{X}_k = \begin{bmatrix} \dot{y} & y - y_t & \dot{\Psi} & \Psi & \dot{\phi} & 1/R & \theta \end{bmatrix}^T$$

$$A_k = \begin{bmatrix} -\frac{2f_{22}}{mv} & 0 & 0 & \frac{2f_{22}}{m} & 0 & v^2 & -g \\ 1 & 0 & 0 & 0 & 0 & 0 & 0 \\ 0 & -\frac{2f_{11}l\lambda}{Ir_0} & -\left(\frac{2f_{11}l^2}{Iv}+\frac{c_t}{I}\right) & 0 & -\frac{2f_{11}lr_0}{Iv} & \frac{2f_{11}l^2}{I} & 0 \\ 0 & 0 & 1 & 0 & 0 & 0 & 0 \\ 0 & -\frac{f_{11}\lambda}{I_\emptyset} & -\frac{f_{11}lr_0}{I_\emptyset v} & 0 & -\frac{f_{11}{r_0}^2}{I_\emptyset v} & \frac{f_{11}lr_0}{I_\emptyset} & 0 \\ 0 & 0 & 0 & 0 & 0 & -\omega_2 & 0 \\ 0 & 0 & 0 & 0 & 0 & 0 & -\omega_2 \end{bmatrix}$$

Equation 4.3 - State space matrix of RKF

$$C_k = \begin{bmatrix} -\frac{2f_{22}}{mv} & 0 & 0 & \frac{2f_{22}}{m} & 0 & 0 & 0 \\ 0 & 0 & 1 & 0 & 0 & -v & 0 \\ 0 & 0 & 0 & 0 & 1 & 0 & 0 \end{bmatrix}$$

Equation 4.4 - Output matrix RKF

Thus the state space matrix now becomes:

$$\frac{dx}{dt} = \hat{X}_k = \begin{bmatrix} \widehat{\dot{y}} \\ y - y_t \\ \dot{\Psi} \\ \Psi \\ \dot{\emptyset} \\ \frac{1}{R} \\ \theta \end{bmatrix} = \begin{bmatrix} -\frac{2f_{22}}{mv} & 0 & 0 & \frac{2f_{22}}{m} & 0 & v^2 & -g \\ 1 & 0 & 0 & 0 & 0 & 0 & 0 \\ 0 & -\frac{2f_{11}l\lambda}{Ir_0} & -\left(\frac{2f_{11}l^2}{Iv}+\frac{c_t}{I}\right) & 0 & -\frac{2f_{11}lr_0}{Iv} & \frac{2f_{11}l^2}{I} & 0 \\ 0 & 0 & 1 & 0 & 0 & 0 & 0 \\ 0 & -\frac{f_{11}\lambda}{I_\emptyset} & -\frac{f_{11}lr_0}{I_\emptyset v} & 0 & -\frac{f_{11}{r_0}^2}{I_\emptyset v} & \frac{f_{11}lr_0}{I_\emptyset} & 0 \\ 0 & 0 & 0 & 0 & 0 & -\omega_2 & 0 \\ 0 & 0 & 0 & 0 & 0 & 0 & -\omega_2 \end{bmatrix} \begin{bmatrix} \widehat{\dot{y}} \\ y - y_t \\ \dot{\Psi} \\ \Psi \\ \dot{\emptyset} \\ \frac{1}{R} \\ \theta \end{bmatrix} + \begin{bmatrix} 0 & 0 & 0 \\ 0 & 0 & -1 \\ 0 & 0 & 0 \\ 0 & 0 & 0 \\ 0 & 0 & 0 \\ 1 & 0 & 0 \\ 0 & 1 & 0 \end{bmatrix} \begin{bmatrix} \dot{\frac{1}{R}} \\ \dot{\theta} \\ \dot{y}_t \end{bmatrix}$$

Equation 4.5 - RKF applied to single IRW

$$\hat{Y}_k = \begin{bmatrix} \ddot{y} \\ \dot{\Psi} \\ \dot{\emptyset} \end{bmatrix} = \begin{bmatrix} -\frac{2f_{22}}{mv} & 0 & 0 & \frac{2f_{22}}{m} & 0 & 0 & 0 \\ 0 & 0 & 1 & 0 & 0 & -v & 0 \\ 0 & 0 & 0 & 0 & 1 & 0 & 0 \end{bmatrix} \begin{bmatrix} \widehat{\dot{y}} \\ y - y_t \\ \dot{\Psi} \\ \Psi \\ \dot{\emptyset} \\ \frac{1}{R} \\ \theta \end{bmatrix}$$

Equation 4.6 **- RKF output equation**

The matrix D_m represents the inputs measured from an absolute reference on the dynamic system. This means that the centrifugal forces that are usually observed are not. C_m represents the measured output matrix; this is similar to the theoretical output matrix and seldom differs. ω_2 represents the integrator cut off for curvature and cant.

4.2.3 Design Scheme

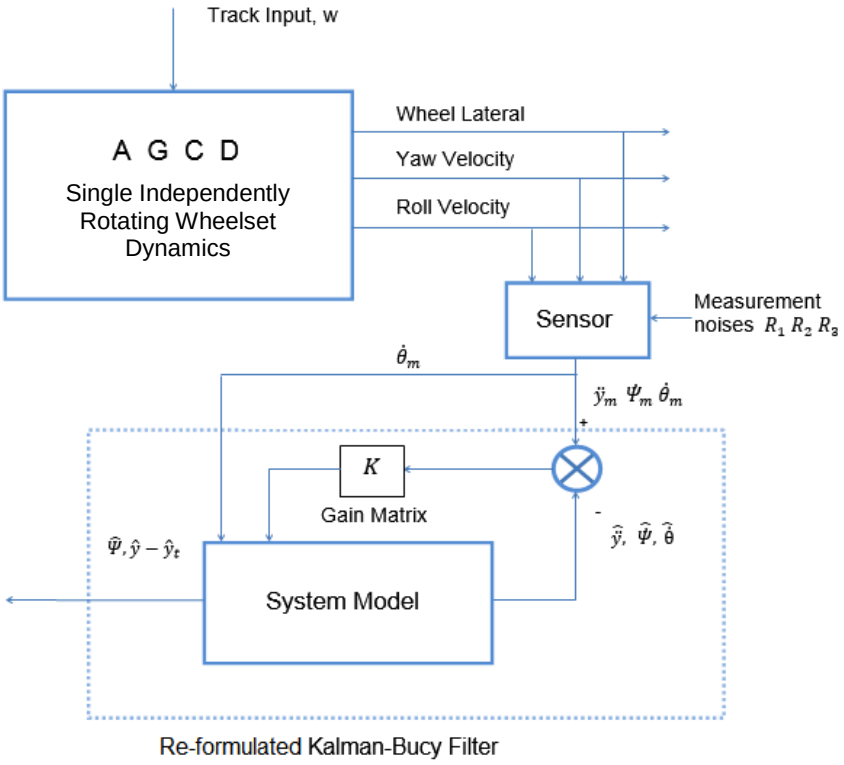

Figure 4.1 - Block diagram sensing scheme

Figure 4.1 provides a block diagram of the sensing scheme, using 3 sensors to measure a single IRW's lateral acceleration; yaw velocity and roll velocity,

$$Y_m = \begin{bmatrix} \ddot{y}_m \\ \dot{\Psi}_m \\ \dot{\phi}_m \end{bmatrix} = \begin{bmatrix} -\frac{2f_{22}}{mv} & 0 & 0 & \frac{2f_{22}}{m} & 0 \\ 0 & 0 & 1 & 0 & 0 \\ 0 & 0 & 0 & 0 & 1 \end{bmatrix} \begin{bmatrix} \dot{y} \\ y - y_t \\ \dot{\psi} \\ \Psi \\ \dot{\phi} \end{bmatrix} + \begin{bmatrix} 0 & 0 & 0 \\ -v & 0 & 0 \\ 0 & 0 & 0 \end{bmatrix} \begin{bmatrix} \frac{1}{R} \\ \theta \\ \dot{y}_t \end{bmatrix} + \begin{bmatrix} 1 & 0 & 0 \\ 0 & 1 & 0 \\ 0 & 0 & 1 \end{bmatrix} \begin{bmatrix} v_1 \\ v_2 \\ v_3 \end{bmatrix}$$

Equation 4.7 - 3 sensor output equation

Y_m shown in figure 4.5 is derived from the wheelset output equation (3.21), but it is modified to represent the measured signals. The difference between the theoretical output equation and the measured output equation is that the input matrix is derived from an absolute reference. This means that the centrifugal forces, which are usually observed by the dynamic system, are no longer available as the sensors in theory would not measure these inputs. The measurement noise signals are generated as vectors v_1, v_2 and v_3; which are treated as white noise and are expressed as covariances $R1$, $R2$ and $R3$; with an associated random noise on top of the signal. All measurement covariances are generated by taking three times the true root mean square (R.M.S) value on the straight track with irregularities; plus the peak value of their responses on the pure curved track, and using 2% of the overall value. A, G, C, D are the state space and output

matrices for the single IRW, as derived in equation 3.22. K_r is the stationary gain matrix which is designed offline using the function (LQE) in $\mathrm{MATLAB}^{\mathrm{TM}}$. Expressing both the inputs ($\frac{\dot{\mathrm{i}}}{R}$, $\dot{\theta}$ & $\dot{y}_t$) and the measurement signals as covariances allows the linear quadratic generator to produce an optimal stationary gain matrix offline; this is then used to provide an optimised estimate of the vehicles states.

4.2.4 Results

There is a trade-off between improving both the estimation accuracy for straight and curved track responses for wheel-rail lateral displacement, and wheelset angle of attack. This trade-off associated with the performance of the Kalman-Bucy filter has been covered in (Li, 2001), which discusses how tuning the intelligent sensing scheme can improve the accuracy of the estimations of the states from the Kalman-Bucy filter. This same method of tuning the state estimator will be applied to a two axle IRW vehicle.

Table 4.1 provides the parameters used to represent the single IRW, and to generate the offline gain matrix K_r. The same build function (lsim) is used in $\mathrm{MATLAB}^{\mathrm{TM}}$ to simulate the dynamic system.

Symbol	Quantity	Value
m	Wheelset mass	1250kg
θ	Track cant	6°
v	Forward velocity	10 m/s
λ	Conicity	0.15
l	Half gauge	0.75 m
f_{11}	Longitudinal creep coefficient	10 MN
f_{22}	Lateral creep coefficient	10 MN
I	Wheelset yaw inertia	700 kgm^2
$I_{\emptyset}$	Wheel rotational Inertia	100 kgm^2
r_0	Nominal wheel radius	0.5 m
R	Curve radius	100 m
C_t	Yaw Damper	2.8kN
$C_{\emptyset}$	Rotational damper between wheels	0.1N
$R1$	Measured lateral acceleration signal covariance	6.30e-6
$R2$	Measured yaw velocity signal covariance	4.78e-6
$R3$	Measured difference in rotational velocity signal covariance	1.12e-7
Q_1	Curve velocity Covariance	1e-7
Q_2	Cant velocity covariance	2e-5
Q_3	Track lateral velocity covariance	3.26e6

Table 4.1 Single IRW parameters

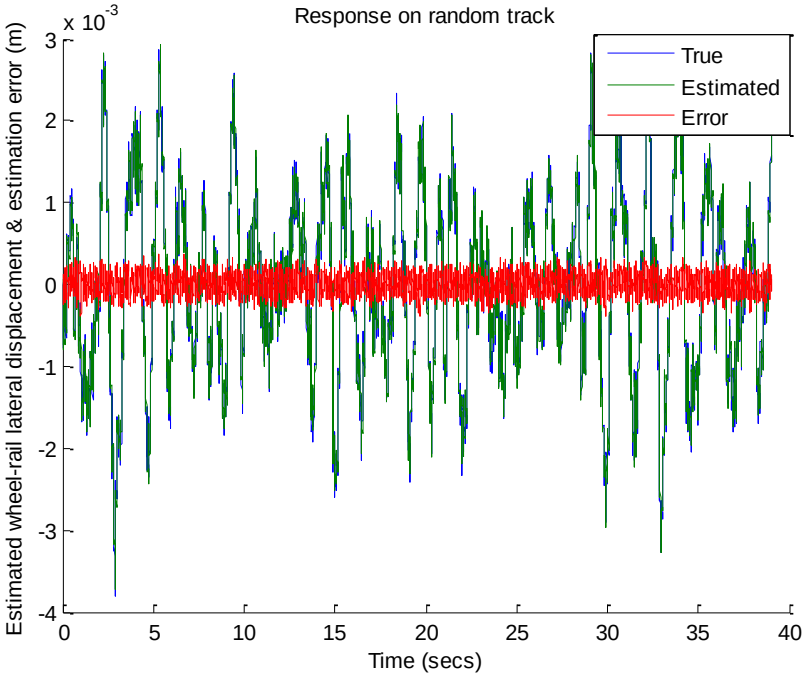

Figure 4.2 Response to random track

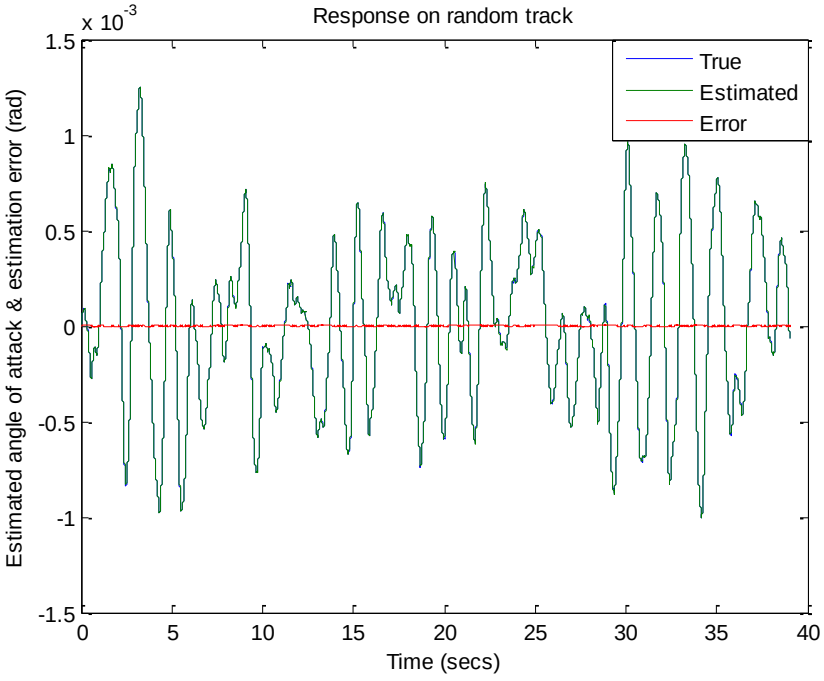

Figure 4.3 - Response to random track

Figure 4.2 and Figure 4.3 shows the estimates of relative lateral displacement and the wheelsets' relative yaw angle, compared to the true ideal response of the system. The estimation error, between the true and estimated responses, is also presented. The figures show that the re-formulated Kalman-Bucy filter provides a good estimation of the straight track responses.

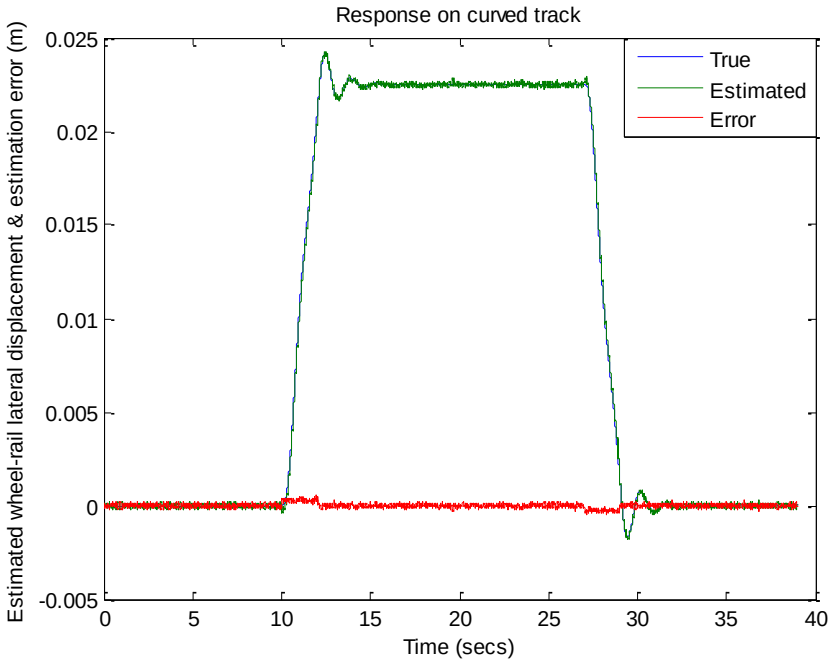

Figure 4.4 - Response to curved track

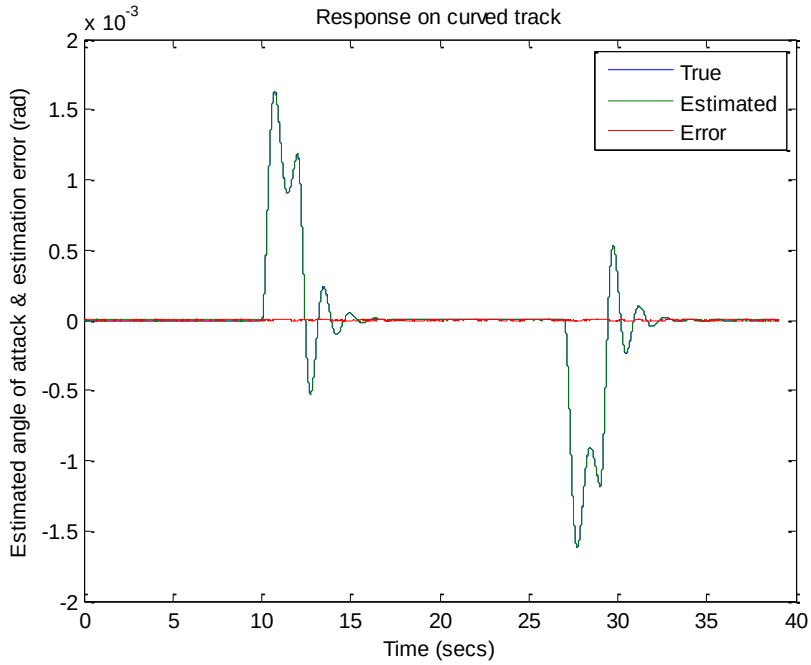

Figure 4.5 - Response to curved track

Figure 4.4 and figure 4.5 illustrates the true and estimated curved track response of the system. The re-formulated Kalman-Bucy filter is able to accurately estimate the response of the wheelset and is shown in the low error between the true and estimated responses.

4.2.5 Robustness Checking

Robustness is defined as the ability to tolerating perturbations that might affect the system's functional body. The intelligent sensing scheme must be able to tolerate perturbations when applied to a real world application as there will be variations which will occur such as parameter,

variations which it must be able to adapt to. This project will illustrate the sensing scheme's response of the system under parameter variations, which will replicate real world events and ultimately show robustness.

Figure 4.6 and figure 4.7 illustrate the response of the system with varying longitudinal creep coefficients.

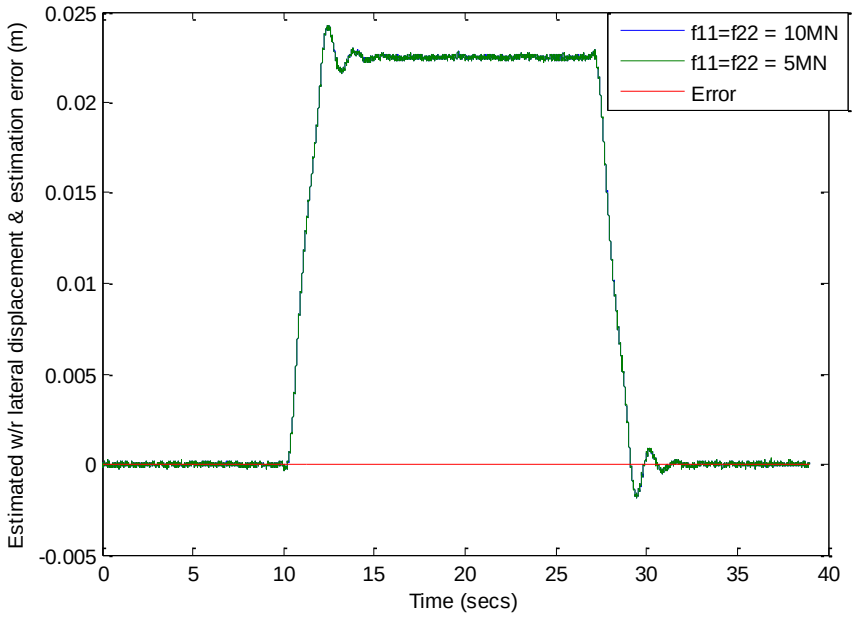

Figure 4.6 - Estimated w/r lat. displacement at f11 & f22 = 10 & 5MN

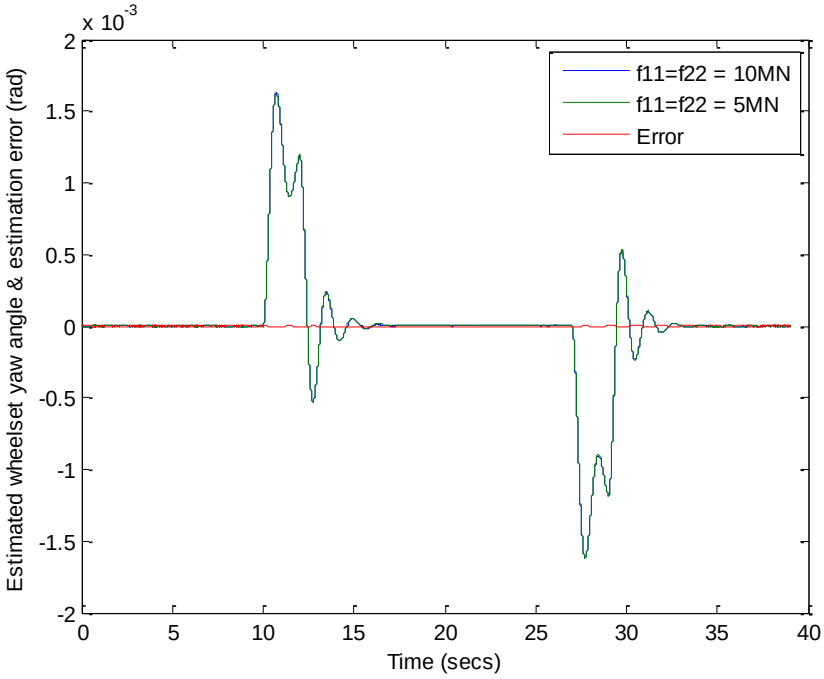

Figure 4.7 - Estimated yaw angle at f11 & f22 = 5 & 10MN

The figures show that the estimated lateral displacement and angle of attack are estimated very accurately under varying longitudinal and lateral creep forces.

Figure 4.8 and figure 4.9 show the estimated response of the system under varying wheelset conicity and creep coefficients.

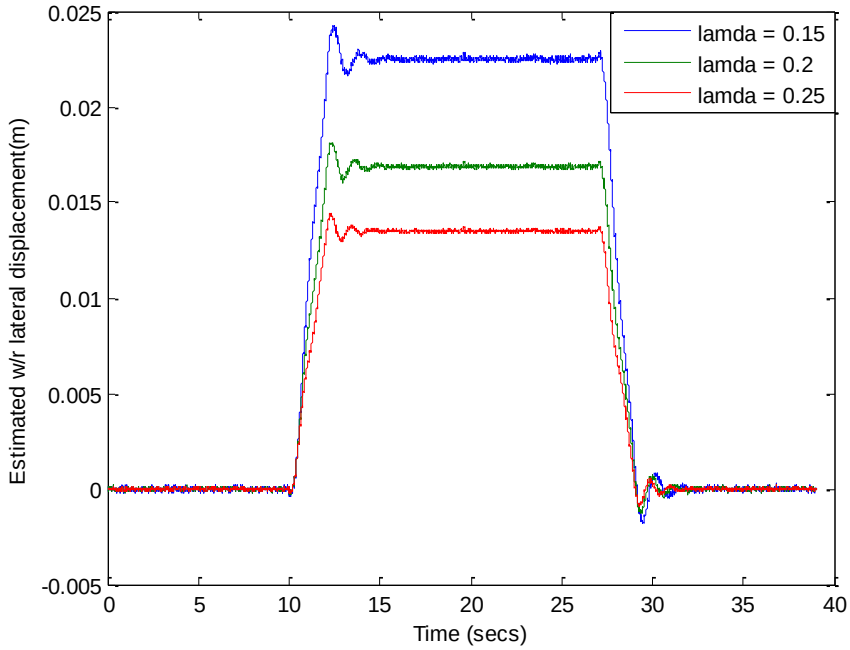

Figure 4.8 - Estimated w/r lateral displacement changing wheel conicity

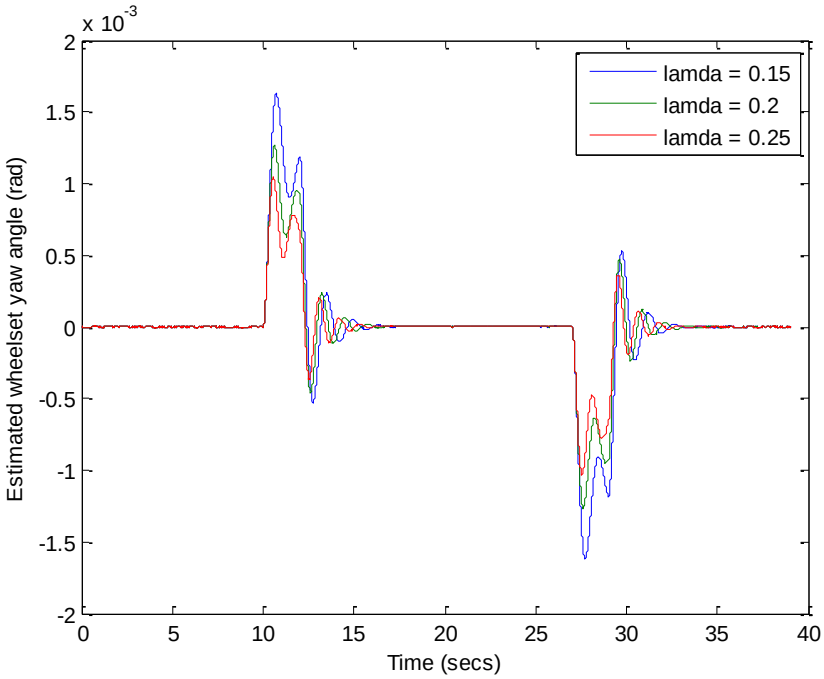

Figure 4.9 - Estimated wheelset yaw angle changing wheel conicity

The results show that, under varying parameters, the system is able to adapt and maintain robustness.

4.2.6 Conclusion

A brief explanation of the Kalman-Bucy filter has been provided; explaining why the estimation technique will provide full state feedback of the system. Re-formulation of the Kalman-Bucy filter to include curvature and cant has been explained to provide the system with an improved estimation of the state variables.

A 3 sensor approach, in line with a re-formulated Kalman-Bucy filter has been used to conduct this preliminary study. The sensing scheme has been able to provide good evidence to suggest that the re-formulated Kalman-Bucy filter can provide an accurate estimate of the state variables such as wheel/rail lateral displacement, and angle of attack.

This section has also applied robustness techniques to see how the wheelset performs under parameter variations, to imitate real world changes the system may incur. The results show that the estimation technique estimates the state variables accurately, and adapts to the variations well.

4.3. Kalman-Bucy Filter Applied to a 2 Axle Mechatronic Vehicle with IRW

Previous studies have concentrated on using the Kalman-Bucy filter to provide full state feedback of a two axle IRW vehicle, but have all concentrated on mounting the sensors directly to the wheelset in order to obtain the necessary feedback signals for the estimator to produce an accurate estimation of the states (Mei and Goodall, 2001; Goodall and Mei, 2000; Li and Goodall, 1999). The issue with mounting the sensors directly to the wheelsets of the vehicles is that the environment that the sensors are in is arduous and, therefore, reliability and robustness are of great concern. In order to avoid reliability and robustness concerns, this study will assess the performance of the sensing scheme using only body mounted sensors to provide the necessary feedback signals for the controller.

4.3.1 Design Scheme

Taking the equations of motion, detailed in 3.4 of the thesis; the state space and input representations are:

$$\dot{X} = A \cdot X_k + B \cdot u + G \cdot w \qquad (4.8)$$

Where A and G can be derived from equations (3.36) ~ (3.43), and are illustrated in state space format. $X, u \text{ and } w$ are the state variables, torque input and track vectors.

$$X_k = \left[\dot{y_{w1}} \quad y_{w1} \quad \dot{\Psi_{w1}} \quad \Psi_{w1} \quad \dot{\phi}_{w1} \quad \dot{y_{w2}} \quad y_{w2} \quad \dot{\Psi_{w2}} \quad \Psi_{w2} \quad \dot{\phi}_{w2} \quad \dot{y_b} \quad y_b - \left(\frac{y_{t1} + y_{t2}}{2}\right) \quad \dot{\Psi_b} \quad \Psi_b \quad y_{t1} \quad y_{t2} \quad \right]^T$$

$$w = \left[\dot{y_{t1}} \quad \dot{y_{t2}} \quad {}^1/_{R_1} \quad \emptyset_1 \quad {}^1/_{R_2} \quad \emptyset_2 \right]^T \qquad u = [T_{w1} \quad T_{w2}]^T$$

Symbol	Quantity	Value
r_0	Nominal wheel radius	$0.45\ m$
λ	Conicity	0.2
v	Forward velocity	$60\ m/s$
a	Half space of the vehicle	$3.7\ m$
l	Half gauge	$0.7\ m$
I_w	Wheelset yaw inertia	$700\ kgm^2$
$I_\emptyset$	Wheel rotational inertia	$100\ kgm^2$
I_b	Vehicle yaw inertia	$170{,}000\ kgm^2$
m_w	Wheelset mass	$1250\ kg$
m_b	Vehicle mass	$13{,}500\ kg$
f_{11}	Longitudinal creep coefficient	$10\ MN$
f_{22}	Lateral creep coefficient	$10\ MN$
$\theta_{1,2}$	Track cant angle at the two wheels	21.04°
$R_{1,2}$	Curve radius at the two wheels	$1000\ m$
k_y	Lateral Stiffness per wheelset	$230\ kN/m$
C_y	Lateral damper per wheelset	$50\ kNs/m$
C_r	Rotational damping between each wheelset	0.1

Table 4-2 - Parameters for a plan view two-axle vehicle

Figure 4.10 shows the design scheme in block diagram form. The diagram illustrates the closed loop control of the 2-axle vehicle with IRW. The outputs are measured by the sensors, which are mounted to the body of the vehicle. Measurement of body lateral acceleration, yaw velocity and the leading and trailing suspensions' lateral and yaw displacements will be used to provide the necessary feedback signals for the controller. A simple model-based Kalman-Bucy filter is used and the curved track features (curvature and cant angle) are set as known values at this stage of the study, however in practice, the curved track features would not be known track inputs. A simple Proportional, (P) controller is used to generate the control torques required by the actuators to actively steer each wheelset. The dynamics of the actuators required to implement the control actions are neglected in the model at this stage; therefore the feedback signal which is generated from the Kalman-Bucy filter will be fed directly back into the vehicle model.

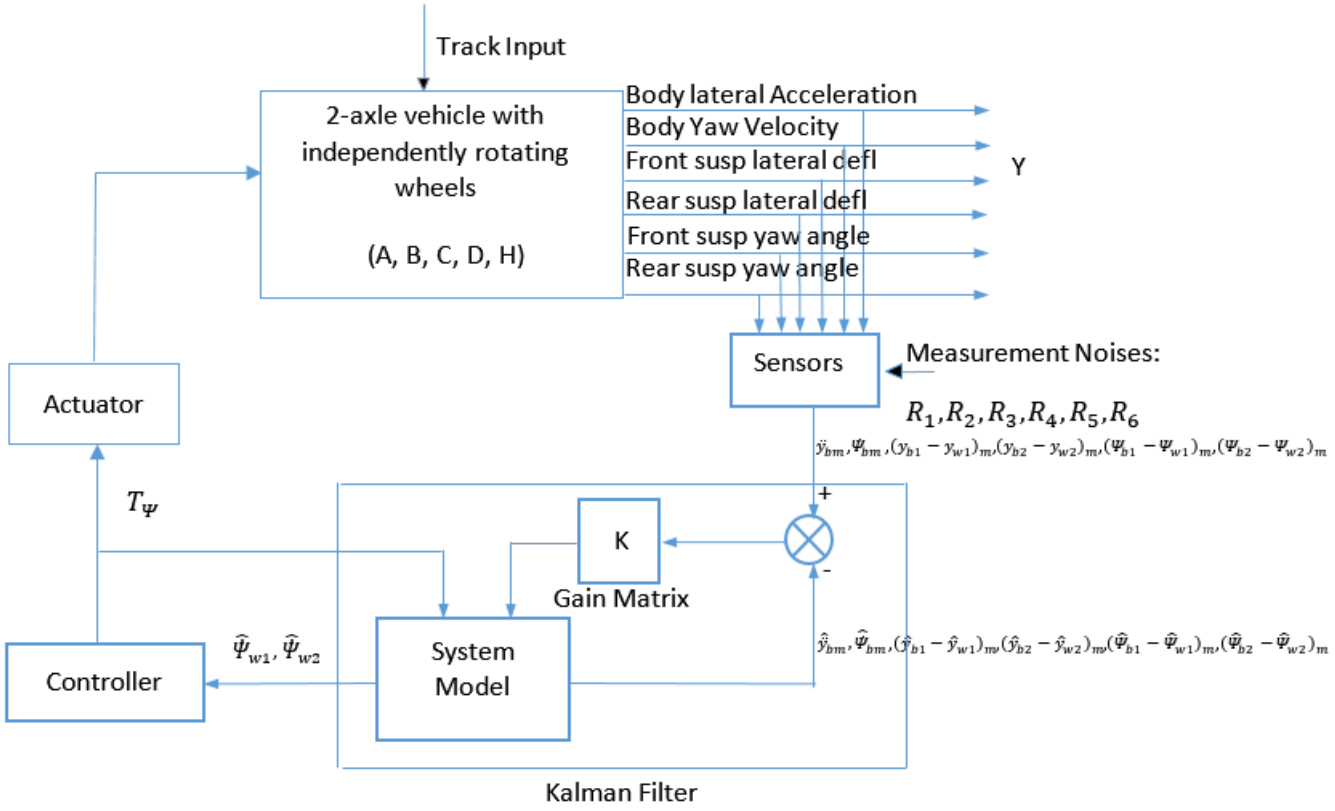

Figure 4.10 - Block diagram of sensing scheme

4.3.2 Simulation Results

In order to assess the performance of the sensing scheme, both track types are used in the simulation. A curved track of 1000m and a canted track of 21.04° are used to return zero cant deficiency.

The purpose of this control scheme is twofold; firstly we must provide steering to the IRW, as the design loses its self-centring ability, which is usually inherent of the conventional axle. Secondly, we must maintain the ride performance on the straight track; provided by the conventional passive

suspension. Therefore, the selection of a suitable covariance matrix, representing the track inputs is crucial in returning a good estimation of the states. The covariance matrix Q_k represents the inputs to the leading and trailing wheelset, as a covariance, and can be expressed as $diag[Q_{l\,track} \quad Q_{t\,track}]$. The measurement noise covariances $R1$ to $R6$ are initially set to the square of 2% of their maximum values, which is determined by taking three times their true root mean square (R.M.S) value, on the straight track with irregularities; plus the peak value of their responses on the pure curved track. The measurement noise covariances can also be expressed as one covariance (R_k); in the same manner as Q_k. Both the input covariance and the measurement noise covariance are then used to generate the gain matrix K, to optimise the state estimation of the Kalman-Bucy filter.

Figures 4.11 ~ 4.15 show the measured response of the front and rear wheelsets' wheel-rail lateral displacement and yaw angle.

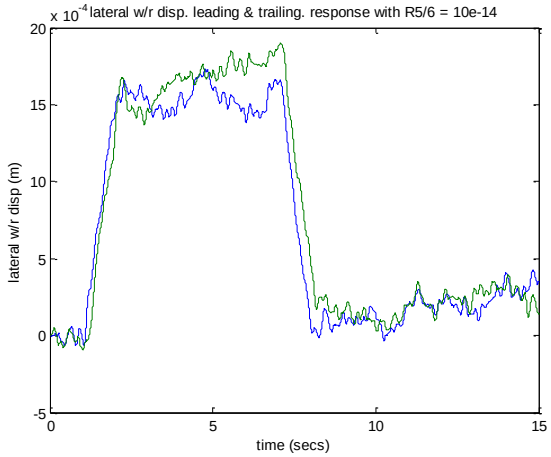

Figure 4.11 – Measured response (lat. displacement)

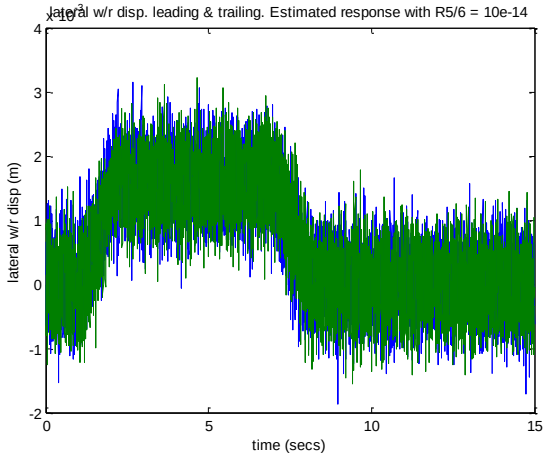

Figure 4.12 – Estimated response (lat. displacement)

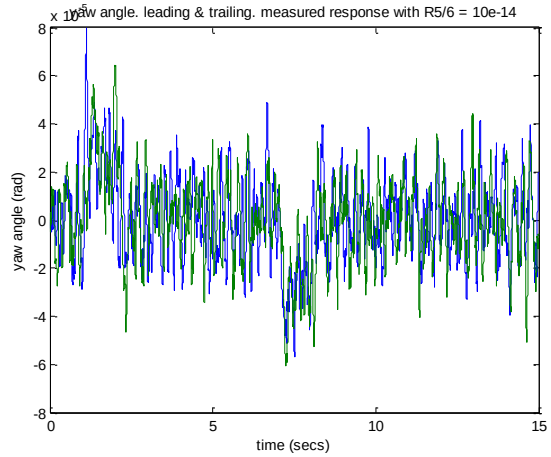

Figure 4.13 – Measured response (angle of attack)

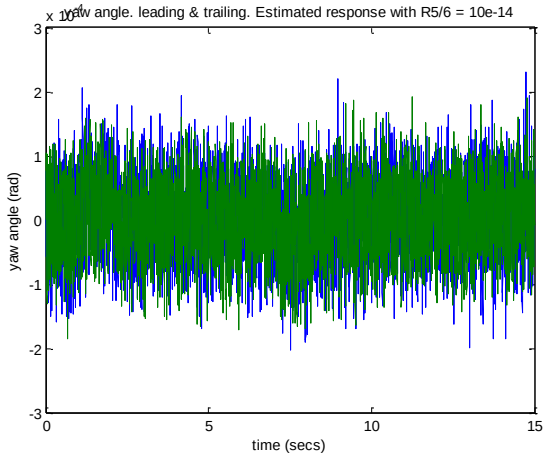

Figure 4.14 – Estimated response (angle of attack)

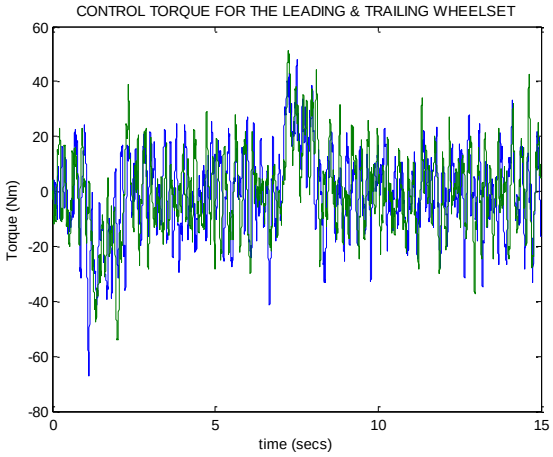

Figure 4.15 – Measured response (control torque)

The figures illustrate the level of accuracy the sensing scheme returns with all measurement noise covariances set to the square of 2% of their maximum values, which is determined by taking 3 times their true root mean square (R.M.S) value on the straight track with irregularities; plus the peak value of their responses on the pure curved track. Setting the covariances to the values is considered to represent a low cost sensor. The results show that, in general, a large amount of noise can be observed. This is the result of an inadequate level of accuracy from the measurements taken. In order to provide active steering, an accurate level of measurements must be taken in order to produce an accurate estimation of the states. As the level of accuracy of the measurement was poor, the next logical step is to improve the accuracy of the sensors, to see if it will improve the performance of the estimate of the states.

4.3.3 Increasing measurement accuracy

Increasing the accuracy of the sensors is reflected by reducing the noise on top of the measured signals, this in turn reduces the error between the measured output and the theoretical output which is used to generate the gain matrix (K). The smaller the margin of error between the two, the fewer steps the gain matrix takes in correcting the error, thus a better estimate is achieved. The next section shows the process of reducing the measurement noises, $R1$ to $R6$, to see which combinations of sensors return good straight and curved track performance. Ideally, as this project aims to provide a low cost sensing approach, the fewer the high accuracy sensors required, the more cost effective the sensing scheme becomes.

4.3.4 Improving measurement sensors.

Figures 4.16 ~ 4.20 show the response of the system when sensor combinations $R1$ and $R6$, and $R5$ and $R6$ are set to 10^{-12}

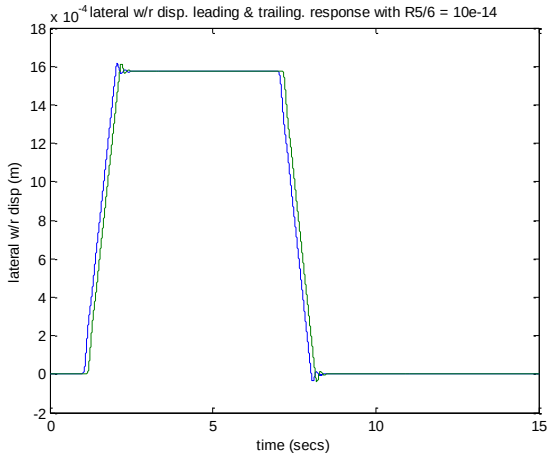

Figure 4.16 – Measured response (lat. displacement)

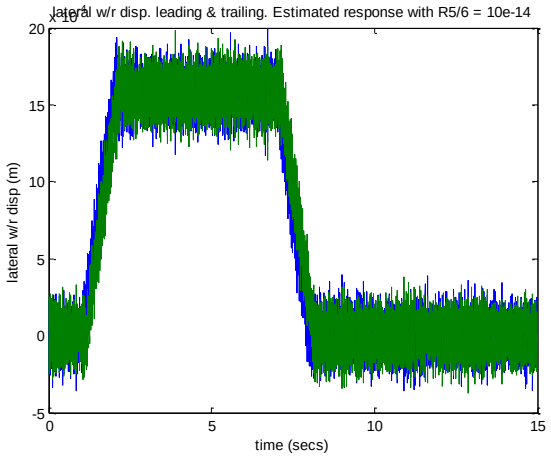

Figure 4.17 – Estimated response (lat. Displacement)

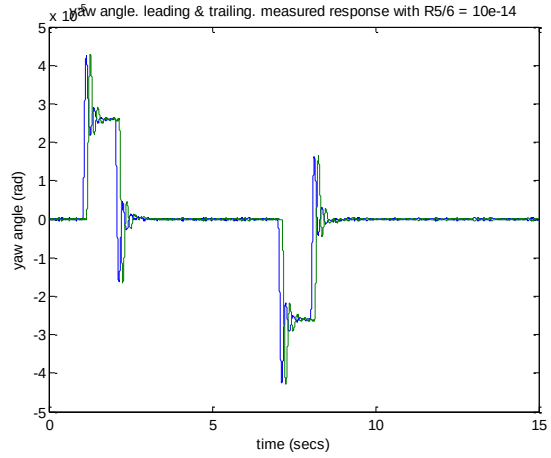

Figure 4.18 – Measured response (angle of attack)

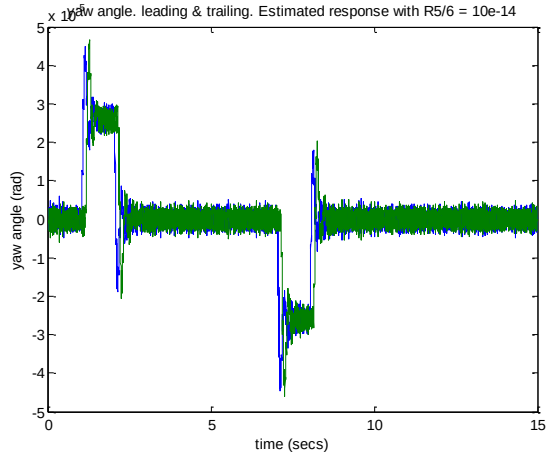

Figure 4.19 – Estimated reposnse (angle of attack)

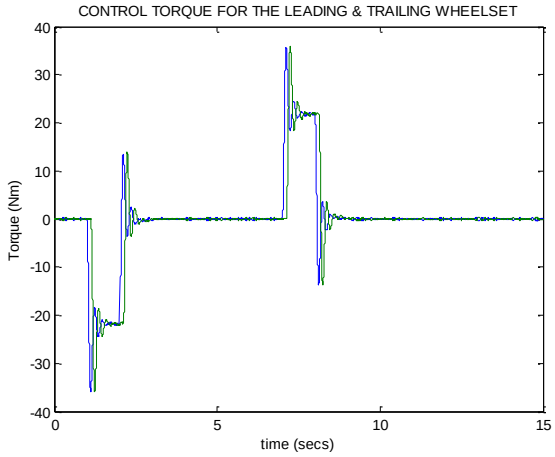

Figure 4.20 – Measured response (control torque)

It can be seen that there has been a significant improvement in the estimation of the states and as a result, the curving performance of the system has improved. Setting the sensors ($R1$, $R2$ and

$R5$), ($R1$, $R4$ and $R5$) and ($R1$, $R3$ and $R5$) to a value of 10^{-12} has also provided the same curving performance as reducing sensors $R1$ and $R6$, and $R5$ and $R6$. However, as mentioned previously, the aim of this project is to produce a practical sensing scheme; and so the aim is to use as many low cost sensors as possible. Thus, for this particular sensing scheme, improving the sensors $R1$ and $R6$, or $R5$ and $R6$ will be the minimum requirement in order to return a performance adequate for good curving.

4.3.5 Response of Mechatronic Vehicle with Active and Passive Suspension

Figures 4.21 and 4.22 compare the curving performance of the mechatronic vehicle with passive and active suspension used to provide the steering action required for the IRW vehicle.

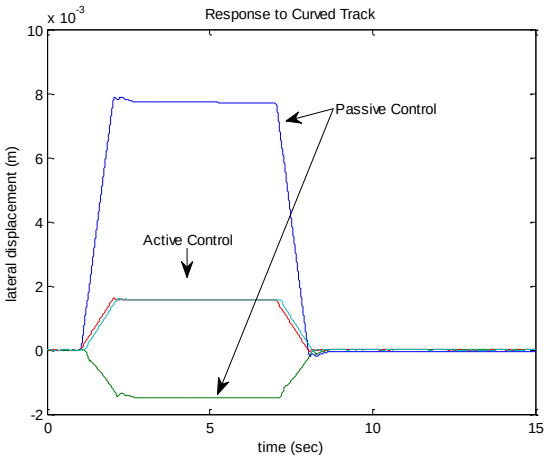

Figure 4.21 – Active vs. passive (lat. Displacement)

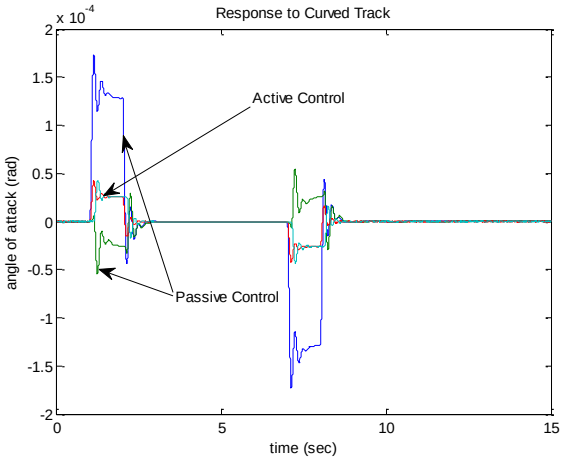

Figure 4.22 – Active vs. passive (angle of attack)

The passive yaw damping and active control torque have both been set to provide 23kNm of torque to steer the vehicle. A significant improvement of curving performance is achieved by the proposed actively controlled scheme. The quasi-static lateral displacement (only 1.6mm) and the angle of attack (0.03 mrads) are shown to improve greatly.

Ride quality is a criterion of its effectiveness in providing isolation from the track roughness, and is quantified in terms of the root mean square (R.M.S.) of the vehicle body acceleration. Figure 4.23 compares the vehicle body accelerations for the active and passive systems when running along the random track. It is noted that the ride quality has improved by 19.5% as the percentage G has reduced from 2.77%g to 2.23%g compared to the passive suspensions performance, whilst the active control achieves a good curving performance on the track as demonstrated above.

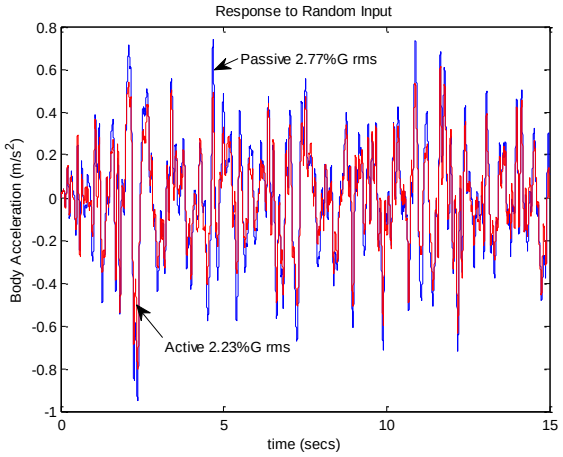

Figure 4.23 – Active vs. passive (body lateral acceleration)

4.3.6 Robustness Checking

The railway wheelset is subject to parameter variations, such as the conicity and creep coefficients at the wheel/rail interface. Therefore, any closed loop system must be robust against variations of operational parameter, in order to ensure the reliability and, ultimately, the safety of the system.

Figure 4.24 and figure 4.25 show the wheel-rail lateral displacement and yaw angle on the curved track, when the conicity in the physical model, changes in the range of 0.2±0.05. The simulation results clearly indicate that the overall control system is stable, although there is a scaling factor on the quasi-static lateral displacement, and on the yaw angle on the curve transition, due to the change in the wheelset conicity.

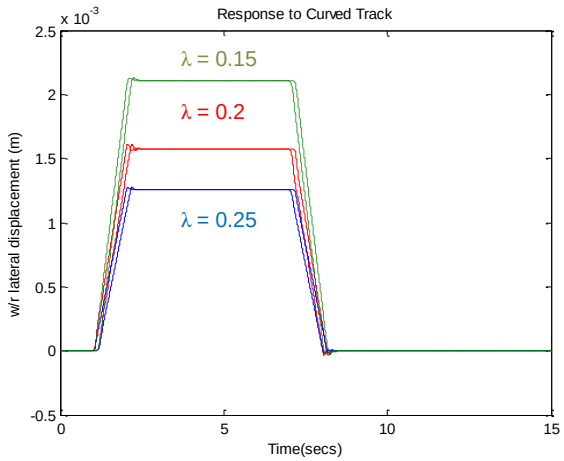

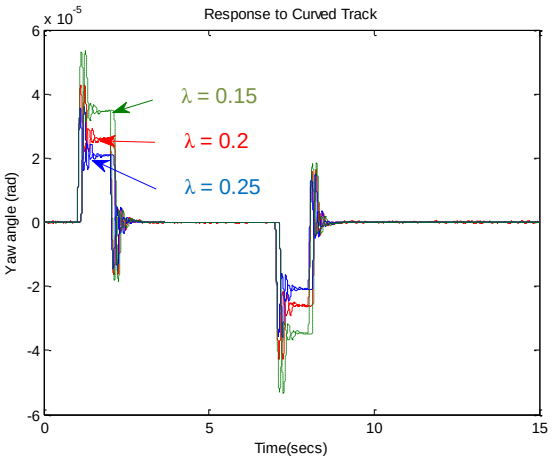

Figure 4.24 – Robustness check (lat. Displacement) Figure 4.25 – Robustness check (angle of attack)

Figure 4.26 and figure 4.27 present the simulation results when the lateral and longitudinal creep coefficient are varied from 10MN to 5MN. It shows clearly from the figures that the proposed scheme is very robust. The relative wheel-rail lateral displacements, and yaw angles for both leading and trailing wheelsets, remain largely unchanged; and there is only a small scaling factor error for yaw angle on both curve transition and steady-state curve.

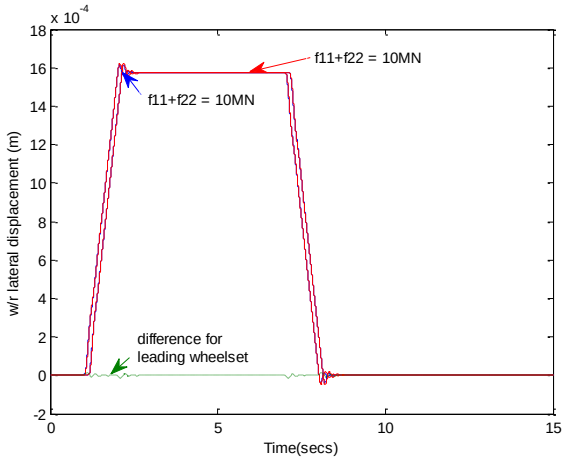

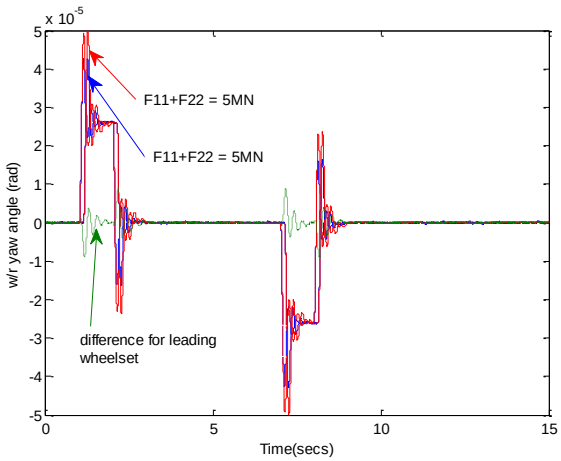

Figure 4.26 – Robustness check (lat. Displacement) Figure 4.27 – Robustness check (angle of attack)

4.3.7 Conclusions

This section of the thesis has presented the development of a novel model based sensing scheme to provide high integrity feedback variables in order to enable the practical implementation of the active control for a railway vehicle. This study is based upon a two-axle mechatronic railway vehicle with independently rotating wheels running on both random and curved tracks. In order to avoid the reliability and robustness concerns with axle mounted sensors for the railway industry, only sensors mounted on the body have been used in the design to provide the necessary feedback signals for the controller.

The simulation results have shown that, by carefully selecting the correct values of measurement noise covariance, the proposed scheme can not only steer the independently rotating wheels to follow the curve track, but also improve the vehicle ride quality by 19.5% compared with the passive system.

The robustness of the proposed sensing scheme is also examined in the presence of the creep coefficient and the conicity variations. The simulation results have shown that, in general, the proposed scheme is stable and is able to maintain a good curving performance, except the fact that the lateral wheel-rail displacement essentially has a scale factor error when the wheelset conicity varies.

4.4. Re-formulated Kalman-Bucy Filter Applied to a 2 Axle Mechatronic Vehicle with IRW

In the previous section, the curved track features (curvature and cant angle) are set as known input values. However, it does not represent a realistic and practical sensing approach. This is because the curve radius and track cant features are difficult to provide in practice. Therefore, an

alternative method of providing the sensing scheme with the deterministic curved track information is to re-formulate the Kalman-Bucy filter. The re-formulated Kalman-Bucy Filter (RKBF) includes the curvature and cant within the state space representation of the mechatronic vehicle.

The following study will show how the sensing scheme performs using the re-formulated Kalman-Bucy filter approach; and will see if the addition of the deterministic track features as two extra states, returns the same curving and ride performance seen from the basic Kalman-Bucy; with curved track features set as known.

4.5. Design Scheme

The change to the re-formulated Kalman-Bucy filter sensing scheme is the approach of the state space representation of the vehicle. The RKBF state space equation is given in (4.9):

$$\dot{X_{kr}} = A_{kr} \cdot X_{kr} + G_{kr} \cdot w_{kr} + T \cdot u \tag{4.9}$$

Where:

$$X_{kr} = \left[\dot{y_{w1}} \quad y_{w1} - y_{t1} \quad \dot{\Psi_{w1}} \quad \Psi_{w1} \quad \dot{\emptyset}_{w1} \quad \dot{y_{w2}} \quad y_{w2} - y_{t2} \quad \dot{\Psi_{w2}} \quad \Psi_{w2} \quad \dot{\emptyset}_{w2} \quad \dot{y_b} \quad y_b - (\frac{y_{t1} + y_{t2}}{2}) \quad \dot{\Psi_b} \quad \Psi_b \quad y_{t1} \quad y_{t2} \quad {}^{1}/_{R_1} \quad \theta_1 \quad {}^{1}/_{R_2} \quad \theta_2\right]^T$$

$$u = [T_{w1} \quad T_{w2}]^T \qquad w_{kr} = \left[\dot{y_{t1}} \quad \dot{y_{t2}} \quad \dot{{}^{1}/_{R_1}} \quad \dot{\emptyset_1} \quad \dot{{}^{1}/_{R_2}} \quad \dot{\emptyset_2}\right]^T$$

$$A = \begin{bmatrix}
-\left(\frac{2f_{22}}{m_w v}+\frac{c}{m_w}\right) & -\frac{k}{m_w} & 0 & \frac{2f_{22}}{m_w} & 0 & 0 & 0 & 0 & 0 & 0 & \frac{c}{m_w} & \frac{k}{m_w} & \frac{ca}{m_w} & \frac{ka}{m_w} & -\frac{k}{2m_w} & \frac{k}{2m_w} & v^2 & -g & 0 & 0 \\
1 & 0 & 0 & 0 & 0 & 0 & 0 & 0 & 0 & 0 & 0 & 0 & 0 & 0 & 0 & 0 & 0 & 0 & 0 & 0 \\
0 & -\frac{2f_{11}l\lambda}{Ir_0} & -\left(\frac{2f_{11}l^2}{Iv}+\frac{c_t}{I}\right) & 0 & -\frac{2f_{11}lr_0}{Iv} & 0 & 0 & 0 & 0 & 0 & 0 & 0 & 0 & 0 & 0 & 0 & \frac{2f_{11}l^2}{I} & 0 & 0 & 0 \\
0 & 0 & 1 & 0 & 0 & 0 & 0 & 0 & 0 & 0 & 0 & 0 & 0 & 0 & 0 & 0 & 0 & 0 & 0 & 0 \\
0 & -\frac{f_{11}\lambda}{I_a} & -\frac{f_{11}lr_0}{I_a v} & 0 & -\left(\frac{f_{11}{r_0}^2}{I_a v}+\frac{c_r}{I_a}\right) & 0 & 0 & 0 & 0 & 0 & 0 & 0 & 0 & 0 & 0 & 0 & \frac{f_{11}lr_0}{I_a} & 0 & 0 & 0 \\
0 & 0 & 0 & 0 & 0 & -\left(\frac{2f_{22}}{m_w v}+\frac{c}{m_w}\right) & -\frac{k}{m_w} & 0 & \frac{2f_{22}}{m_w} & 0 & \frac{c}{m_w} & \frac{k}{m_w} & -\frac{ca}{m_w} & -\frac{ka}{m_w} & \frac{k}{2m_w} & -\frac{k}{2m_w} & 0 & 0 & v^2 & -g \\
0 & 0 & 0 & 0 & 0 & 1 & 0 & 0 & 0 & 0 & 0 & 0 & 0 & 0 & 0 & 0 & 0 & 0 & 0 & 0 \\
0 & 0 & 0 & 0 & 0 & 0 & -\frac{2f_{11}l\lambda}{Ir_0} & -\left(\frac{2f_{11}l^2}{Iv}+\frac{c_t}{I}\right) & 0 & -\frac{2f_{11}lr_0}{Iv} & 0 & 0 & 0 & 0 & 0 & 0 & 0 & 0 & \frac{2f_{11}l^2}{I} & 0 \\
0 & 0 & 0 & 0 & 0 & 0 & 0 & 1 & 0 & 0 & 0 & 0 & 0 & 0 & 0 & 0 & 0 & 0 & 0 & 0 \\
0 & 0 & 0 & 0 & 0 & 0 & -\frac{f_{11}\lambda}{I_a} & -\frac{f_{11}lr_0}{I_a v} & 0 & -\left(\frac{f_{11}{r_0}^2}{I_a v}+\frac{c_r}{I_a}\right) & 0 & 0 & 0 & 0 & 0 & 0 & 0 & 0 & \frac{f_{11}lr_0}{I_a} & 0 \\
\frac{c}{m_b} & \frac{k}{m_b} & 0 & 0 & 0 & \frac{c}{m_b} & \frac{k}{m_b} & 0 & 0 & 0 & -\frac{2c}{m_b} & -\frac{2k}{m_b} & 0 & 0 & 0 & 0 & \frac{v^2}{2} & -\frac{g}{2} & \frac{v^2}{2} & -\frac{g}{2} \\
0 & 0 & 0 & 0 & 0 & 0 & 0 & 0 & 0 & 0 & 1 & 0 & 0 & 0 & 0 & 0 & 0 & 0 & 0 & 0 \\
\frac{ca}{I_b} & \frac{ka}{I_b} & \frac{c_t}{I_b} & 0 & 0 & -\frac{ca}{I_b} & -\frac{ka}{I_b} & \frac{c_t}{I_b} & 0 & 0 & 0 & 0 & -\frac{2ca^2}{I_b} & -\frac{2ka^2}{I_b} & \frac{ka}{I_b} & -\frac{ka}{I_b} & 0 & 0 & 0 & 0 \\
0 & 0 & 0 & 0 & 0 & 0 & 0 & 0 & 0 & 0 & 0 & 0 & 1 & 0 & 0 & 0 & 0 & 0 & 0 & 0 \\
0 & 0 & 0 & 0 & 0 & 0 & 0 & 0 & 0 & 0 & 0 & 0 & 0 & 0 & -\omega_1 & 0 & 0 & 0 & 0 & 0 \\
0 & 0 & 0 & 0 & 0 & 0 & 0 & 0 & 0 & 0 & 0 & 0 & 0 & 0 & 0 & -\omega_1 & 0 & 0 & 0 & 0 \\
0 & 0 & 0 & 0 & 0 & 0 & 0 & 0 & 0 & 0 & 0 & 0 & 0 & 0 & 0 & 0 & -\omega_2 & 0 & 0 & 0 \\
0 & 0 & 0 & 0 & 0 & 0 & 0 & 0 & 0 & 0 & 0 & 0 & 0 & 0 & 0 & 0 & 0 & -\omega_2 & 0 & 0 \\
0 & 0 & 0 & 0 & 0 & 0 & 0 & 0 & 0 & 0 & 0 & 0 & 0 & 0 & 0 & 0 & 0 & 0 & -\omega_2 & 0 \\
0 & 0 & 0 & 0 & 0 & 0 & 0 & 0 & 0 & 0 & 0 & 0 & 0 & 0 & 0 & 0 & 0 & 0 & 0 & -\omega_2
\end{bmatrix}$$

Equation 4.10 – RKF applied to two axle IRW vehicle

$$\boldsymbol{G_{kr}} = \begin{bmatrix} \mathbf{0} & \mathbf{0} & \mathbf{0} & \mathbf{0} & \mathbf{0} & \mathbf{0} \\ \mathbf{-1} & \mathbf{0} & \mathbf{0} & \mathbf{0} & \mathbf{0} & \mathbf{0} \\ \mathbf{0} & \mathbf{0} & \mathbf{0} & \mathbf{0} & \mathbf{0} & \mathbf{0} \\ \mathbf{0} & \mathbf{0} & \mathbf{0} & \mathbf{0} & \mathbf{0} & \mathbf{0} \\ \mathbf{0} & \mathbf{0} & \mathbf{0} & \mathbf{0} & \mathbf{0} & \mathbf{0} \\ \mathbf{0} & \mathbf{0} & \mathbf{0} & \mathbf{0} & \mathbf{0} & \mathbf{0} \\ \mathbf{0} & \mathbf{-1} & \mathbf{0} & \mathbf{0} & \mathbf{0} & \mathbf{0} \\ \mathbf{0} & \mathbf{0} & \mathbf{0} & \mathbf{0} & \mathbf{0} & \mathbf{0} \\ \mathbf{0} & \mathbf{0} & \mathbf{0} & \mathbf{0} & \mathbf{0} & \mathbf{0} \\ \mathbf{0} & \mathbf{0} & \mathbf{0} & \mathbf{0} & \mathbf{0} & \mathbf{0} \\ \mathbf{0} & \mathbf{0} & \mathbf{0} & \mathbf{0} & \mathbf{0} & \mathbf{0} \\ \mathbf{-\frac{1}{2}} & \mathbf{-\frac{1}{2}} & \mathbf{0} & \mathbf{0} & \mathbf{0} & \mathbf{0} \\ \mathbf{0} & \mathbf{0} & \mathbf{0} & \mathbf{0} & \mathbf{0} & \mathbf{0} \\ \mathbf{0} & \mathbf{0} & \mathbf{0} & \mathbf{0} & \mathbf{0} & \mathbf{0} \\ \mathbf{1} & \mathbf{0} & \mathbf{0} & \mathbf{0} & \mathbf{0} & \mathbf{0} \\ \mathbf{0} & \mathbf{1} & \mathbf{0} & \mathbf{0} & \mathbf{0} & \mathbf{0} \\ \mathbf{0} & \mathbf{0} & \mathbf{1} & \mathbf{0} & \mathbf{0} & \mathbf{0} \\ \mathbf{0} & \mathbf{0} & \mathbf{0} & \mathbf{1} & \mathbf{0} & \mathbf{0} \\ \mathbf{0} & \mathbf{0} & \mathbf{0} & \mathbf{0} & \mathbf{1} & \mathbf{0} \\ \mathbf{0} & \mathbf{0} & \mathbf{0} & \mathbf{0} & \mathbf{0} & \mathbf{1} \end{bmatrix}$$

Equation 4.11 – Input matrix for RKF two axle IRW vehicle

$$T = \begin{bmatrix} 0 & 0 & 0 & 0 & 0 & 0 & 0 & -1 & 0 & 0 & 0 & 0 & 1 & 0 & 0 & 0 & 0 & 0 & 0 & 0 \\ 0 & 0 & -1 & 0 & 0 & 0 & 0 & 0 & 0 & 0 & 0 & 0 & 1 & 0 & 0 & 0 & 0 & 0 & 0 & 0 \end{bmatrix}^T$$

Equation 4.12 - Control torque matrix

The re-formulated state space matrix, A_{kr} now has the leading and trailing wheelsets' curve radius and cant angle features included as 4 extra states. They can clearly be seen in the state variables in X_{kr}. The extra states have been produced from the previous input matrix, G, and, in turn, have created a new input matrix, G_{kr} which has the curved track features represented as their derivatives, and are shown in w_r. The control torque generated to actively steer the mechatronic vehicle is represented in matrix u. It is represented to replicate the control torque applied from a practical approach. This means that the torque is generated using the estimated yaw velocities $\widehat{\dot{\Psi}_{w1}}$ and $\widehat{\dot{\Psi}_{w2}}$, as the control torque signal will be derived from the estimated states, and not the theoretical states, which represent the dynamic system. A simple P controller is again used in this sensing approach. The dynamics of the actuators required to implement the control actions are neglected in the model. However, in practice, the dynamics of the actuator would contribute to the performance of the overall system.

6 practical sensors have been used for the re-formulated Kalman-Bucy Filter sensing scheme. The sensing scheme continues with the approach of using accelerometers and yaw gyroscopes mounted to the body of the vehicle to measure the body lateral acceleration and yaw velocity.

Suspension lateral and yaw displacements are also measured to provide the necessary feedback signals for the controller. The output equation is detailed in 4.14.

$$Y_m = C_{kr} \cdot X_{kr} + H \cdot v \tag{4.13}$$

Where:

$$C_{kr} = \begin{bmatrix} \frac{c}{m_b} & \frac{k}{m_b} & 0 & 0 & 0 & \frac{c}{m_b} & \frac{k}{m_b} & 0 & 0 & 0 & -\frac{2c}{m_b} & -\frac{2k}{m_b} & 0 & 0 & 0 & 0 & 0 & 0 & 0 & 0 \\ 0 & 0 & 0 & 0 & 0 & 0 & 0 & 0 & 0 & 0 & 0 & 0 & 0 & 0 & 1 & 0 & -\frac{v}{2} & 0 & -\frac{v}{2} & 0 \\ 0 & -1 & 0 & 0 & 0 & -\frac{1}{2} & 0 & 0 & 0 & 0 & 0 & \frac{1}{2} & 0 & 1 & 0 & a & 0 & 0 & 0 & 0 \\ 0 & 0 & 0 & 0 & 0 & \frac{1}{2} & 0 & -1 & 0 & 0 & 0 & -\frac{1}{2} & 0 & 1 & 0 & -a & 0 & 0 & 0 & 0 \\ 0 & 0 & 0 & -1 & 0 & 0 & 0 & 0 & 0 & 0 & 0 & 0 & 0 & 0 & 0 & 1 & \frac{a}{2} & 0 & \frac{a}{2} & 0 \\ 0 & 0 & 0 & 0 & 0 & 0 & 0 & 0 & 0 & -1 & 0 & 0 & 0 & 0 & 0 & 1 & -\frac{a}{2} & 0 & -\frac{a}{2} & 0 \end{bmatrix}$$

Equation 4.14 - RKF output equation

C_k is formed using rows 2,4,7,9,10,11,12 and 14 of A_k, v are the vectors representing the measurement noises of the sensors, which in this case are:

$$[\dot{y}_b \quad \dot{\Psi}_b \quad y_{b1} - y_1 \quad y_{b2} - y_2 \quad \Psi_{b1} - \Psi_1 \quad \Psi_{b2} - \Psi_{b2}]^T$$

They are represented in the matrix form as follows:

$$H = \begin{bmatrix} 1 & 0 & 0 & 0 & 0 & 0 \\ 0 & 1 & 0 & 0 & 0 & 0 \\ 0 & 0 & 1 & 0 & 0 & 0 \\ 0 & 0 & 0 & 1 & 0 & 0 \\ 0 & 0 & 0 & 0 & 1 & 0 \\ 0 & 0 & 0 & 0 & 0 & 1 \end{bmatrix} \quad v = [v_1 \quad v_2 \quad v_3 \quad v_4 \quad v_5 \quad v_6]^T$$

Equation 4.15 - Measurement noise matrix and vector

The estimated states are calculated using equation (4.16).

$$\hat{\dot{X}}_{kr} = A_{kr}\, \hat{X}_{kr} + K_r(Y_m - \hat{Y}_k) \tag{4.16}$$

Where K_r is the gain matrix designed offline, $\mathrm{MATLAB}^{\mathrm{TM}}$ is used to create the gain matrix using the function (LQE). Expressing both the input and measurement signals as covariances, allows the linear quadratic generator to produce an optimal stationary gain matrix offline. This is then used to provide an optimised estimate of the vehicles states.

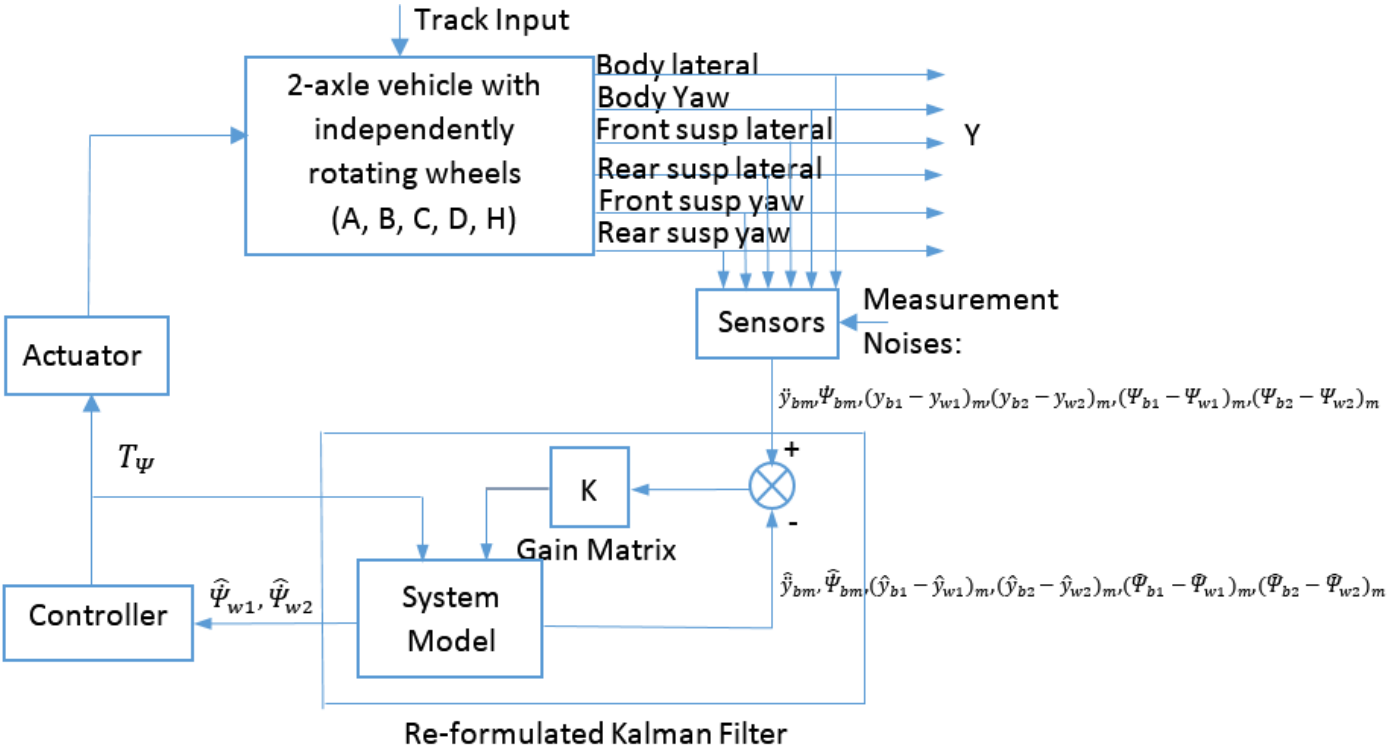

Figure 4.28 - Block diagram of sensing scheme

Figure 4.28 provides a block diagram of the closed loop sensing scheme. The figure shows how the control torque is generated, using the estimated yaw velocities of the leading and trailing wheelset. This signal is given to the actuator that is converted into an actuation torque to actively steer the vehicle.

4.6. Simulation Results

To assess the performance of the sensing scheme, with the use of the re-formulated Kalman-Bucy filter approach, both straight and curved track features are considered. A curved track radius of 1000m connected to a straight track on either end, via a transition, is used. The curved track is also canted inwards to give zero cant deficiency

The same sensing approach has been initially used with the re-formulated Kalman-Bucy filter sensing scheme. Therefore, the covariance of measurement noises $R1$, $R2$, $R3$ and $R4$ have remained set to 2% of their maximum values which is determined by taking three times their true R.M.S value on the straight track with irregularities; plus the peak value of their responses on the pure curved track. Furthermore, measurement noises $R5$ & $R6$ are set to 10^{-12} to maintain good curving performance.

4.6.1 The 'Hunting' Method

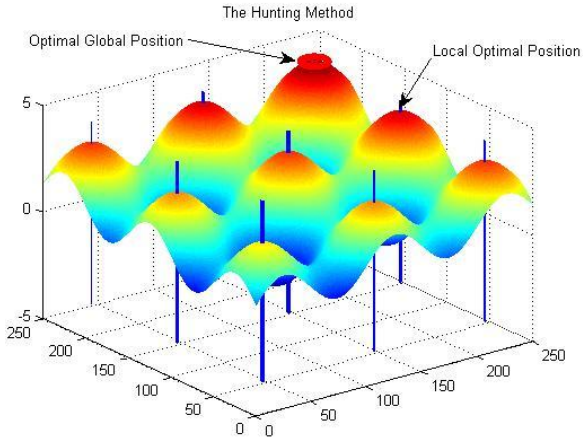

Figure 4.29 - The 'hunting' method

Previous studies on the optimisation of the state estimations using RKBF have shown that there is a design trade-off inherent of the re-formulated Kalman-Bucy filter (Li, 2001). This is because the gain matrix designed offline produces either good straight or curved track performance. Previous methods of trying to optimise the sensing scheme have minimised the error between the true and estimated responses of the system, on both the straight and curved track. Although this process is useful at quantifying the performance of the system well, the method becomes increasingly complex when the number of input variables increases as the amount of variants of covariance values increases exponentially. Moreover, the method cannot 'self-learn' as it has predetermined values of input covariances pre-set.

A new approach to returning the optimum response of the sensing scheme on both the straight and curved track has been devised for this study; a process named 'hunting', which is a mathematical optimising technique called hill climbing. The iterative algorithm enables the user to define an ideal target score; in this case the ideal score is to return zero error between the measured and estimated responses for both the curved and straight track of the system, and to send a 'hunter' to find a set of covariance values which will return that performance. The rule of the method attempts to better the previous output performance. This means that the algorithm will always work towards 'self-learning'. Varying the amount of 'hunters' and the amount of steps improves the effectiveness of the algorithm. However, as a result, it increases the simulation time.

Figures 4.30 ~ 4.35 show the comparison of the sensing scheme using the re-formulated Kalman Filter and the basic Kalman filter which assumes that the curved track features are known values. The figures compare the responses of the measured (how the vehicle responds) and estimated (what the RKF estimates) responses of the leading and trailing wheelsets.

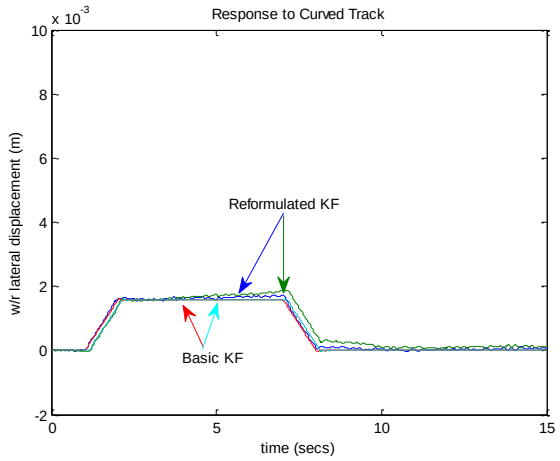

Figure 4.30 – RKF vs. KF lat. disp

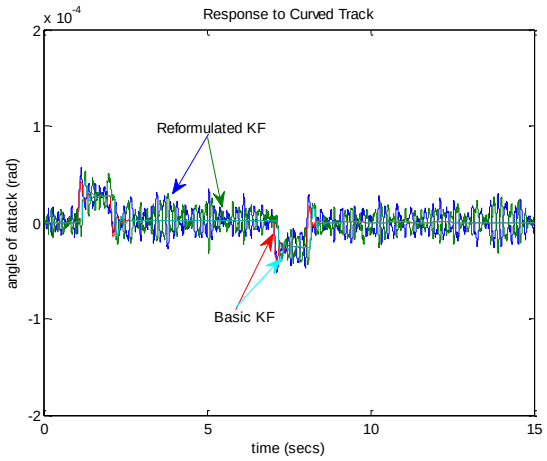

Figure 4.31 - – RKF vs. KF angle of attack

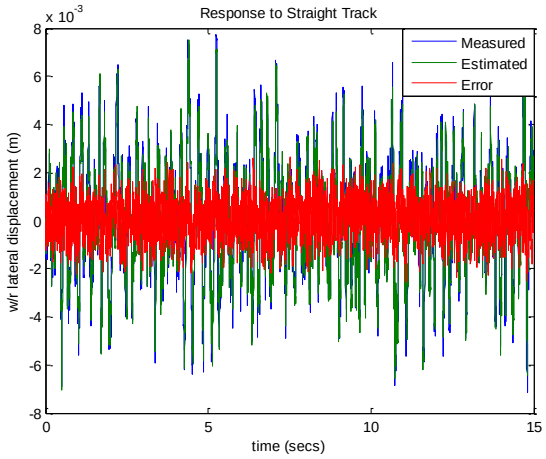

Figure 4.32 - – RKF vs. KF (lat. disp)

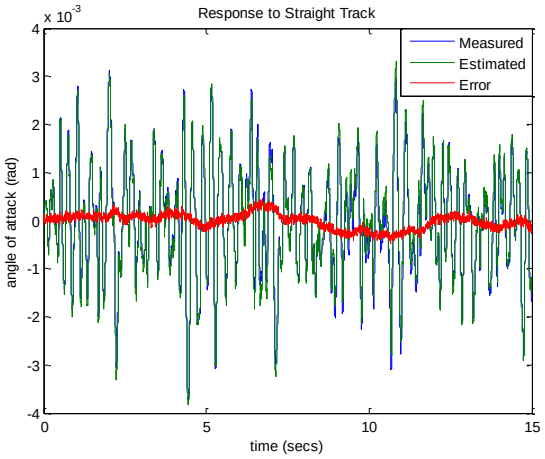

Figure 4.33 - – RKF vs. KF (angle of attack)

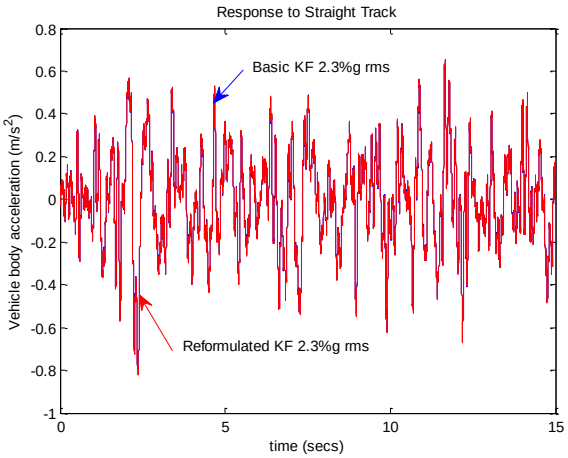

Figure 4.34 - – RKF vs. KF (lat. acceleration)

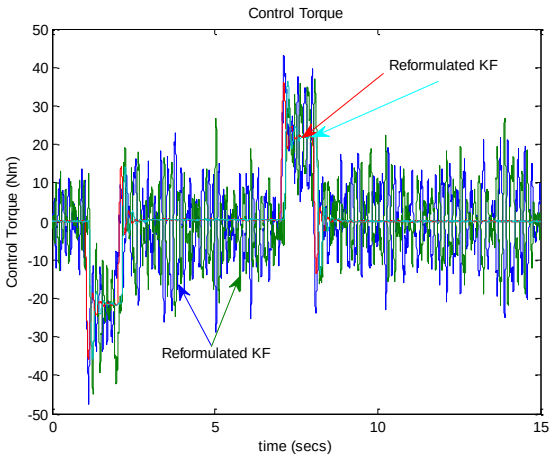

Figure 4.35 - – RKF vs. KF (control torque)

The comparison of the responses shows that there is still a level of inaccuracy present. The control torque generated has a relatively large amount of noise on top of the signal; which has resulted in a poor curving performance from the system. The straight track performance of the sensing scheme using the reformulated Kalman filter is shown in figures 4.32 and figure 4.33. The relatively large error shows that the performance has been hindered as a result of the poor

feedback from the sensors. This in turn causes a poor estimation of the states as a result. The ride comfort, however, has maintained its level of performance compared to the ideal Kalman filter sensing approach.

4.6.2 Improving Measurement Sensors

The previous section of this study highlighted that although the sensing scheme, using the re-formulated Kalman filter provides similar straight and curved track performance compared to the sensing scheme using the basic Kalman filter with the curved track features assumed known, there is still a level of inaccuracy due to the level of noise associated with the responses; in particular the noise on the control torques generated to provide active steering of the mechatronic vehicle. Therefore, as a result, improving the body yaw velocity sensors accuracy by setting the measurement noise to 10^{-12} is a necessity to improving the overall performance of the sensing scheme.

Figures 4.36 ~ 4.39 compare the curving performance of the actively controlled railway vehicle using the basic Kalman-Bucy filter with curvature and cant angle features set to known against the actively controlled railway vehicle using the re-formulated Kalman-Bucy filter approach with the improved yaw gyroscope sensor.

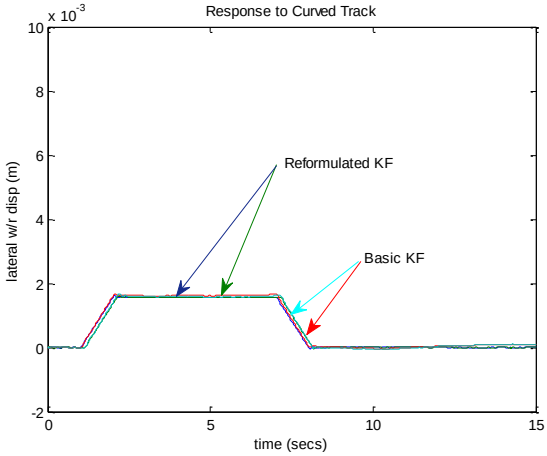

Figure 4.36 - – RKF vs. KF (lat. disp)

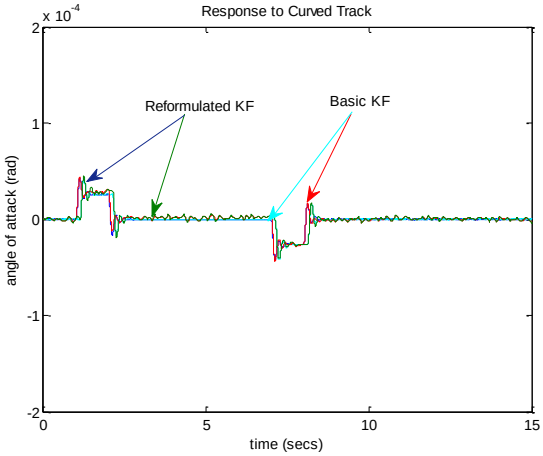

Figure 4.37 – RKF vs. KF (angle of attack)

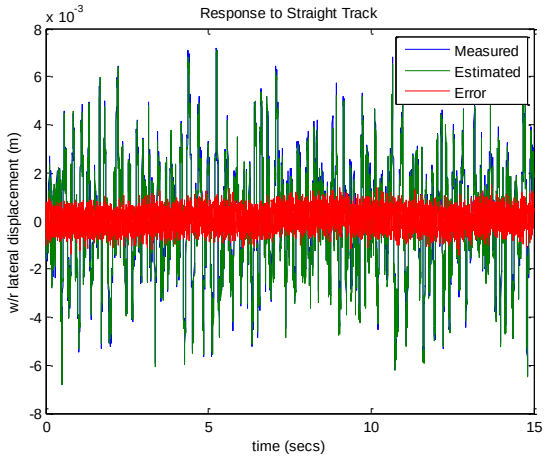

Figure 4.38 - RKF vs. KF (lat. disp)

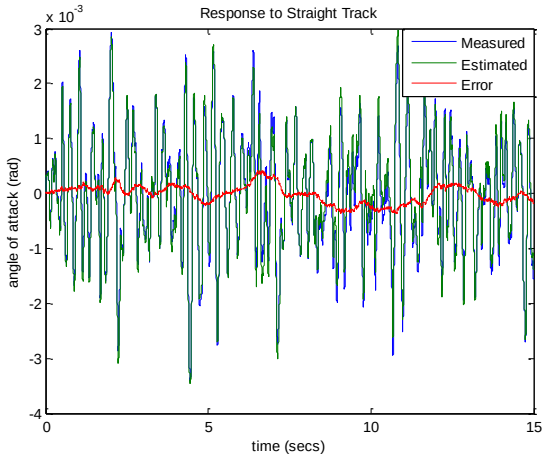

Figure 4.39 - RKF vs. KF (angle of attack)

The track input covariance Q_{kr} was determined using the 'hunting' method and produced the covariance matrix: $Q_{kr} = [1e^{-4} \quad 1e^{-4} \quad 2e^{-7} \quad 2e^{-3} \quad 2e^{-7} \quad 2e^{-3}]$.

The figures show that an improved overall average optimal performance across the curved and straight tracks has been achieved. The re-formulated Kalman filter sensing scheme has maintained the curving performance compared to the basic Kalman filter, using the curved track features as known 'inputs'.

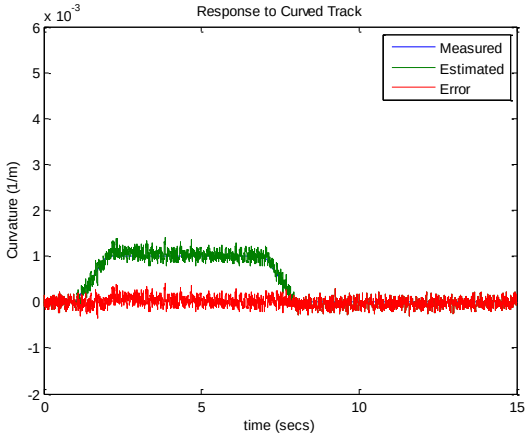

Figure 4.40 – Estimation of curved track

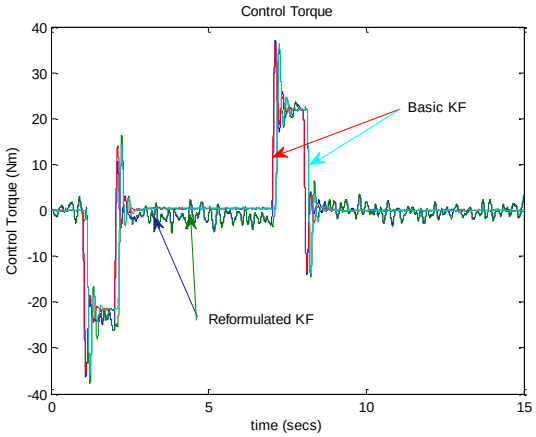

Figure 4.41 – Estimation of contol torque

Figure 4.40 and figure 4.41 show the re-formulated Kalman filters' estimation of the curvature and control torque; which is essential for the system to provide an accurate optimal gain matrix (K_r), to actively steer the vehicle. The figures show that, compared to the ideal curvature and control torque required and represented in the basic Kalman filter model, the re-formulated Kalman filter model has maintained that level of accuracy with minimal error.

Contrary to previous studies, the performance on the straight track does not appear to be hindered by the trade-off that is usually associated from reformulating the Kalman-Bucy filter (Li, 2001).

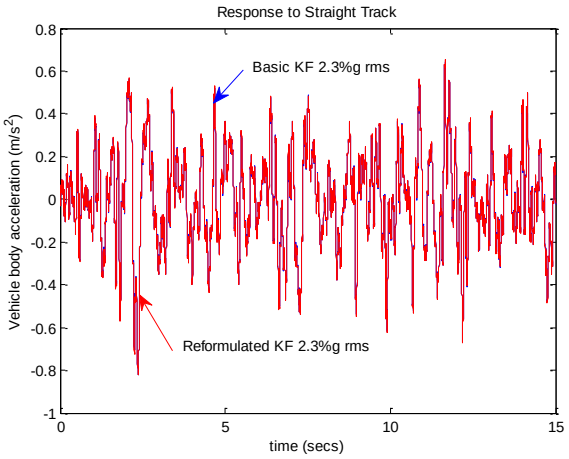

Figure 4.42 – RKF vs. KF – Ride performance

Figure 4.42 shows the comparison in body lateral acceleration between the basic active control strategy using the basic Kalman Filter assuming the curved track features as known values; and the re-formulated Kalman Filter approach. The responses have been quantified by taking the route mean square (R.M.S) of the signal. It can be seen that the lateral acceleration exerted on the passenger has maintained at a low percentage g force which is essential as one of the criterion for the control scheme is to maintain or improve the ride comfort of the vehicle.

4.7. Robustness

Another criterion of the effectiveness of the sensing scheme is whether the system can maintain its level of performance under parameter variations, especially at the wheel/rail contact. Therefore it is important to ensure the robustness of the sensing scheme in terms of its stability and curving performance.

This section of the study will assess the performance of the sensing scheme, whilst varying wheel conicity and longitudinal creep forces.

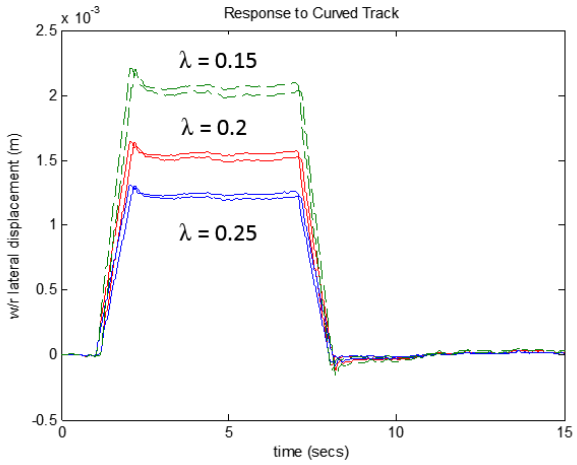

Figure 4.43 - Robustness check (lat. displacement)

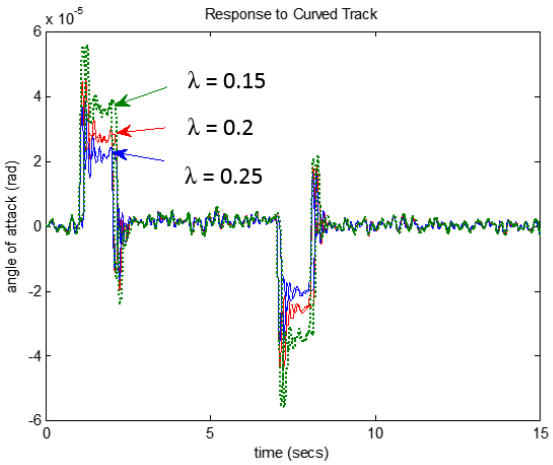

Figure 4.44 - Robustness check (angle of attack)

Figure 4.43 and figure 4.44 show the wheel-rail lateral displacement and yaw angle on the curved track when the conicity in the physical model changes in the range of 0.2±0.05. The simulation results show that the system is stable under variations in conicity; although there is a scaling factor on the quasi-static lateral displacement and the yaw angle during the curve transition due to the change in wheelset conicity.

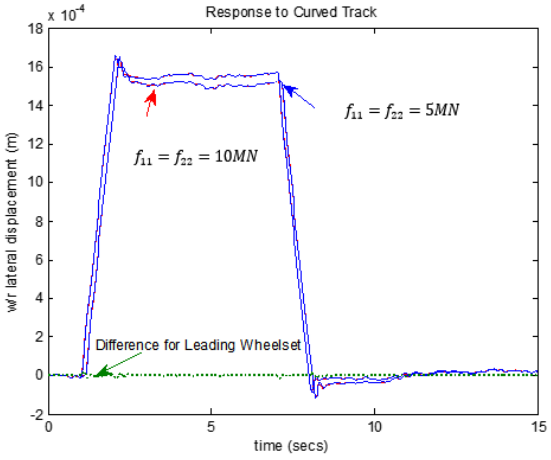

Figure 4.45 - Robustness check (lat. displacement)

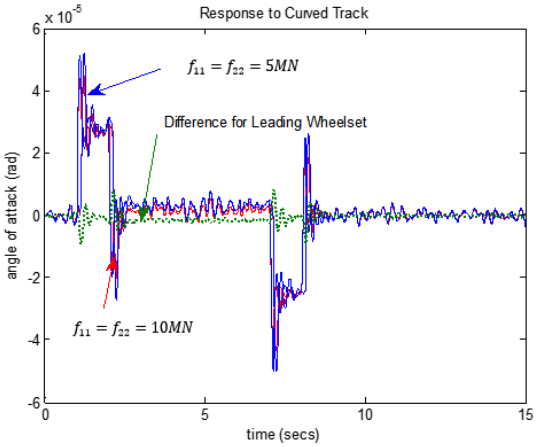

Figure 4.46 - Robustness check (angle of attack)

Figure 4.45 and 4.46 present the simulation results when the lateral and longitudinal creep coefficient are varied from 10MN to 5MN. The figures show that the proposed scheme reminas robust, as the wheel-rail lateral displacement and yaw angle of the leading wheelset remain largely unchanged and only a small scaling factor error is shown.

4.8. Conclusions

This study has presented the development of a novel model based sensing scheme to provide high integrity feedback variables, to enable the practical implementation of the active control of a railway vehicle with IRW. The study has shown that reformulating can provide the same curving performance as the previous study, which uses a basic Kalman-Bucy Filter assuming the curved track features as known. Furthermore, the re-formulated Kalman Filter model has shown to maintain the same level of straight track stability and ride comfort as the ideal active control model.

Initial results using measurement noises $R5$ and $R6$, set as 10^{-12}, have shown that, although the sensing scheme provided good curving and straight track stability, there was a relatively large inaccuracy due to the number of noise associated with the signals. This inaccuracy was assumed to be due to the lack of accuracy from the sensors. Measurement noise covariance $R2$, representing the noise of the sensor measuring the vehicles yaw velocity, was set to the same as $R5$ and $R6$; to see if the system could maintain the level of performance seen from the Kalman Filter model, with the curved track features set to known values. The results show that the sensing scheme produces similar levels of curved and straight track performances as the ideal active control model.

The robustness of the proposed sensing scheme has also been examined, to show that the sensing scheme can maintain the same level of performance when varying the wheelset conicity and creep forces. The simulation results have shown that the proposed scheme is stable and maintains a good level of curving performance; the only issue is that the lateral wheel-rail displacement has a scale factor error when the wheelset conicity varies.

4.9. Sensor Optimisation

Part of the optimisation process of this study is to produce a cost effective sensing scheme using practical sensors. The following study uses the previous model's re-formulated Kalman-Bucy filter approach, to return active steering of the railway vehicle; but will assess the performance of the system with a reduced number of sensors.

The same body mounted sensors have been used again to maintain a sensing scheme that avoids mounting any sensors onto the bogies or wheelsets, to avoid the sensors being mounted in an arduous environment.

As the previous section of the performance study of the re-formulated Kalman filter has shown it was essential to have measurement noises $R2$, $R5$ and $R6$ set to 10^{-12}, to return good curving

performance. As a result, a three sensor approach has been used in this section, which represent the vehicle body yaw velocity, and the leading and trailing suspension yaw deflections.

Figure 4.47 and figure 4.48 compare the curving performance of the six sensor Kalman-Bucy filter using curved track features as known inputs to the system; and the three sensor re-formulated Kalman-Bucy filter.

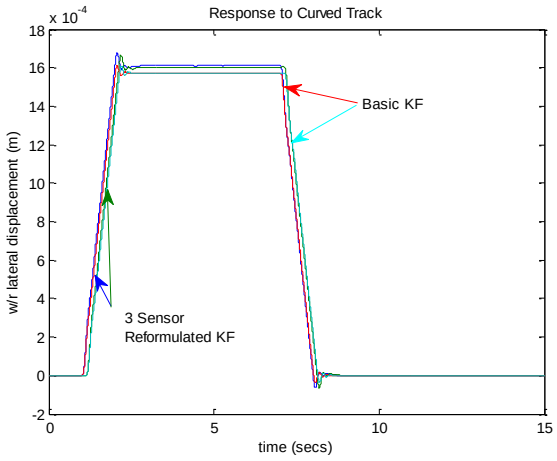

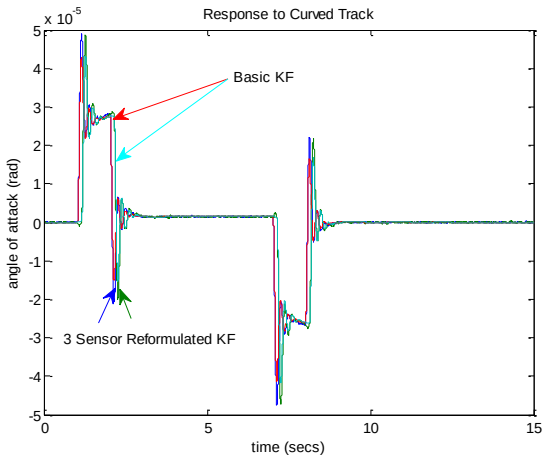

Figure 4.47 – Sensor optimisation (lat. displacement) **Figure 4.48 - Sensor optimisation (angle of attack)**

The figures show that the curving performance has been maintained when compared to the ideal case.

Figure 4.49 and figure 4.50 also show that the estimation of the curved track features has been maintained with little error between the measured and estimated response.

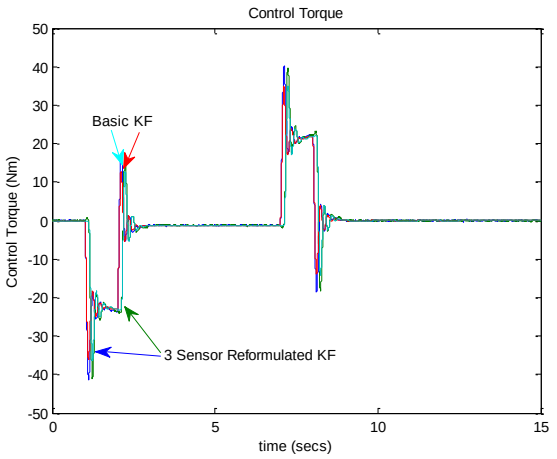

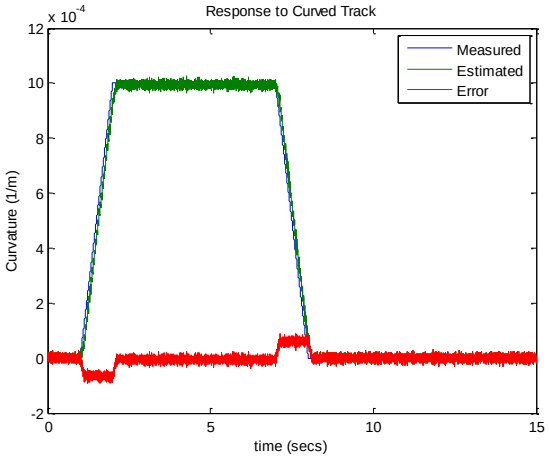

Figure 4.49 - Sensor optimisation (control torque) **Figure 4.50 - Sensor optimisation (curved track estimation)**

This low amount of error can be understood when looking at the effectiveness of the three sensor re-formulated Kalman filter model, estimating the control torques required to actively steer the vehicle.

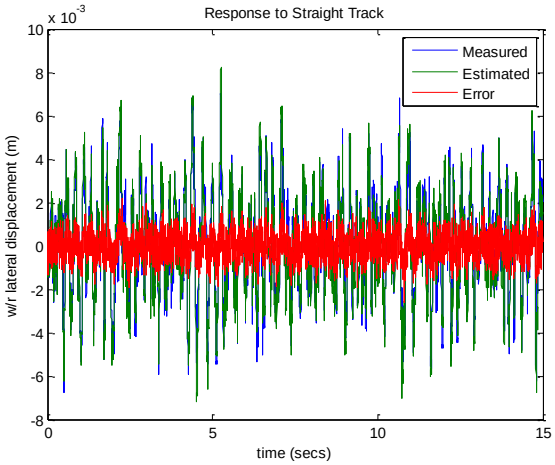

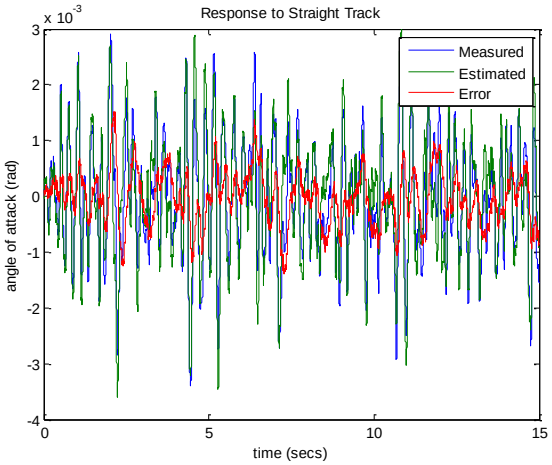

Figure 4.51 - Sensor optimisation (straight track lat. disp) **Figure 4.52 - Sensor optimisation (straight track angle of attack)**

The stability on the straight track has suffered as a result of the reduction in sensors. The lateral displacement error between the measured and estimated response has increased by 30%, and the error on the yaw angle has tripled, however the error between the measured and estimated is still low (0.54mm lateral displacement error and 0.48mrad yaw angle error).

Figure 4.53 and figure 4.54 show that if the offline gain matrix is tuned to provide better straight track performance, the reduced sensing scheme can provide good straight track performance.

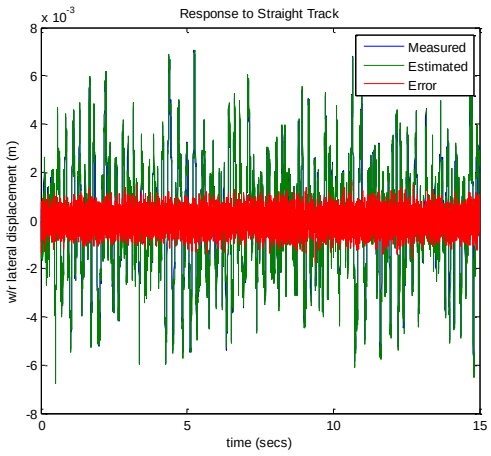

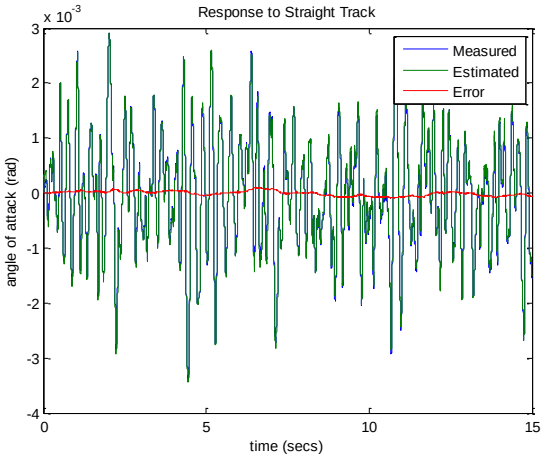

Figure 4.53 - Sensor optimisation (straight track lat. disp) **Figure 4.54 - Sensor optimisation (straight track angle of attack)**

4.10. Robustness Check

It is important to ensure that the reduced sensing scheme can maintain its curving performance under parameter variations which is a common occurrence in the real world. Therefore, the following section is going to assess the performance of the reduced sensor sensing scheme, under variations of conicity, and longitudinal and lateral creep force.

Figure 4.55 and figure 4.56 present the simulation results when the wheelset conicity is altered between 0.2±0.05.

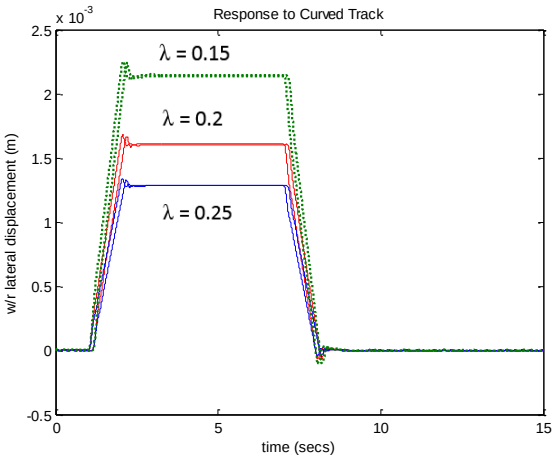

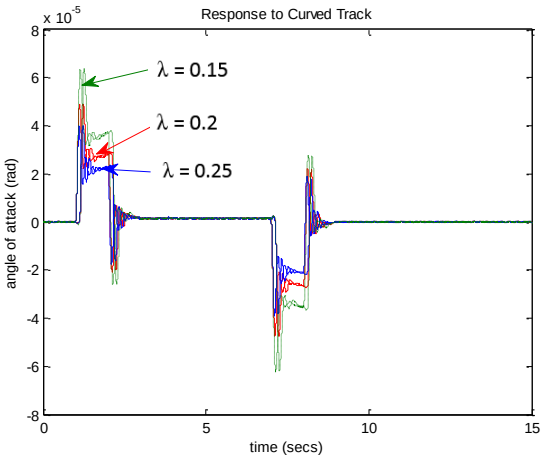

Figure 4.55 – Robustness check (lateral displacement) Figure 4.56 - Robustness check (angle of attack)

The simulation results show that the curving performance is maintained for both the leading and trailing wheelset: with the only error being the scaling factor on both the lateral displacement and yaw angle on the curve transitions; due to the change in wheelset conicity.

Figure 4.57 and figure 4.58 present the simulation results when the lateral and longitudinal creep coefficients are varied from 10MN to 5MN.

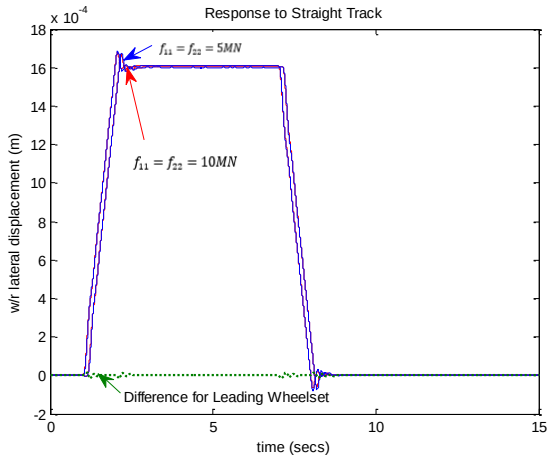

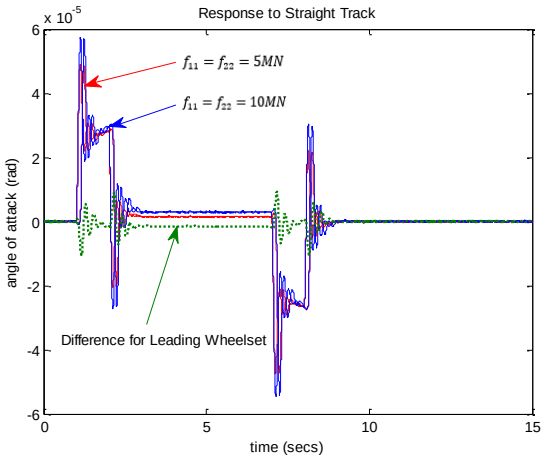

Figure 4.57 - Robustness check (lateral displacement) Figure 4.58 - Robustness check (angle of attack)

The figures show that the reduced sensor sensing scheme remains robust. Wheel-rail lateral displacements for both leading and trailing wheelsets remain largely unchanged; and only a small scaling factor error for the yaw angle on both curve transition and steady state curve is seen.

4.11. Conclusion

This study has presented an optimised sensing scheme using only three sensors mounted to the body of the vehicle to provide active steering of a mechatronic railway vehicle. The sensing scheme has used a re-formulated Kalman filter to estimate the curved track features as well as the necessary feedback signals for the controller.

The simulation results have shown that the proposed scheme maintains its control to actively steer the vehicle and also maintains its stability and isolation on the straight track. The findings show that the straight track performance is hindered slightly as a result of the reduction in measurements taken; but is considered to still provide a sufficient estimate of the states. The findings have also discussed that if the gain matrix is weighted towards improving better straight track performance, the sensing scheme can provide the same level of response as the six sensor version of the scheme. This will, however, hinder the curved track performance as a result: it may be considered that if the same level of straight and curved track performance is required, that ~~a~~ two Kalman filters are used; with two separate Kalman gains designed to provide both straight and curved track performance. This method would only be considered if it were a more cost effective approach to providing the six sensor re-formulated-Kalman-Bucy filter; which has proven to provide a high level of response on both the straight and curved track.

The robustness of the proposed sensing scheme is also examined to assess the stability and curving performance of the system, under varying parameters. The simulation results have concluded that the sensing scheme is stable and is able to maintain god curving performance, with the exception of that the lateral wheel-rail displacements and yaw angle, which has a scale factor error as the conicity varies.

Chapter 5 Overall Conclusions & Further Work

5.1. Overall Conclusions

This thesis has presented the development of an active control system which may be implemented onto a mechatronic vehicle. It has provided an insight into a possible solution to the problem with mounting the sensors onto the axle in order to gain the full state feedback signals for optimal control of independently rotating wheels. Sensors mounted to the vehicle body, using practical and low cost sensors, have been used to overcome the arduous environment at the axle.

A mathematical representation of a single axle independently rotating wheelset taking lateral, yaw and rotational degrees of freedom, has been initially used; and a re-formulated Kalman-Bucy filter has been used to estimate the state variables of the IRW. Good straight and curved track performances were achieved. A two-axle mechatronic railway vehicle, with independently rotating wheels running on both random and curved tracks, has been derived, and used, in a state space form. An initial study using six sensors, and a basic Kalman-Bucy filter, has been used to provide the optimal controller with the signals to actively steer the IRW vehicle. In this initial study, the curved track features were set as known values. Simulations results have shown that, by carefully selecting the correct values of measurement noise covariances, the sensing scheme could not only provide positive steering to the IRW vehicle, but also improve the vehicle ride quality by 19.5% compared with the passive suspension. The robustness of the sensing scheme has also been examined in the presence of the creep coefficient and the conicity variations. The simulation results have shown that, in general, the proposed scheme is stable and is able to maintain a good curving performance; although the lateral wheel-rail displacement essentially has a scale factor error when the wheelset conicity varies.

Using a re-formulated Kalman-Bucy filter to include the curved track features into the state space representation of the mechatronic vehicle in the same six sensor control scheme has provided the same curving performance as the basic Kalman-Bucy filter assuming the curved track features as known. The re-formulated Kalman filter model has shown to maintain the same level of straight track stability and ride comfort as the ideal active control model. The robustness of the proposed sensing scheme has also been examined. The simulation results show that the sensing scheme is stable and maintains a good level of curving performance, except, there is a scale factor error when the wheelset conicity varies.

An optimisation process has been undertaken to produce the most cost effective sensing scheme. Three sensors mounted to the body of the vehicle, to provide active steering of a mechatronic

railway vehicle, using the re-formulated Kalman-Bucy filter, maintains its control to actively steer the vehicle. The findings have shown that the straight track performance is hindered slightly as a result of the reduction in measurements is taken; however if the gain matrix is weighted correctly, an improved straight track performance is observed. The robustness of the proposed sensing scheme is also examined to assess the stability and curving performance of the system under varying parameters. The simulation results have concluded that the sensing scheme is stable and is able to maintain god curving performance, although there is a scale factor error as the conicity varies.

5.2. Further work

This study has continued with the development of a sensing scheme. However there are still various areas in which the project can be further developed.

The previous chapter highlighted that the re-formulated Kalman-Bucy works well to estimate the curved track features. However, when reducing the sensors, a typical compromise had to be made in order to provide both good straight and curved track performance of the sensing scheme. The model has only used a simple P controller to develop the signal to provide active steering of the system; one possible development of the sensing scheme would be to change the type of controller used to a PI or PID controller.

The use of real track data may be considered to develop the sensing scheme. One of the main issues with developing artificial track data from a power spectral density is that the features of the track are lost. The use of real track data would be a natural progression of the development of this sensing scheme.

(Mei and Goodall, 2001) included actuator dynamics into the case to provide an even more practical example of the system. The addition of actuator dynamics would further develop the sensing scheme as actuator dynamics would affect the performance of the active control of the system.

The modelling of the system is solely a linear approach; whereas the dynamics of a railway vehicle are highly non-linear. A possible development of the project would be to include non-linearities within the dynamic representation of the mechatronic railway vehicle to further develop the project.

The intuitively formulated method to actively steer the vehicle could be developed to compare the performance of the optimal control strategy produced in this thesis. It is understood that full state feedback isn't necessary to actively steer the vehicle, and by using a low pass filter to eradicate

any high frequencies as well as integrating the lateral acceleration and yaw velocity, using a filtering technique, the necessary states to feed into the controller could be generated.

References

Akbari, A. and Lohmann, B. (2010) 'Output feedback H ∞/GH 2 preview control of active vehicle suspensions: a comparison study of LQG preview.' *Vehicle System Dynamics*, 48(12) pp. 1475-1494.

Bruni, S., Goodall, R., Mei, T. X. and Tsunashima, H. (2007) 'Control and monitoring for railway vehicle dynamics.' *Vehicle System Dynamics*, 45(7-8) pp. 743-779.

Charles, G., Goodall, R. and Dixon, R. (2008) 'Model-based condition monitoring at the wheel–rail interface.' *Vehicle System Dynamics*, 46(sup1) pp. 415-430.

Cheli, F., Corradi, R., Mapelli, F. and Mauri, M. (2002) *Motion control of a bogie with independently motorised wheels.*

Chi, M., Zeng, J., Guo, W., Zhang, W. and Jin, X. (2009) 'Analysis on Steering Capability of a New Bogie with Independently Rotating Wheels.' *International Journal of Railway*, 2(4) pp. 164-169.

Chui, C. K. and Chen, G. (2009) *Kalman filtering: With real-time applications.* Springer.

Diana, G., Bruni, S., Cheli, F. and Resta, F. (2003) 'Active control of the running behaviour of a railway vehicle: stability and curving performances.' *Vehicle System Dynamics*, 37 pp. 157-170.

Dukkipati, R. V. and Narayanaswamy, S. (1999) 'Performance of a Rail car equipped with Independently Rotating Wheelsets Having Yaw Control.' *Journal of Rail and Rapid Transit*, 213(1) pp. 31-38.

Dukkipati, R. V., Narayana Swamy, S. and Osman, M. O. M. (1992) 'Independently Rotating Wheel System for Railway Vehicles - A State of the Art Review.' *Vehicle System Dynamics*, 21 pp. 297 - 330.

Eickhoff, B. (1991) 'The application of independently rotating wheels to railway vehicles.' *Proceedings of the Institution of Mechanical Engineers, Part F: Journal of Rail and Rapid Transit*, 205(1) pp. 43-54.

Eickhoff, B. and Harvey, R. (1989) 'Theoretical and experimental evaluation of independently rotating wheels for railway vehicles.' *The Dynamics of Vehicles on Roads and Tracks, Proceedings of 11th IAVSD Symposium*, pp. 190-202.

Fallah, M. S., Bhat, R. and Xie, W. F. (2009) 'H ∞ robust control of semi-active Macpherson suspension system: new applied design.' *Vehicle System Dynamics*, 48(3) pp. 339-360.

Frederich, F. (1989) 'Dynamics of a bogie with independent wheels.' *Vehicle System Dynamics: International Journal of Vehicle Mechanics and Mobility,*, 19 pp. 271-232.

Goodall and Li (2000) 'Solid Axle and Independently-Rotating Railway Wheelsets - A Control Engineering Assessment of Stability.' *Vehicle System Dynamics*, 33(1) pp. 57-67.

Goodall, R. (1997) 'Active Railway Suspensions: Implementation Status and Technological Trends.' *Vehicle System Dynamics*, 28(2-3) pp. 87-117.

Goodall, R. (1998) 'Steer-by-Wire - A Railway Technology for the Future?' *International Congress Railtech*, 98(1) pp. 67-76.

Goodall, R. and Mei, T. (2000) 'LQG and GA Solutions for Active Steering of Railway Vehicles.' *IEE Proceedings - Control Theory and Applications*, 147(1) pp. 111-117.

Goodall, R. and Mei, T. X. (2001) 'Mechatronic strategies for controlling railway wheelsets with independently rotating wheels.' *Advanced Intelligent Mechatronics*, 1 pp. 225-230.

Goodall, R. M. and Kortüm, W. (1983) 'Active Controls in Ground Transportation — A Review of the State-of-the-Art and Future Potential.' *Vehicle System Dynamics*, 12(4-5) pp. 225-257.

Goodall, R. M. and Kortüm, W. (2002) 'Mechatronic developments for railway vehicles of the future.' *Control Engineering Practice*, 10(8) pp. 887-898.

Gretzschel and Bose. (2000) 'A Mechatronic Approach for Active Influence on Railway Vehicle Running Behaviour.' *In Proceeding of 16th IAVSD Symposium – The Dynamics of Vehicle on Roads and on Tracks.* Vol. 33. Pretoria, South Africa: pp. 418-430.

Gretzschel, M. and Bose, L. (2002) 'A new concept for integrated guidance and drive of railway running gears.' 10(9) pp. 1013-1021.

Gretzschel, M. and Jaschinski, A. (2004) 'Design of an Active Wheelset on a Scaled Roller Rig.' *Vehicle System Dynamics*, 41(5) pp. 365-381.

Grewal, M. S. and Andrews, A. P. (1993) *Kalman filtering: theory and practice.* Prentice-Hall.

Gruszecki, J., Grzybowski, J. and Rzucidło, P. (2005) 'Electro-mechanical actuators for general aviation fly-by-wire aircraft.' *Aviation*, 9(1) pp. 19-25.

Iwnicki, S. (2006) *Handbook of railway vehicle dynamics.* crc Press.

Jiang, Z., Matamoros-Sanchez, A. Z., Zolotas, A., Goodall, R. and Smith, M. (2013) 'Passive suspensions for ride quality improvement of two-axle railway vehicles.' *Proceedings of the Institution of Mechanical Engineers, Part F: Journal of Rail and Rapid Transit*, December 19, 2013,

Kalman, R. E. (1960) 'A new approach to linear filtering and prediction problems.' *Journal of basic Engineering*, 82(1) pp. 35-45.

Karnopp, D. (1978) 'Are active suspensions really necessary?' *In Mechanical Engineering.* Vol. 101. New York: ASME, pp. 86-86.

Kim, M. S. (2011) 'Measurement of the wheel-rail relative displacement for the active wheelsets steering system using the image processing algorithm.' *In Proceedings of the 13th WSEAS international conference on mathematical and computational methods in science and engineering*. Catania, Sicily, Italy, 2074904: World Scientific and Engineering Academy and Society, pp. 242-246.

Kleine, S. and Niekerk, J. L. V. (1998) 'Modelling and Control of a Steer-By-Wire Vehicle.' *Vehicle System Dynamics*, 29(sup1) pp. 114-142.

Li, H. (2001) *Measuring systems for active steering of railway vehicles.* Doctor of Philosophy. Loughborough University.

Li, H. and Goodall, R. M. (1999) 'Linear and non-linear skyhook damping control laws for active railway suspensions.' *Control Engineering Practice*, 7(7) pp. 843-850.

Li, H. and Goodall, R. M. (1999) 'State estimation for active steering of railway vehicles.' *In 14th World Congress of IFAC.* Vol. 1. Beijing: pp. 133-138.

Li, H., Mei, T., Pearson, J. and Goodall, R. (2002) 'Non-linear Kalman filter estimation for active steering of profiled rail-wheels.' *In 15th Triennial World Congress, IFAC.* Vol. 15. Barcelona, Spain: pp. 424-424.

Li, P., Goodall, R., Weston, P., Seng Ling, C., Goodman, C. and Roberts, C. (2007) 'Estimation of railway vehicle suspension parameters for condition monitoring.' *Control Engineering Practice*, 15(1) pp. 43-55.

Liang, B. and Iwnicki, S. D. (2007) 'An Experimental Study of Independently Rotating Wheels for Railway Vehicles.' *In Mechatronics and Automation, 2007. ICMA 2007. International Conference on.* Vol. 1, 5-8 Aug. 2007: pp. 2282-2286.

Liang, B., Iwnicki, S. D. and Swift, F. J. (2004) 'Independently Rotating Wheels with Induction Motors for High-Speed Trains.' *In ASME 7th Biennial Conference on Engineering Systems Design and Analysis.* Vol. 2. Manchester, England: pp. 21-26.

Matsumoto, A., Sato, Y., Ohno, H., Shimizu, M., Kurihara, J., Tomeoka, M., Saitou, T., Michitsuji, Y., Tanimoto, M., Sato, Y. and Mizuno, M. (2012) 'Continuous observation of wheel/rail contact forces in curved track and theoretical considerations.' *Vehicle System Dynamics*, 50(sup1) pp. 349-364.

Mei and Goodall. (2000) 'Wheelset control strategies for a two-axle railway vehicle.' *In The dynamics of vehicles on roads and on tracks. Vehicle System Dynamics.* Vol. 33. Pretoria, South Africa: IAVSD,

Mei, T. and Goodall, R. (2003) 'Practical strategies for controlling railway wheelsets independently rotating wheels.' *Journal of dynamic systems, measurement, and control*, 125(3) pp. 354-360.

Mei, T. and Li, H. (2008a) 'Control design for the active stabilization of rail wheelsets.' *Journal of Dynamic Systems, Measurement, and Control*, 130(1) p. 011002.

Mei, T. and Li, H. (2008b) 'Monitoring train speed using bogie mounted sensors—Accuracy and robustness.' *In Railway Condition Monitoring, 4th IET International Conference*. Derby: IET, pp. 1-6.

Mei, T., Nagy, Z., Goodall, R. and Wickens, A. (2002) 'Mechatronic solutions for high-speed railway vehicles.' *Control Engineering Practice*, 10(9) pp. 1023-1028.

Mei, T. X. and Goodall, R. M. (1999) '*Optimal Control strategies for Active Steering of Railway Vehicles*.' *In Proceedings of IFAC World Congress 99.* Vol. F. Beijing, China: pp. 251-256.

Mei, T. X. and Goodall, R. M. (2000) 'Modal Controllers for Active Steering of Railway Vehicles with Solid Axle Wheelsets.' *Vehicle System Dynamics*, 34(1), 2013/12/06, pp. 25-41.

Mei, T. X. and Goodall, R. (2001) 'Robust Control for Independently Rotating Wheelsets on a Railway Vehicle Using Practical Sensors.' *Control Systems Technology*, 9(4) pp. 509-607.

Mei, T. X. and Goodall, R. M. (2006) 'Stability control of railway bogies using absolute stiffness: sky-hook spring approach.' *Vehicle System Dynamics*, 44(sup1) pp. 83-92.

Mei, T. X. and Li, H. (2008) 'A novel approach for the measurement of absolute train speed.' *Vehicle System Dynamics*, 46(sup1) pp. 705-715.

Mei, T. X., Goodall, R. and Li, H. (1999) 'Kalman filter for the state estimation of a 2-axle railway vehicle.' *In 5th European Control Conference.* Vol. 99:

Mei, T. X., Perez, J. and Goodall, R. M. (2000) 'Design of optimal PI controls for perfect curving of railway vehicles with solid-axle wheelsets.' *In UKACC International Conference on Control.* Vol. 31. Cambridge: IEE, pp. 6-25.

Mei, T. X., Lu, J. W. and Abe, M. (2005) 'On the interaction and integration of wheelset control and traction system.' *In The Dynamics of Vehicles on Roads and on Tracks Supplement to Vehicle System Dynamics: Proceedings Of The 18th Iavsd Symposium.* Vol. 41. Kanagawa, Japan: CRC Press, pp. 123-132.

Michitsuji, Y. and Suda, Y. (2006) 'Running performance of power-steering railway bogie with independently rotating wheels.' *Vehicle System Dynamics*, 44(sup1) pp. 71-82.

Pearson, J., Goodall, R., Mei, T. and Himmelstein, G. (2004) 'Active stability control strategies for a high speed bogie.' *Control engineering practice*, 12(11) pp. 1381-1391.

Pearson, J., Goodall, R., Mei, T., Shen, S. and Zolotas, A. (2004) 'Kalman Filter Design for a High Speed Bogie Active Stability System.' *UKACC Control, Bath, UK*,

Pearson, J. T., Goodall, R. M., Mei, T. X., Shuiwen, S., Kossmann, C., Polach, O. and Himmelstein, G. (2004) 'Design and Experimental Implementation of an Active Stability System for a High Speed Bogie.' *Vehicle System Dynamics*, 41 pp. 43-52.

Perez, J., Mauer, L. and Busturia, J. (2003) 'Design of active steering systems for bogie-based railway vehicles with independently rotating wheels.' *Vehicle System Dynamics*, 37 pp. 209-220.

Perez, J., Busturia, J. M., Mei, T. and Vinolas, J. (2004) 'Combined active steering and traction for mechatronic bogie vehicles with independently rotating wheels.' *Annual Reviews in Control*, 28(2) pp. 207-217.

Powell, A. J. (1998) 'On The Dynamics of Actively Steered Railway Vehicles.' *Vehicle System Dynamics*, 29(sup1) pp. 506-520.

Powell, A. J. and Wickens, A. H. (1996) 'Active Guidance of Railway Vehicles Using Traction Motor Torque Control.' *Vehicle System Dynamics*, 25(sup1) pp. 573-584.

Pèrez, J., Busturia, J. and Goodall, R. (2002) 'Control strategies for active steering of bogie-based railway vehicles.' *Control Engineering Practice*, 10(9) pp. 1005-1012.

Shen, G. and Goodall, R. (1997) 'Active Yaw Relaxation For Improved Bogie Performance.' *Vehicle System Dynamics*, 28(4-5) pp. 273-289.

Suda, Y., Wang, W., Nishina, M., Lin, S. and Michitsuji, Y. (2012) 'Self-steering ability of the proposed new concept of independently rotating wheels using inverse tread conicity.' *Vehicle System Dynamics*, 50(sup1) pp. 291-302.

Sugiyama, H., Yamashita, S. and Suda, Y. (2010) 'Curving Simulation of Ultralow-Floor Light Rail Vehicles With Independently Rotating Wheelsets.' *In ASME 2010 International Mechanical Engineering Congress and Exposition.* Vol. 11: American Society of Mechanical Engineers, pp. 869-875.

Tanifuji, K., Sato, T. and Goodall, R. (2003) 'Active steering of a rail vehicle with two-axle bogies based on wheelset motion.' *Vehicle System Dynamics*, 39(4) pp. 309-327.

Ward, C. P., Weston, P., Stewart, E., Li, H., Goodall, R. M., Roberts, C., Mei, T., Charles, G. and Dixon, R. (2011) 'Condition monitoring opportunities using vehicle-based sensors.' *Proceedings of the Institution of Mechanical Engineers, Part F: Journal of Rail and Rapid Transit*, 225(2) pp. 202-218.

Wickens, A. (1969) 'General aspects of the lateral dynamics of railway vehicles.' *Journal of Engineering for Industry*, 91(3) pp. 869-875.

Zhaijun, L., Hongqi, T. and Yinglong, L. (2011) 'Measuring Technology of Rail Vehicle's Offset Caused by Vibration.' *In Measuring Technology and Mechatronics Automation, Third International Conference on.* Vol. 2: IEEE, pp. 529-533.

Zhou, R., Zolotas, A. and Goodall, R. (2014) 'Robust system state estimation for active suspension control in high-speed tilting trains.' *Vehicle System Dynamics:International Journal of Vehicle Mechanics and Mobility*, 52 pp. 1-15.

Zolotas, A. C. and Goodall, R. (2000) 'Advanced control strategies for tilting railway vehicles.' *In UKACC Control*. Cambridge:

Zolotas, A. C., Halikias, G. D. and Goodall, R. (2000) 'A comparison of tilt control approaches for high speed railway vehicles.' *In Proceedings of the 14th International Conference on Systems Engineering*: pp. 632-636.